PB80-176852

Red Clay Turbidity and Its Transport in Lake Superior

Minnesota Univ.-Duluth

Prepared for

Environmental Protection Agency
Chicago, IL

Jan 79

U.S. Department of Commerce
National Technical Information Service
NTIS

United States
Environmental Protection
Agency
Region V

Great Lakes
National Program Office
536 South Clark Street
Chicago, Illinois 60605

EPA 905/9-79-004
January 1979

PB80-176852

EPA

Red Clay Turbidity and Its Transport in Lake Superior

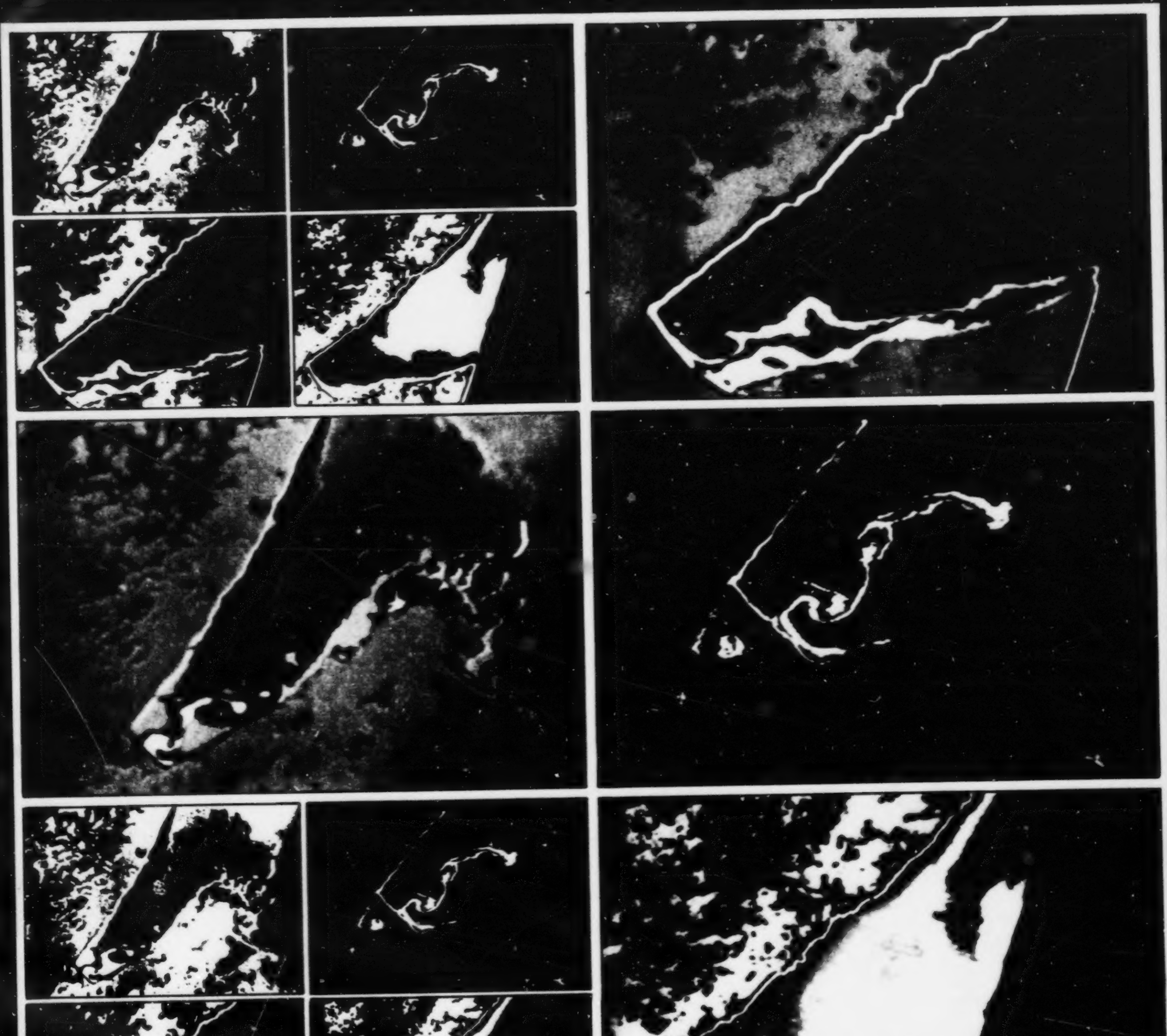

REPRODUCED BY
NATIONAL TECHNICAL
INFORMATION SERVICE
U.S. DEPARTMENT OF COMMERCE
SPRINGFIELD, VA 22161

TECHNICAL REPORT DATA
(Please read Instructions on the reverse before completing)

1. REPORT NO.
EPA-905/9-79-004

2.

3. RECIPIENT'S ACCESSION NO.
PB80-176852

4. TITLE AND SUBTITLE
Red Clay Turbidity and Its Transport
in Lake Superior

5. REPORT DATE
January 1979

6. PERFORMING ORGANIZATION CODE

7. AUTHOR(S)
Michael Sydor, Richard T. Clapper, Gordon J. Oman,
and Kirby R. Stortz

8. PERFORMING ORGANIZATION REPORT NO.

9. PERFORMING ORGANIZATION NAME AND ADDRESS
Physics Department
University of Minnesota, Duluth
Duluth, Minnesota 55812

10. PROGRAM ELEMENT NO.
2BA645

11. CONTRACT/GRANT NO.
R005175-01

12. SPONSORING AGENCY NAME AND ADDRESS
Great Lakes National Program Office
U.S. Environmental Protection Agency, Region V
536 South Clark Street
Chicago, Illinois 60605

13. TYPE OF REPORT AND PERIOD COVERED
Final

14. SPONSORING AGENCY CODE

15. SUPPLEMENTARY NOTES
Undertaken in support of the Upper Lakes Reference Group studies of pollution in Lake Superior and Lake Huron.

16. ABSTRACT

Red clay plumes in western Lake Superior are studied using Landsat satellite imagery to determine the relative magnitude of the three sources of the observed turbidity: erosion of the Wisconsin south shore red clay banks, resuspension of bottom sediments, and runoff from the many streams which flow through the red clay belt and then into the lake. A comprehensive sampling program was conducted during the spring of 1975 to determine the runoff contribution to the total load observed in the lake. Analysis of Landsat transparency data coupled with weather records enabled contributions from erosion and resuspension to be separated. It was found that approximately 75% of the observed load in the lake during the ice-free season, from May to November, is from erosion, 20% is from resuspension, and 5% is from runoff.

A numerical model for water transports in Lake Superior as a function of winds is developed. This model is verified by comparison of observed and predicted water levels at several locations around the lake, and by comparison of the predicted transport patterns to actual turbidity distributions observed in Landsat imagery. Transport patterns are shown for western Lake Superior and the entire lake for both an easterly and westerly wind. A model of current profile with depth is also developed. The results of the transport model are used to predict distributions of red clay from the south shore and taconite tailings discharged into the lake at Silver Bay, Minnesota.

17. KEY WORDS AND DOCUMENT ANALYSIS

a. DESCRIPTORS	b. IDENTIFIERS/OPEN ENDED TERMS	c. COSATI Field/Group
Turbidity Sediment transport Erosion Runoff Water quality Hydrodynamics Remote sensing	Red clay, Landsat Lake Superior, Numerical transport models Upper Lakes Reference Group International Joint Commission	

18. DISTRIBUTION STATEMENT RELEASE TO PUBLIC	**19. SECURITY CLASS** *(This Report)* UNCLASSIFIED	**21. NO. OF PAGES** 139
	20. SECURITY CLASS *(This page)* UNCLASSIFIED	**22. PRICE**

EPA Form 2220-1 (Rev. 4-77) PREVIOUS EDITION IS OBSOLETE

EPA-905/9-79-004
January 1979

RED CLAY TURBIDITY AND ITS TRANSPORT IN LAKE SUPERIOR

by

Michael Sydor
Richard T. Clapper
Gordon J. Oman
Kirby R. Stortz

Physics Department
University of Minnesota, Duluth
Duluth, Minnesota 55812

E.P.A. Grant No. R005175-01

Project Officer

Anthony G. Kizlauskas
U.S. Environmental Protection Agency
Region V
Great Lakes National Program Office
Chicago, Illinois 60605

GREAT LAKES NATIONAL PROGRAM OFFICE
U.S. ENVIRONMENTAL PROTECTION AGENCY
REGION V
CHICAGO, ILLINOIS 60605

DISCLAIMER

This report has been reviewed by the Great Lakes National Program Office, Region V, U.S. Environmental Protection Agency, and approved for publication. Approval does not signify that the contents necessarily reflect the views and policies of the U.S. Environmental Protection Agency, nor does mention of trade names constitute endorsement or recommendation for use.

FOREWORD

The U.S. Environmental Protection Agency (EPA) was created because of increasing public and governmental concern about the dangers of pollution to the health and welfare of the American people. Noxious air, foul water, and spoiled land are tragic testimony to the deterioration of our natural environment.

The Great Lakes National Program Office (GLNPO) of the U.S. EPA was established in Region V, Chicago, to provide a specific focus on the water quality concerns of the Great Lakes. GLNPO provides funding and personnel support to the International Joint Commission activities under the U.S.-Canada Great Lakes Water Quality Agreement.

Several water quality studies have been funded to support the Upper Lakes Reference Group (ULRG) under the Agreement to address specific objectives related to pollution in the Upper Lakes (Lake Superior and Lake Huron). This report describes some of the work supported by this Office to carry out ULRG study objectives.

We hope that the information and data contained herein will help planners and managers of pollution control agencies make better decisions for carrying forward their pollution control responsibilities.

Dr. Edith J. Tebo
Director
Great Lakes National Program Office

ABSTRACT

Through the use of Landsat satellite imagery from 1972 - 1975, red clay plumes in western Lake Superior are studied in order to determine the relative magnitude of the three sources of the observed turbidity: erosion of the Wisconsin south shore red clay banks, resuspension of bottom sediments, and runoff from the many streams which flow through the red clay belt and then into the lake. A comprehensive sampling program was conducted during the spring of 1975 in order to determine the runoff contribution to the total load observed in the lake. Analysis of Landsat transparency data coupled with weather records enabled contributions from erosion and resuspension to be separated. It was found that approximately 75% of the observed load in the lake during the ice free season, from May to November, is from erosion, 20% is from resuspension, and 5% is from runoff.

A numerical model for water transports in Lake Superior as a function of winds is developed. This model is verified by comparison of observed and predicted water levels at several locations around the lake, and by comparison of the predicted transport patterns to actual turbidity distributions observed in Landsat imagery. Transport patterns are shown for western Lake Superior and the entire lake for both an easterly and westerly wind. A model of current profile with depth is also developed. The results of the transport model are used to predict distributions of red clay from the south shore and taconite tailings discharged into the lake at Silver Bay, Minnesota.

This report was submitted in fulfillment of Grant No. R005175-01 by the Great Lakes National Program Office, Region V under the sponsorship of the U.S. Environmental Protection Agency. This report covers a period from October, 1974 to March, 1976 and work was completed as of January, 1979.

CONTENTS

Foreword iii
Abstract iv
Figures vi
Tables ix
Acknowledgments x

1. Introduction 1
2. Conclusions 2
3. Recommendations 4
4. Runoff from Douglas County, Wisconsin 5
    Rivers and streams analyzed 5
    Method 7
    Results 20
    Rain Runoff 27
    Conclusions 32
5. Sources and Transports of Turbidity in Western Lake Superior . . . 34
    Estimation of sediment resuspension and total loading 34
    Turbidity transport and the distribution of turbidity sources 48
6. A Numerical Model of Transports in Lake Superior 56
    Description of the model 56
    Results of transport model 61
    Current profile model 88
    Turbidity transport model 95

References 104

Appendix

A. South Shore Data for the 1975 Runoff 105

FIGURES

Number		Page
1	General study area	6
2	Rivers and streams analyzed in Douglas County, Wisconsin . . .	8
3	Nemadji River basin	9
4	Comparison of grabbed and integrated water samples	10
5	Cross sectional areas and discharge rates of analyzed streams	11
6	Discharge vs. stage for the analyzed streams	14
7	Soil map of northern Wisconsin	19
8	Daily snow and runoff data during snow-runoff period	21
9	Daily suspended load for analyzed streams during the entire runoff period	22
10	Turbidity and suspended solids correlation	26
11	Total load vs. total discharge for the large streams	28
12	Daily rainfall and Nemadji River discharge and suspended load data for a summer rain event	32
13	Turbidity calibration of Landsat images	35
14	Representative suspended solids distribution produced from Landsat data	36
15	Lake grid spaces and regions used in Landsat image analysis .	37
16	Spring ice shelf near Amnicon River	41
17	Average lake turbidity near Duluth	42
18	Average turbidity dissipation for easterly and westerly wind storms	45
19	Actual turbidity dissipation for a large easterly storm . . .	45

Number Page

20 Average storm characteristics 46

21 Distribution of storm duration 46

22 Average turbidity distribution and transport for an easterly storm 49

23 Average turbidity distribution and transport for a westerly storm 50

24 Average turbidity distribution and transport by westerly winds 51

25 Average turbidity distribution and transport for variable winds 52

26 Average turbidity distribution for the ice-free season 53

27 Relative south shore erosion rate 54

28 Resuspension areas in Lake Superior 54

29 Duluth water levels for easterly wind 63

30 Actual Duluth water levels for westerly wind 63

31 Western Lake Superior transports for easterly storm 65

32 Landsat image for 11APR75 showing resuspension plume 68

33 Skylab image showing turbidity entrapment near Duluth 68

34 Landsat image for 23NOV73 showing taconite tailings plume off Silver Bay 69

35 Western Lake Superior transports for westerly storm 70

36 Water level as a function of time at Duluth from the transport model 72

37 Water levels for western Lake Superior for an easterly storm . 73

38 Water levels for western Lake Superior for westerly wind . . . 73

39 Water levels for western Lake Superior from the Forristall model 74

40 Entire Lake Superior transports from a 13 m/s NE wind 75

Number		Page
41	Entire Lake Superior transports from a 11 m/s westerly wind. .	80
42	Lake Superior water level station locations	85
43	Modeled Lake Superior water levels from a northeast storm . .	86
44	Current vs. relative depth near surface	91
45	Current meter station locations	91
46	Current profiles for two values of ν	94
47	Peak measured surface currents vs. wind speed for several northeast winds	94
48	Computer bottom currents near Duluth	96
49	Lake sample settling in lab	97
50	Modeled suspended solids distribution at several stages of the storm	98
51	Landsat image for 03APR75	101
52	Modeled sediment accumulation at different stages of the storm	102

TABLES

Number Page

1 Load Transported during April, 1975 25

2 Snow Runoff per Linear km of Stream Length and per Square km of Basin Area for the Period April 10 - 27 29

3 Summer Rain Runoff for Nemadji River (1970 - 1974) 30

4 Yearly Input of Suspended Load 32

5 Percent Abundance of Particle Sizes by Number 33

6 Ratio of Average Turbidity to Surface Turbidity for Western Lake Superior 38

7 Total Suspended Load in Western Lake Superior 39

8 Sources of Lake Turbidity 47

9 Comparison of Periods in Hours of Gravitational Modes in Lake Superior 64

ACKNOWLEDGMENTS

We would especially like to thank Dr. Thomas F. Jordan, Physics Department, University of Minnesota, Duluth, for his derivation of the current profile model solution.

We are grateful to Mr. Steve Diehl, University of Minnesota, Duluth, for his work on the transport model.

We are grateful for the assistance of the following individuals who helped to collect and analyze material in this report: Dr. David G. Darby, University of Minnesota, Duluth; Dr. Albert B. Dickas, University of Wisconsin, Superior; Mr. David Smith, Mr. John Sorensen, Mr. Vasyl Shuter, Mr. Gary Fandrei, and Mr. Wayne Maanum.

We are particularly grateful for the assistance of Mr. Steven Spray, whose photographic and sampling efforts were most helpful during the difficult conditions of early spring.

We are grateful to Mr. Nelson A. Thomas, U.S. Environmental Protection Agency, Large Lakes Research Station, Grosse Ile, Michigan, for performing the particle size analysis.

1. INTRODUCTION

The transport of fine red clay particles from erosion of red clay banks in Douglas County, Wisconsin, over large areas of the lake causes water quality degradation and displeasing aesthetic appearance, which together are often referred to as the Red Clay Problem. The turbidity within the lake plumes results from three processes: lakeshore erosion, sediment resuspension, and stream runoff. The total turbidity within the entire plume can be determined through remote sensing. The relative contribution of each source, however, must be established from measurements of the individual sources. The runoff can readily be evaluated with reasonable accuracy. The magnitude of the other turbidity sources can be established by subtraction of the contribution from runoff. The determination of the relative magnitude of all three sources of red clay turbidity in the lake is essential in evaluation of red clay-related problems, such as the deterioration of water quality and property damage caused by severe erosion of the lakeshore. In the case of water quality, it is particularly important to determine the magnitude of the runoff, since the water quality problems resulting from shore erosion and sediment resuspension may be quite distinct from those resulting from red clay washed out by polluted rivers. For instance, the red clay particles transported by the Nemadji River could adsorb and carry pollutants into the lake. The contribution of runoff to lake turbidity is also useful for determining the effect of various erosion abatement programs currently in progress in the red clay belt of Wisconsin and Minnesota.

2. CONCLUSIONS

1) Turbidity measurements correlated with Landsat satellite data show that lake turbidity originated from erosion of shore banks, resuspension of bottom sediment, and river runoff. Using satellite data from August, 1972 to August, 1975, the contribution of each source per open water season (May - November) was estimated to be 4.0 x 10^6 metric tons from erosion, 1.0 x 10^6 metric tons from resuspension, and .32 x 10^6 metric tons from river runoff. During the open water season, about 75% of the total sediment load is contributed by erosion, 20% by resuspension, and 5% by river runoff.

2) The runoff mainly comes from the Nemadji River, which accounts for over 80% of the total sediment output from streams and rivers in Douglas County, Wisconsin.

3) Winter storms which occur when the lake is ice-free but when the lakeshore and the rivers are iced over, contribute roughly 2 x 10^6 metric tons per season of additional suspended material in the lake. This largely comes from sediment resuspension at the intermediate depths off Wisconsin and Minnesota Points. Resuspension is greater during the winter months because of the higher frequency of northeast winds and more nearly isothermal condition of the lake.

4) A numerical model for transports was devised for the lake. The model was tested using water level data and by comparing the predicted transports to the transport of turbid plumes observed by Landsat. The results of the numerical model and the statistical analysis of Landsat data explain the periodic contamination of the Duluth water intake by high concentrations of red clay particles and asbestos particles.

5) The fine red clay material contaminates much of western Lake Superior from Duluth to the Apostle Islands. The main transport of turbidity for northeast winds occurs along the axis of the western arm of the lake from Duluth towards the Apostle Islands. For west winds, the main transports occur along the Wisconsin shore towards the Apostle Islands.

6) The distribution of lake levels as a function of winds is given for Duluth and extreme western Lake Superior. The height of water level fluctuation due to storm surges is on the order of 20 cm (8 inches), which is comparable to the seasonal fluctuation in the water level. Changes in erosion rates resulting from water level fluctuations could in principle be obtained from Landsat data on the distribution of turbidity along the shore after storm surges.

7) General circulations and transports for the entire lake are discussed. The transport patterns for the two wind directions modeled here do not carry

the fine red clay material directly across the international boundary. However, fine red clay particles are transported in the lake in detectable concentrations (1 mg/ℓ) for over 80 km.

8) The effective area of contamination for a storm surge and the long-range transport of fine sediment was assessed by simulating a turbidity plume generated by a steady two-day northeasterly wind storm with 13 m/sec (30 mph) winds followed by a westerly wind. The results show that an estimated 10^6 metric tons of material would be removed by erosion for such a storm and dispersed in the area of the lake from Duluth to the Apostle Islands. Although the computation simulated dispersion of clay for an equivalent of only a 4-day period, in which time it showed that most of the suspended load was deposited in western Lake Superior between Duluth and the Apostle Islands, it is estimated that on the order of 3% of the material or $\sim 10^5$ metric tons per year would disperse outside of this area. This result is also borne out in the observation of extensive plumes through remote sensing which in some instances shows the plumes extending well past the Apostle Islands.

9) Bottom currents near Duluth for westerly winds favor the presence of an upwelling along the North Shore. The results of the calculation on bottom currents for isothermal conditions indicate that resuspended material off Minnesota Point would move out along an easterly direction for northeast winds. Westerly winds would generally move the resuspended material towards Duluth, with the exception of an area east and southeast of the Superior entry, where the bottom currents point toward the Wisconsin shore.

3. RECOMMENDATIONS

1) Correlation of Erosion and Lake Levels.

Examination of the results from the numerical model shows that the water level along the red clay bank shore is a function of winds. The change in water level produced by the wind appears to be accompanied by a change in the relative turbidity along the shore as observed from the satellite.

Further work including the effects of wind, fetch, and turbidity distribution along the shore in correlation with water level information obtained from the numerical model should be made.

A series of manned overflights of the shore area for various wind conditions using multispectral scanners would be fruitful in establishing the dependence of the erosion rates on water levels. The overflights would also help determine the boundary conditions necessary for modeling the shore erosion as a turbidity source.

2) Water Quality.

The development of the numerical model for transports is a prerequisite for water quality modeling. The next step should be concerned with water quality modeling of the effects of harbor effluents from the St. Louis River. The effluents tend to accumulate in extreme western Lake Superior for variable wind conditions.

The overall quality of the water in the lake should also be considered. The dispersion of very fine particulates and the dispersion of effluents from various point sources should be studied through remote sensing coupled with the modeling of long-range transport events.

Although it would be impractical to run a finer grid model for the entire lake because of computer storage and time requirements, much higher resolution could be obtained by submodeling on a finer grid scale at various locations of interest around the lake. For example, future studies might entail cutting the grid spacing by one half over the entire western arm of Lake Superior, while leaving the remainder of the lake unaltered. This would be especially beneficial for the comparison of modeled plumes to actual satellite images which contain features comparable in size to the present grid spacing.

4. RUNOFF FROM DOUGLAS COUNTY, WISCONSIN

RIVERS AND STREAMS ANALYZED

Streams and rivers passing through Douglas County, Wisconsin were monitored during the entire spring runoff in April, 1975. These streams run through the major deposit of glacial-lacustrine red clay around Lake Superior. The deposit averages 30 meters in depth and covers a 15-km-wide area along nearly all of the Lake Superior shore in Douglas County, Wisconsin, and beyond into Bayfield County, Wisconsin. The clay deposit shows critical erosion along many areas of the lakeshore and along the river banks and road cuts. A large fraction of the clay is made up of very fine particles less than 6 µ in size which are washed out into Lake Superior and are transported in the lake in high concentrations as far as 80 km. The transported particles from the red plumes are frequently observed in western Lake Superior and are a source of contamination of municipal water supplies.

The rivers and streams analyzed in this project include those flowing into the lake between Dutchman Creek, which enters Lake Superior approximately 2.5 km east of the southeastern end of Allouez Bay, and Haukkala Creek, Figure 1. This includes approximately 20 km of lake shoreline and twenty-one rivers and streams. In addition, the Nemadji River was also observed. Although the Nemadji River does not flow directly into Lake Superior but rather into the Superior Harbor Basin of the Duluth-Superior Harbor, its mouth is only 800 meters from the Superior entry to the harbor. Although the percentage of the Nemadji River's suspended load which is deposited in the lake has yet to be determined accurately, it is known that much of the fine load does flow out to the lake. The volume of the Nemadji's load is so great that if only 20% of it reached the lake, its contribution would still be comparable with the combined output of all the other rivers and streams in Douglas and Bayfield Counties.

From west to east, the rivers and streams analyzed and the monitoring sites are as follows: Nemadji River at the bridge near the Nemadji Golf Club in south Superior; Dutchman Creek at Hwy 13, 500 meters from the mouth; Morrison Creek at Hwy 13, 150 meters from the mouth; Amnicon River at Hwy 13; Ten Creek at Hwy 13, 600 meters upstream from the intersection with the Amnicon River; Wagner Creek at Hwy 13, 600 meters upstream from the intersection with the Amnicon River; Hanson Creek at Hwy 13, 300 meters from the mouth; Middle River at Hwy 13, 1 km from the mouth; Poplar River at Hwy 13, 800 meters from the mouth; Bardon River at Hwy 13, 800 meters from the mouth; and Pearson Creek at Hwy 13, 2.5 km from the mouth.

Within the study area investigated by the University of Minnesota, Duluth, there were fifteen unnamed intermittent streams. For purposes of this study the unnamed streams were numbered consecutively from west to east,

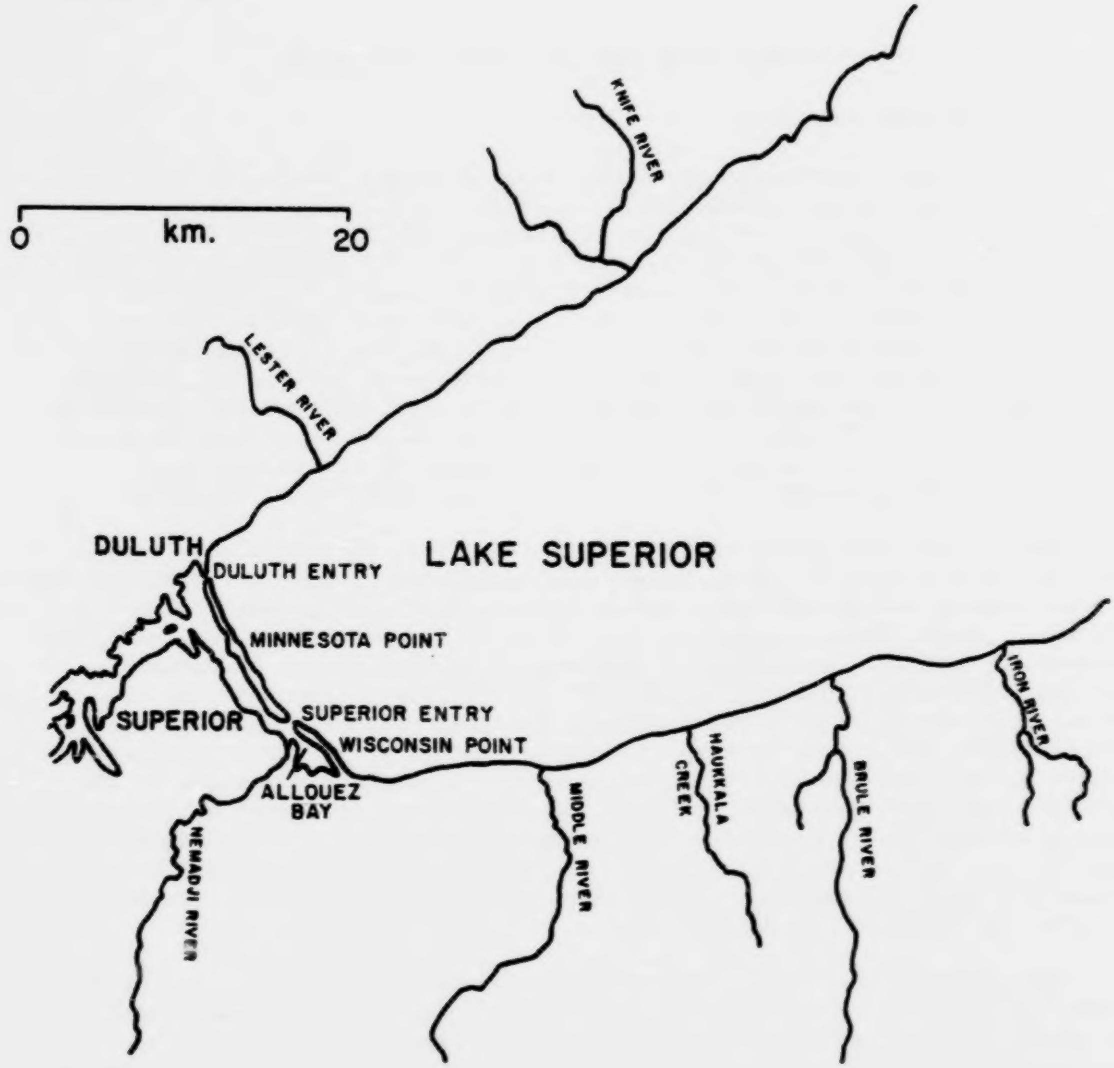

0
km.
20
KNIFE RIVER
LESTER RIVER
DULUTH
LAKE SUPERIOR
DULUTH ENTRY
MINNESOTA POINT
SUPERIOR
SUPERIOR ENTRY
WISCONSIN POINT
ALLOUEZ BAY
NEMADJI RIVER
MIDDLE RIVER
HAUKKALA CREEK
BRULE RIVER
IRON RIVER

Figure 1. General study area.

#1 - #15. Figure 2 presents a map of all of the rivers and streams analyzed, which includes an outline of their drainage basins. Since the United States Geological Survey has conducted considerable analysis of the Nemadji River, their figure for the total drainage area of this river was used. An outline of the Nemadji Basin which was taken from the report Red Clay Project appears in Figure 3.

METHOD

Since it is the suspended material that adversely affects Lake Superior's water quality, it was only the suspended load, or more specifically the wash-load, of the streams that was measured during this study. Particles included in the bed-load and the saltation-load of the streams are too heavy to remain suspended in the lake for any appreciable length of time.

A hand-held, rod-supported US DH-48 integrating sampler was used to collect water samples, which were refrigerated and analyzed within 24 hours. Particle size analyses were performed on selected samples using a HIAC counter.* Turbidity was measured with an AG1 Hach Meter, and suspended solids were determined by filtration through 0.45 μ Millipore filters. On deep, swift rivers such as the Nemadji it was impossible to stand in the river with the US DH-48 sampler. Long extensions for the handle were constructed so as to allow sampling from bridges, culverts, and, at times, trees which had fallen across the channels. To keep the sampler properly orientated in the swift current, i.e., the intake nozzle horizontal to the stream surface and directed directly upstream, thin nylon lines were attached to the handle near the sampler and tied-off upstream. Occasionally during the course of sampling, "dipped" or "grabbed" samples were also obtained for comparison with the integrated samples. A comparison between integrated and dipped samples appears in Figure 4.

Stream discharge rates were determined by measuring stream velocities (v) with a Gurley Meter (622), Pygmy Gurley Meter (625), or both, depending upon the flow-rate and the accessibility. At the same time as the average velocity was measured, the depth profile was measured to determine the cross-sectional area (A) of the stream. Thus discharge (Q) was determined, where $Q = Av$. In addition, marked stakes were driven or marks placed upon permanent fixtures such as culverts, bridge abutments, or trees at each sampling site. Using these marks, the stages of the rivers and streams could be easily and quickly determined when time or conditions prevented a current depth profile from being taken. Provided that subsequent channel profiling indicated that the contour of the channel had not changed, these stage indications were used to interpolate discharge rates. At the sites where the staging marks were not in contact with the stream surface, a hand level was used to determine the difference between the water surface and the staging mark. The cross-sectional areas for irregularly shaped stream contours were determined by reproducing scaled graphs of the profiles and tracing the outlines with a planimeter. Cross sections of the major rivers and streams analyzed appear in Figure 5. Plots of discharge vs. stage are shown in Figure 6.

---

*Particle size analyses were performed by Nelson A. Thomas, U.S. Environmental Protection Agency, Large Lakes Research Station, Grosse Ile, Michigan.

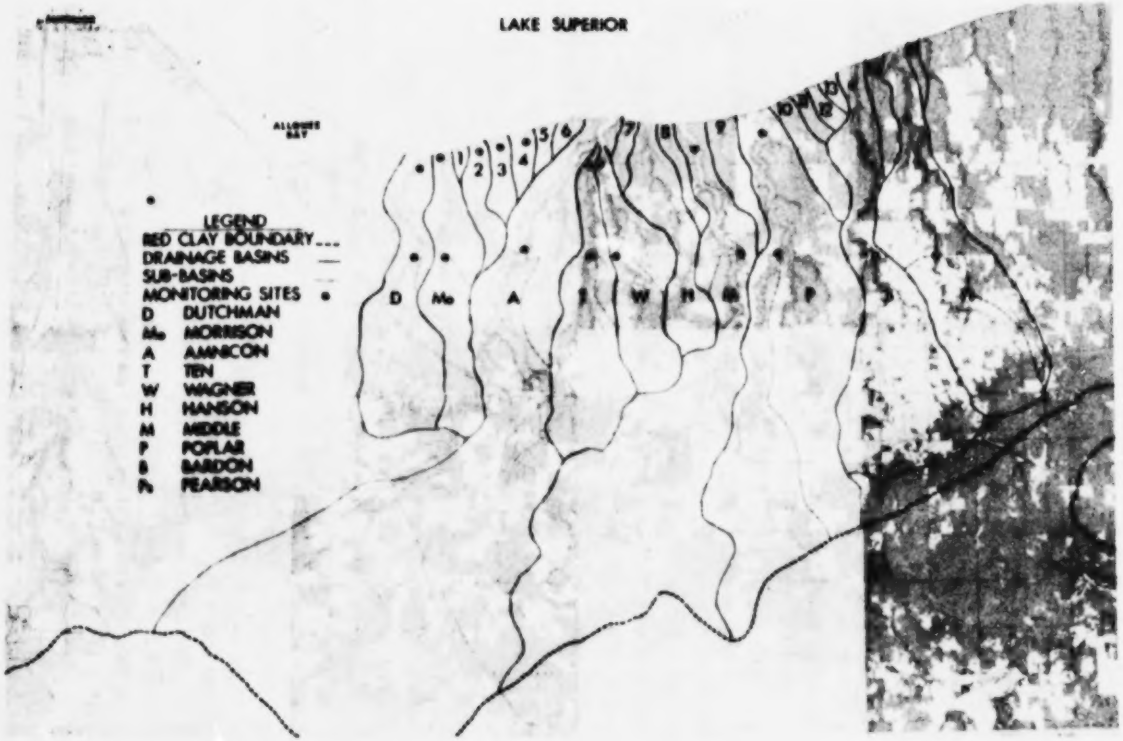
LAKE SUPERIOR
ALLOUEZ BAY
LEGEND
RED CLAY BOUNDARY
DRAINAGE BASINS
SUB-BASINS
MONITORING SITES
D DUTCHMAN
Mo MORRISON
A AMNICON
T TEN
W WAGNER
H HANSON
M MIDDLE
P POPLAR
B BARDON
Pe PEARSON
1
2
3
4
5
6
7
8
9
10
11
12
13
D
Mo
A
T
W
H
M
P
B
Pe

Figure 2. Rivers and streams analyzed in Douglas County, Wisconsin.

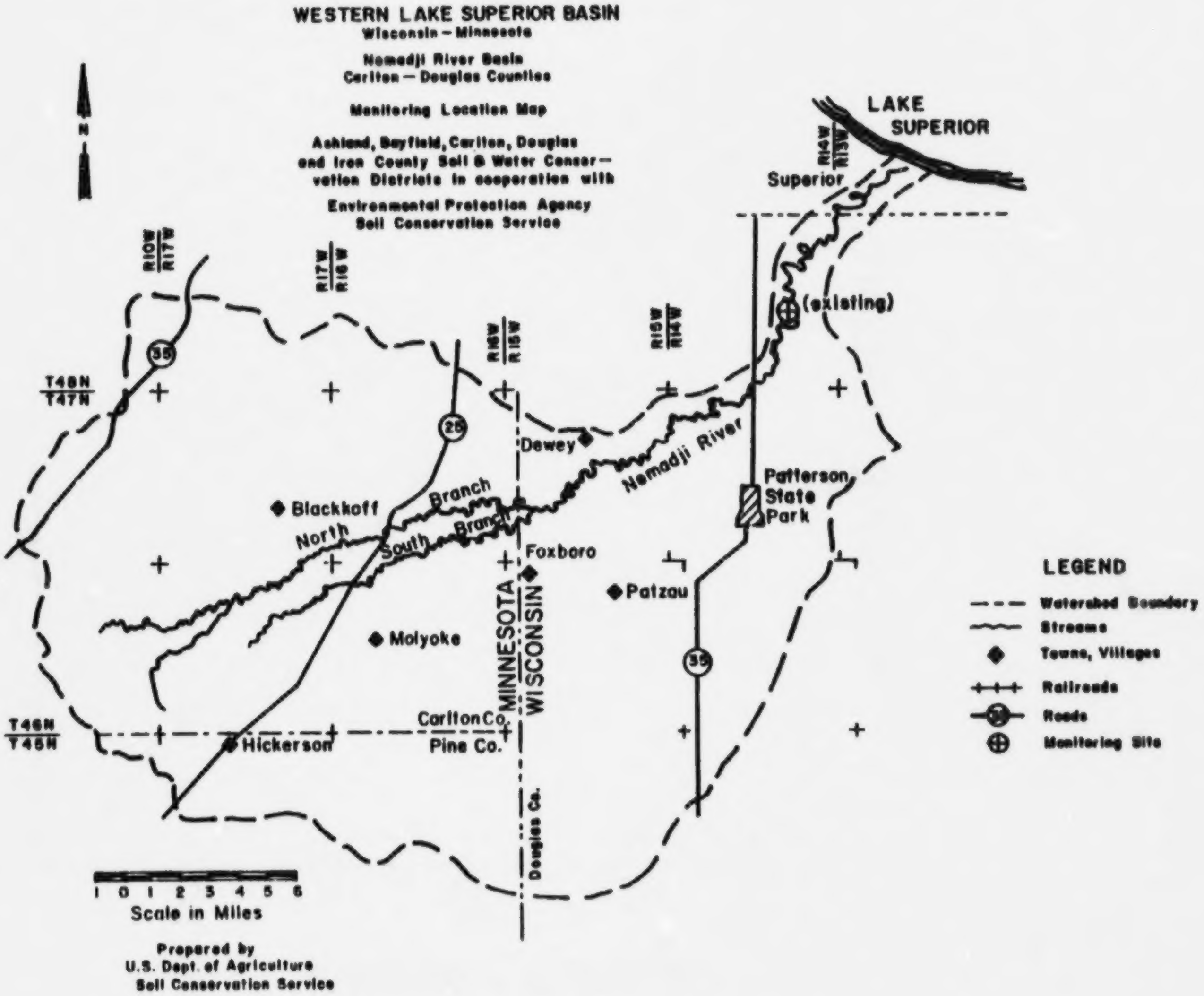
WESTERN LAKE SUPERIOR BASIN
Wisconsin – Minnesota
Nemadji River Basin
Carlton – Douglas Counties
Monitoring Location Map
Ashland, Bayfield, Carlton, Douglas and Iron County Soil & Water Conservation Districts in cooperation with
Environmental Protection Agency
Soil Conservation Service
N
LAKE SUPERIOR
Superior
R14W
R13W
(existing)
R10W
R17W
R17W
R16W
R16W
R15W
R15W
R14W
T48N
T47N
T47N
T46N
T46N
T45N
35
25
35
Dewey
Nemadji River
Patterson State Park
Blackkoff
North
Branch
South
Branch
Foxboro
Patzau
Molyoke
MINNESOTA
WISCONSIN
Carlton Co.
Pine Co.
Hickerson
Douglas Co.
LEGEND
Watershed Boundary
Streams
Towns, Villages
Railroads
Roads
Monitoring Site
1 0 1 2 3 4 5 6
Scale in Miles
Prepared by
U.S. Dept. of Agriculture
Soil Conservation Service

Figure 3. Nemadji River basin.

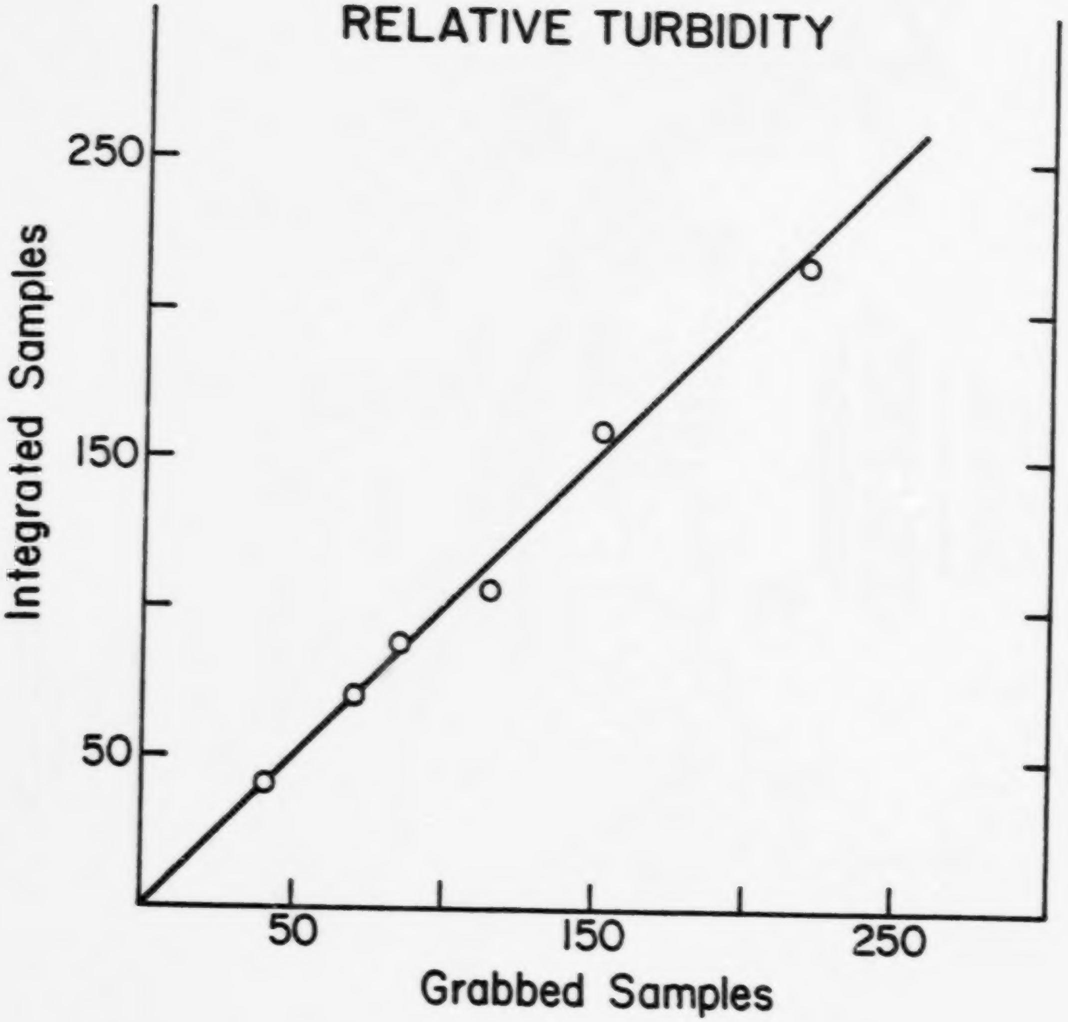

Figure 4. Comparison of grabbed and integrated water samples.

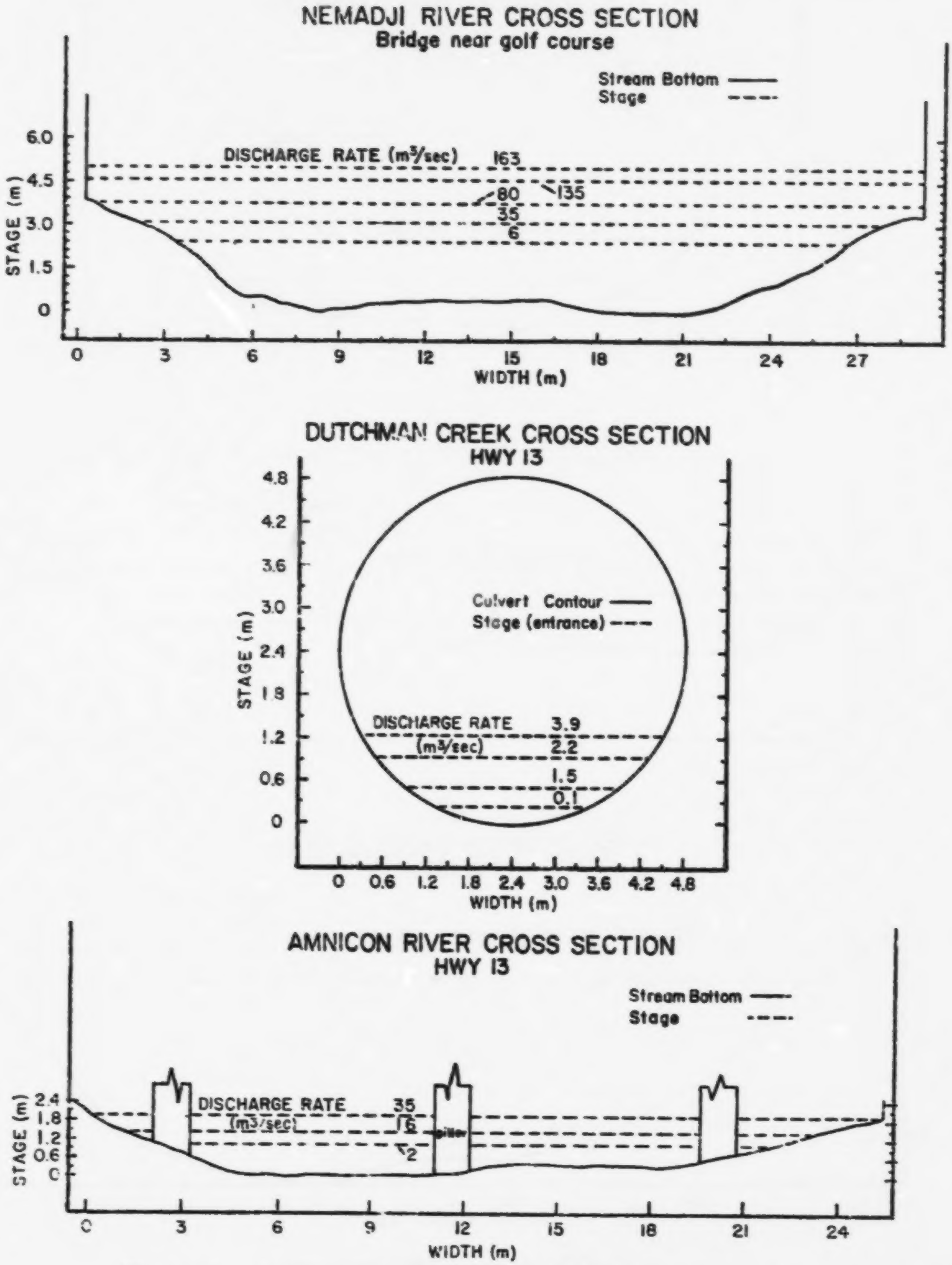

Figure 5. Cross-sectional areas and discharge rates of analyzed streams.

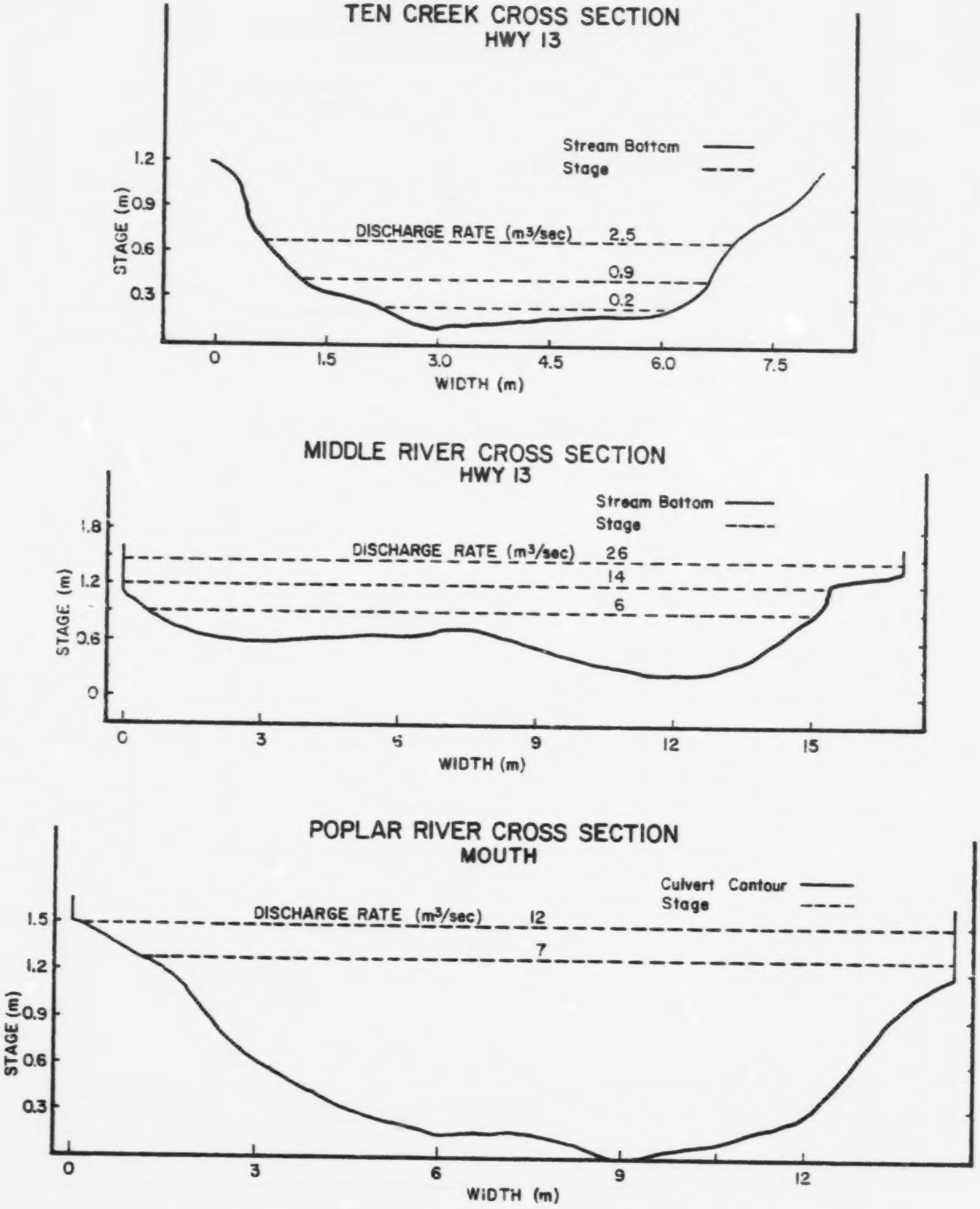

Figure 5. (continued)

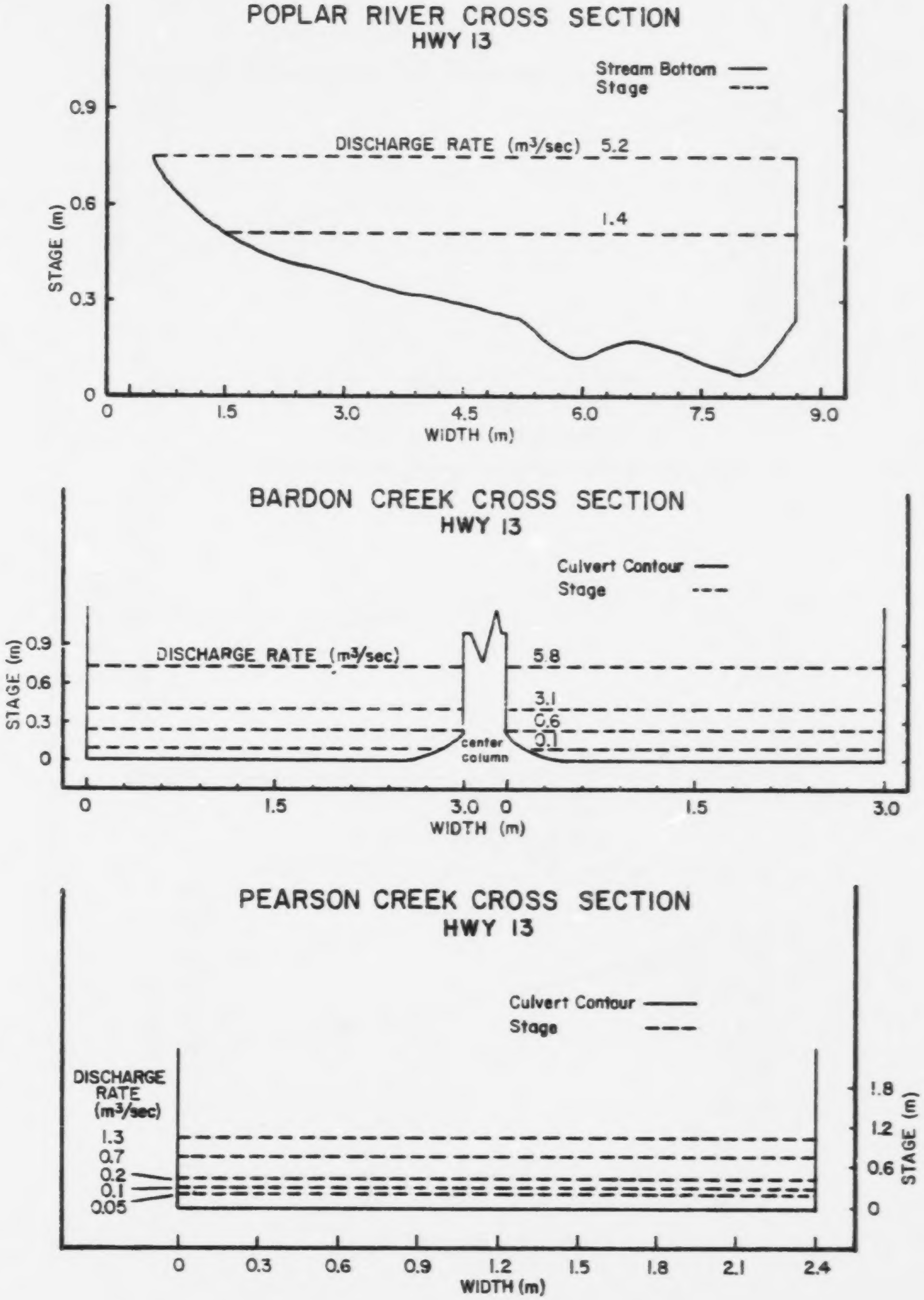

Figure 5. (continued)

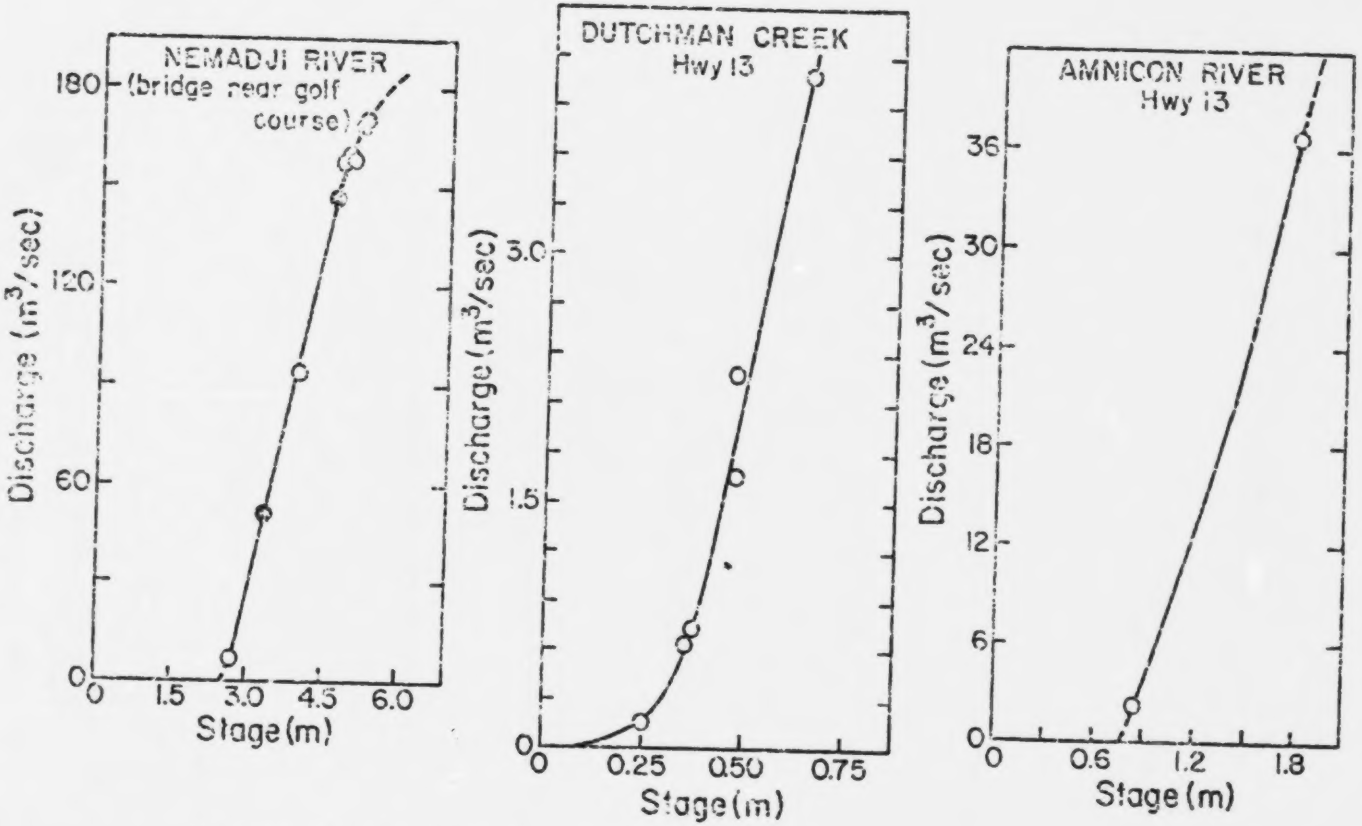

Figure 6. Discharge vs. stage for the analyzed streams.

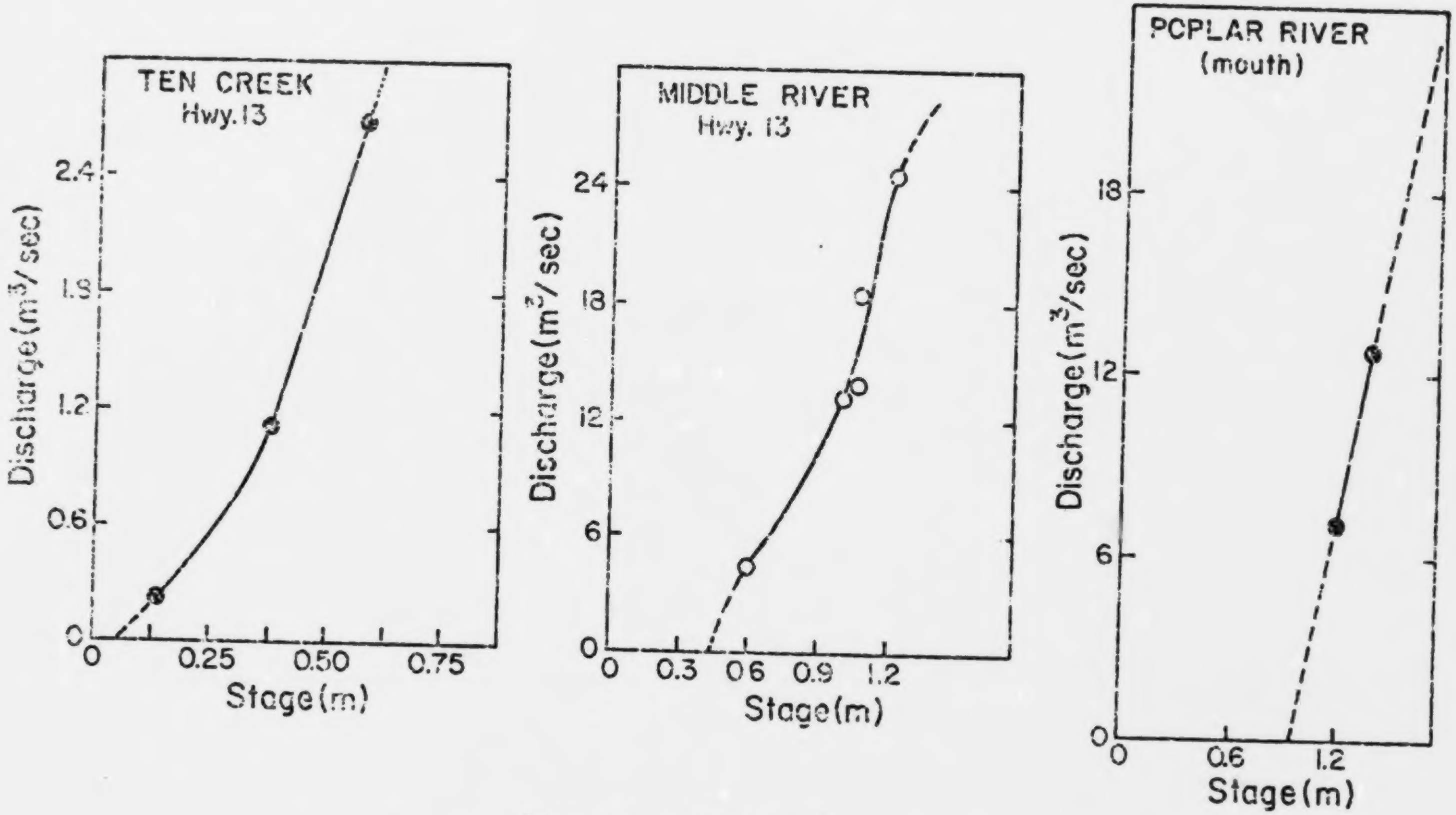

Figure 6. (continued)

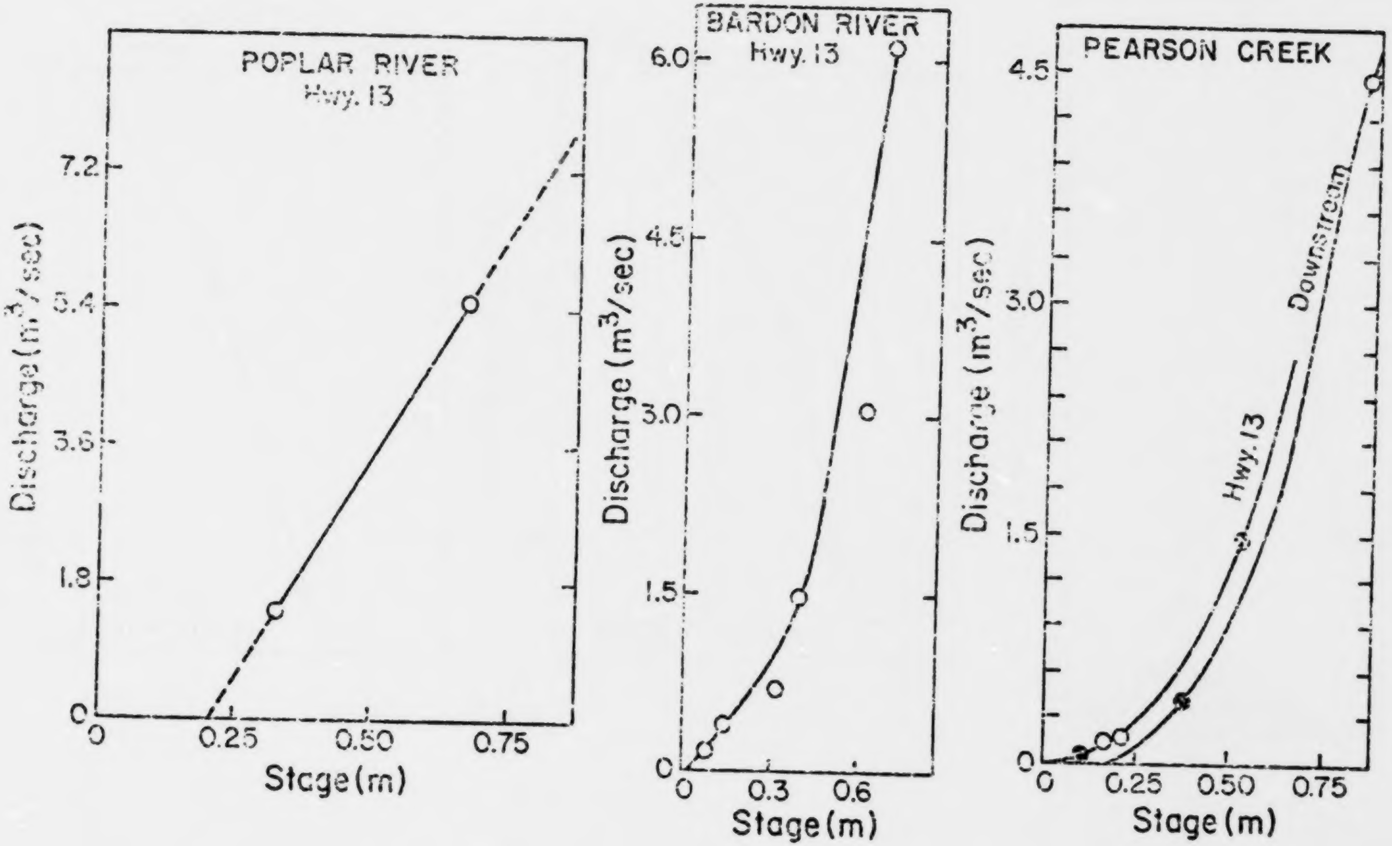

Figure 6. (continued)

Snow depth and the moisture content of the snow were measured by coring the snow at various locations with a 4.45 cm (1.75 inch) diameter clear plastic tube. The depth of the snow at the coring site was measured, and the core was emptied from the plastic tube into a small plastic bag and weighed to the nearest gram with a spring scale. Both the coring tube and the weighing bags were transparent so that the snow could be examined to be sure that debris such as grass, mud, sticks, and gravel were not present in the sample. Accurate snow measurement depends upon the percent of land covered by the snow as well as the depth. As the spring runoff progressed, larger areas of open ground began to appear. Photographs were taken to assist in determining the percent of land covered by the snow as well as the depth.

River and stream sampling for this project was conducted during the period April 9 through May 23, 1975, with intensive sampling taking place during the runoff period April 14 through May 7. During the period April 14 through May 7 stages were noted and water samples collected at all of the major rivers and streams on all but six days, of which no more than two were consecutive. This period was divided into a snow-runoff period, April 14 - 27, and a rain-runoff event, April 28 - May 7. Stream velocities were measured on occasions when significant stage differences were noted. Whenever possible, discharge rates were established and water samples were collected for upstream and downstream sampling sites of the same river. This was done in order to estimate the eroded load per km of stream length for a particular stage. Unfortunately, manpower shortages prevented checking the sampling sites of all the streams on any one day. During the first half of the runoff period nearly all of the sampling sites were taken alternately in order to reduce periods when data was not collected for the major streams to not more than one or two days, although occasionally a three-day period did elapse.

The difficulty in reaching good sampling locations caused certain sacrifices to be made. Ideally, sites should be on uniform, straight sections of the streams. There should be no tributaries or ditches entering above the location which are not well mixed with the main stream before reaching the sampling site. In addition, the site should be on a "high" section of the stream with no obstructions nearby downstream. This is necessary to permit accurate interpolation of the discharge from stage readings. If damming or restriction occurs, the backup destroys the relationship between stage and discharge. One other factor enters into site selection when testing near the lake. The sampling sites must be far enough upstream to prevent lake level from altering water samples and current measurements. This was satisfied for times of high flow for all rivers. The summertime low-flow periods on the Poplar River were subject to storage variation because of the gravel bar buildup at the mouth of the river.

The slope of the stage vs. discharge curve is nearly linear except at the peak flow or when a river rises above its normal banks and flows onto the flood plain. If testing is made in well-confined areas with deep banks, the change of slope due to flood plain overflow need not be determined.

In one way or another nearly all of the sampling sites fell short of the criteria just mentioned. However, the best locations which were reasonably convenient were selected, and appropriate data adjustments were made.

The sheer number of streams in this area prevented most of the intermittent streams (#1 - #15) as well as Hanson Creek from being monitored except by occasional visual inspection. The soil map of the entire test area, Figure 7, and topographical maps of the area, Figure 2, reveal that the soil and topography of the test area are quite uniform. Therefore, estimates of eroded load for the streams not monitored were determined by comparison of their basin areas and stream lengths to those for which considerable data was collected. All values determined strictly by estimate or interpolation appear enclosed in parentheses in the data tables in Appendix A.

Many daily values of discharge and load for the major streams had to be determined by interpolating from known values before and after the day. The accuracy of interpolated values depends on the accuracy of the known points, but it also depends upon assumptions made when interpolating. The following assumptions were made:

1) The increase or decrease of discharge rate is linear between close, consecutive measurements.

2) The increase or decrease of suspended load is linear between close, consecutive measurements.

3) Streams of similar size and length contained within similar geological and topographical boundaries will behave approximately the same.

4) For any stream flowing through unchanging topography and soil conditions the time average eroded load per unit length is constant for short sections.

In estimating the total load carried during the spring runoff, there are two sources of error for which no correction can be made at this time. The first deals with the transport of winter fines at the onset of the runoff. This error is limited primarily to the smaller, shallower streams and rivers which freeze solidly or nearly solidly during the winter. As the streams begin to thaw and flow begins over the frozen streams (often on the ice surface or between the frozen top surface and the frozen bottom), many fine particles are carried to points where ice restrictions cause the flow to decrease to the point that suspended particles are deposited on the icy bottom. After the runoff gains momentum, the bottom ice is freed and floated to the surface. Ice chunks carrying sediment up to 5 cm thick are floated downstream. Many of these chunks are broken up or overturned, thus depositing the sediment into the stream, but many other chunks are carried into the lake. No estimate of the extent of this contribution can be made at this time. The second source of error deals with transport near the river mouths. Wash-load transport is primarily a function of turbulence. As the streams near the lake (most stream mouths are drowned), the channels widen and the

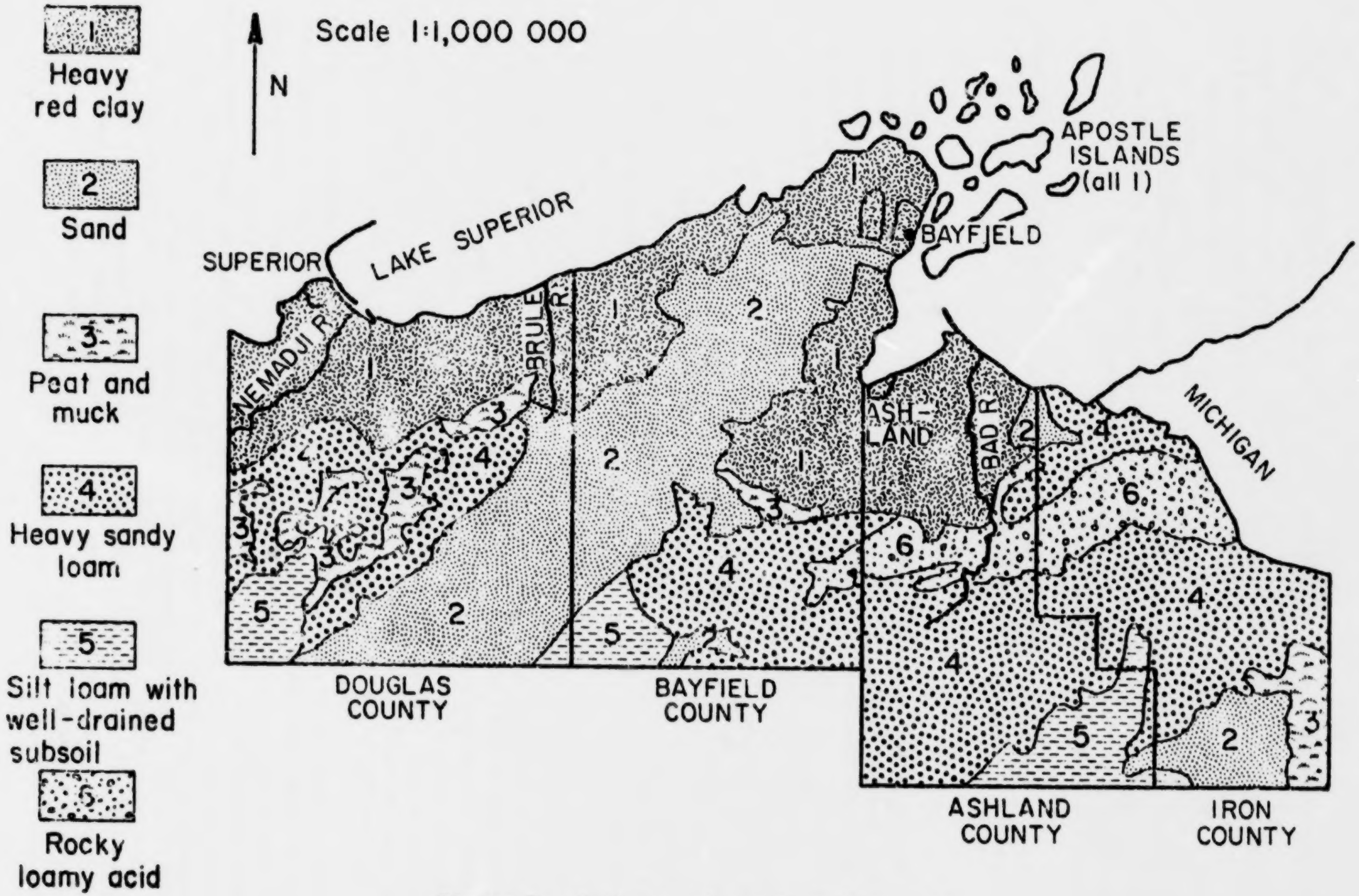
1
Heavy red clay
2
Sand
3
Peat and muck
4
Heavy sandy loam
5
Silt loam with well-drained subsoil
6
Rocky loamy acid
N
Scale 1:1,000 000
APOSTLE ISLANDS (all 1)
BAYFIELD
SUPERIOR
LAKE SUPERIOR
NEMADJI R.
BRULE R.
ASH-LAND
BAD R.
MICHIGAN
DOUGLAS COUNTY
BAYFIELD COUNTY
ASHLAND COUNTY
IRON COUNTY

Figure 7. Soil map of northern Wisconsin.

bottoms become smoother, both resulting in a decrease in turbulence and load transport. Also on occasions high lake level and strong wave action cause the flow to decrease tremendously, sometimes to the point that the flow runs upstream for as much as 1 km. The result of this is heavy deposits of soft, mucky fines above the stream mouths. Periodically high flow rates in the spring or during severe rainfalls scour and cleanse these areas. However, at peak runoff, the conditions are lessened by the high flow conditions. No attempt to estimate the amount of this transient transport of material can be made at this time. It is reasonable to assume that the sources of error due to these factors are reasonably low, say 10%.

All the data collected during this study together with interpolated and estimated values appear in Appendix A.

RESULTS

Snow measurements for the study correlate well with data obtained from the National Weather Service Office, International Airport, Duluth, Minnesota. Comparative plots of the snow remaining at Duluth Airport and the measured rate of runoff vs. date for the period April 7 through April 25 are shown in Figure 8. The data indicate approximately 25 cm more snow near Pearson Creek than Weather Bureau measurements near Duluth. Past experience makes this difference reasonable, although it should be noted that measurements along the South Shore varied considerably, depending upon where the measurements were taken. For instance, on April 14, snow measurements varied from 26 cm near Hwy 13, Dutchman Creek to 34 cm near the mouth of Pearson Creek. Using the snow moisture content of the samples and basin sizes, the calculations of water content for the basins were compared with measured total discharge values for both these river basins. During the period April 7 through April 26, the calculated discharge at Hwy 13, Dutchman Creek was 2.5 x 10^6 m^3. At Hwy 13, the calculated discharge for Pearson Creek during the period April 14 through April 27, was 1.6 x 10^6 m^3. The measured discharge during this period totaled 1.5 x 10^6 m^3. These differences are small and suggest that the snow measurements made at a few points were representative of the entire basin areas. It should be pointed out, however, that snow distribution is not uniform over large areas, and several widely spaced stations must be monitored when determining the spring runoff. Thus, weather data at the Duluth Airport is not sufficient for South Shore runoff studies.

Plots of total daily suspended load vs. date were constructed for all of the major streams and are shown in Figure 9. It is interesting to note that although the plots for all of the streams yield similar curves, a significant difference exists between the large rivers (Nemadji and Amnicon) and all of the smaller streams. In the smaller streams, the highest sediment load transported occurs at the onset of the runoff, although peak discharge does not occur until later. For the large rivers peak daily load occurs during the days of peak discharge. This difference can most likely be attributed to the greater buildup of winter fines in the shallow streams where the flow is reduced by ice obstruction. The large rivers are able to uniformly transport the fines throughout the winter. The peaks of the suspended load curves correlate well with the rate of runoff (Figure 8).

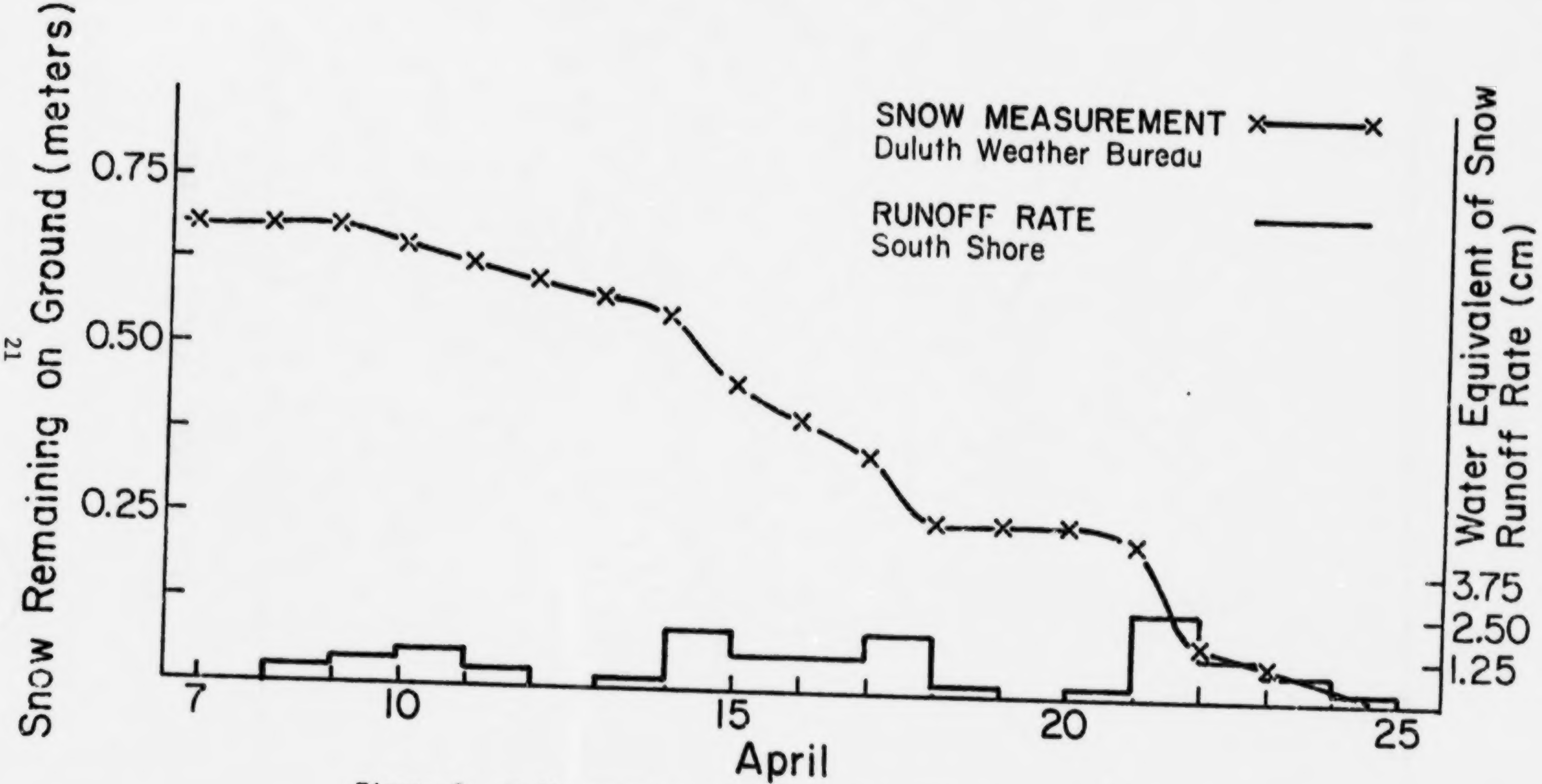

Figure 8. Daily snow and runoff data during snow-runoff period.

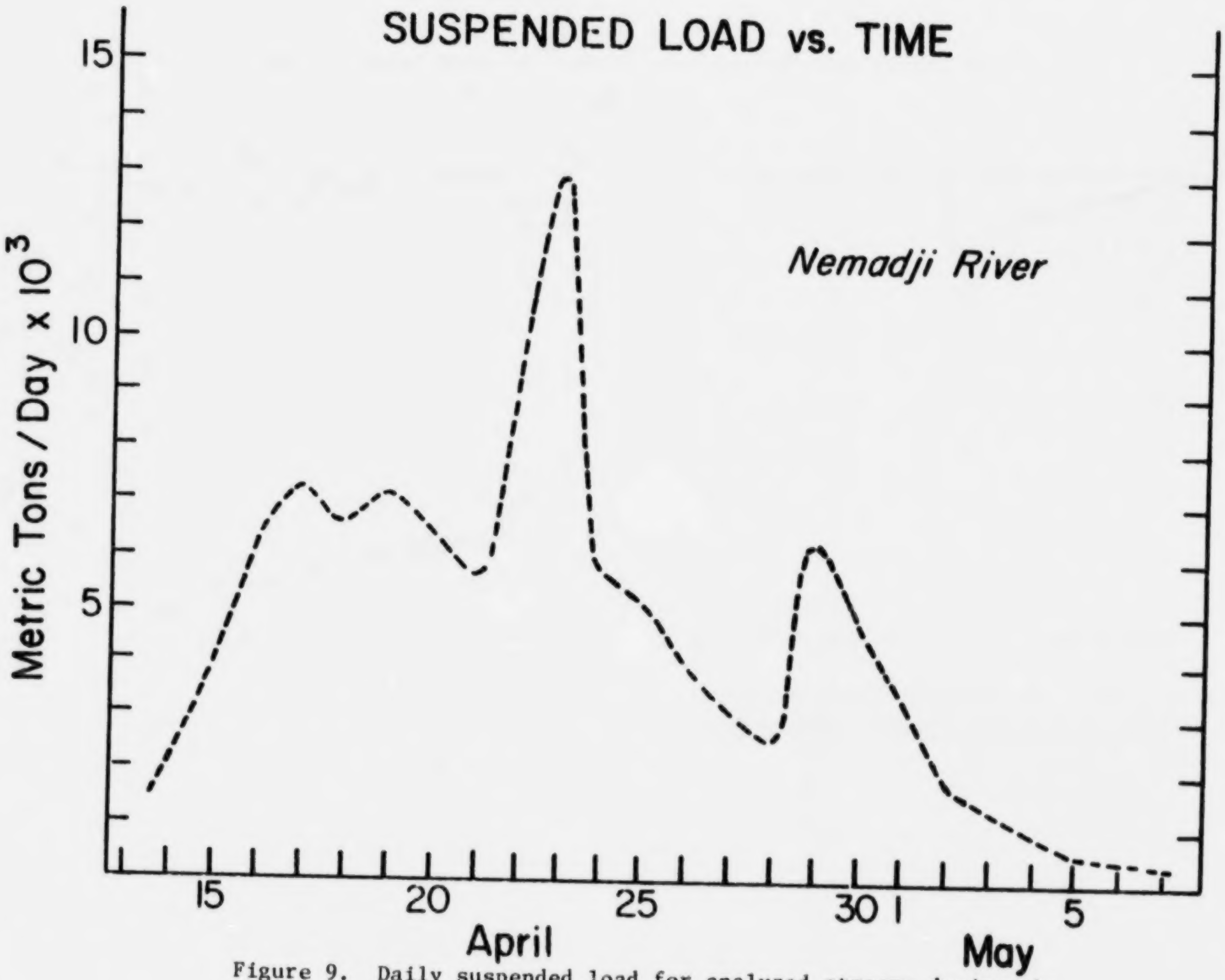

Figure 9. Daily suspended load for analyzed streams during the entire runoff period.

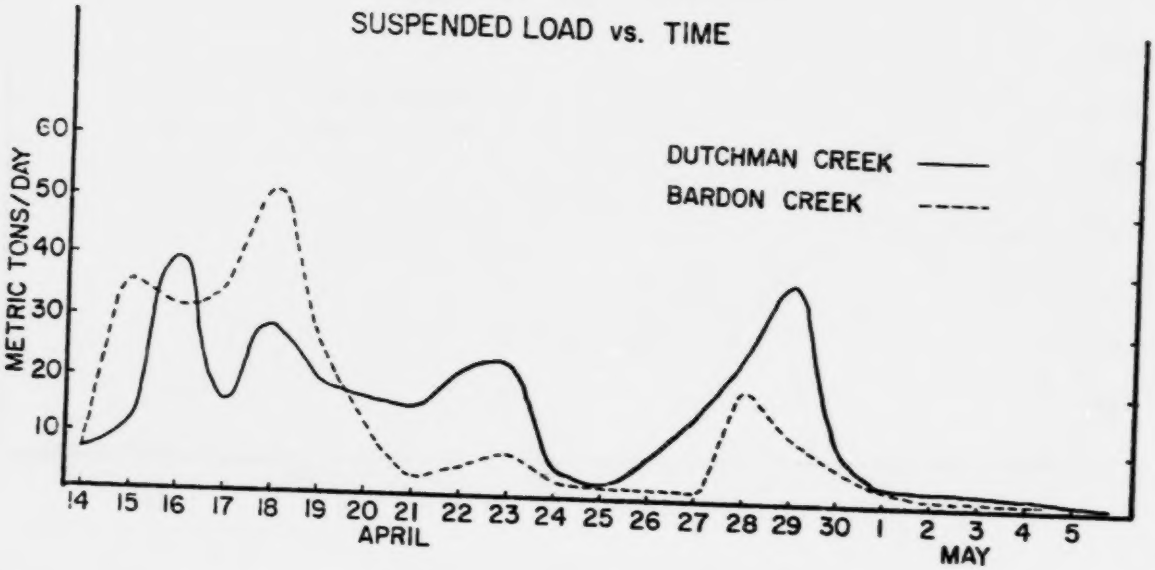

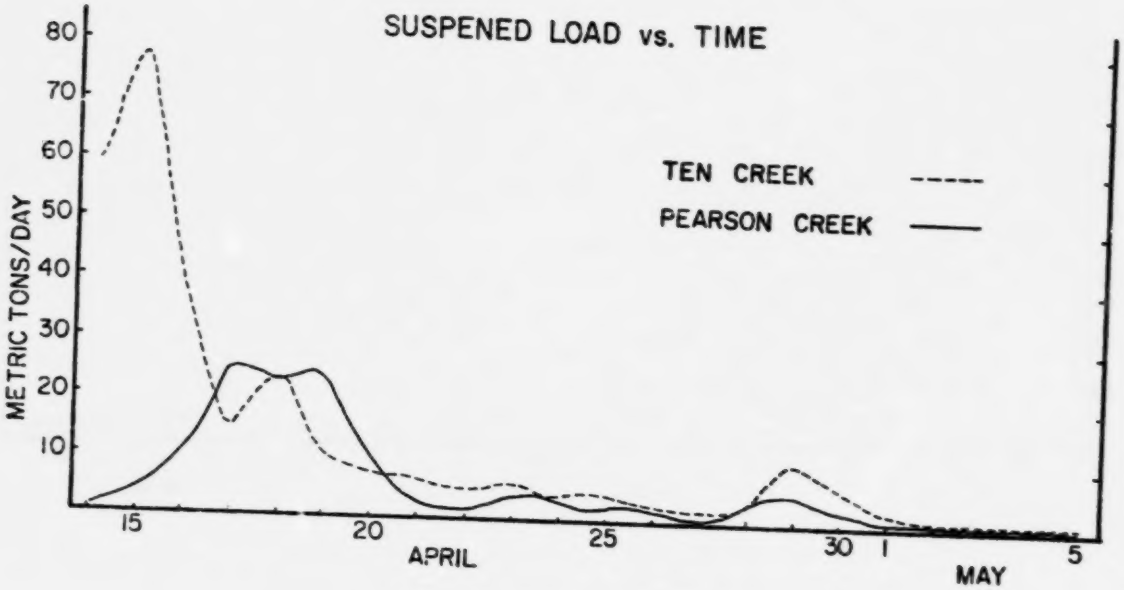

Figure 9. (continued)

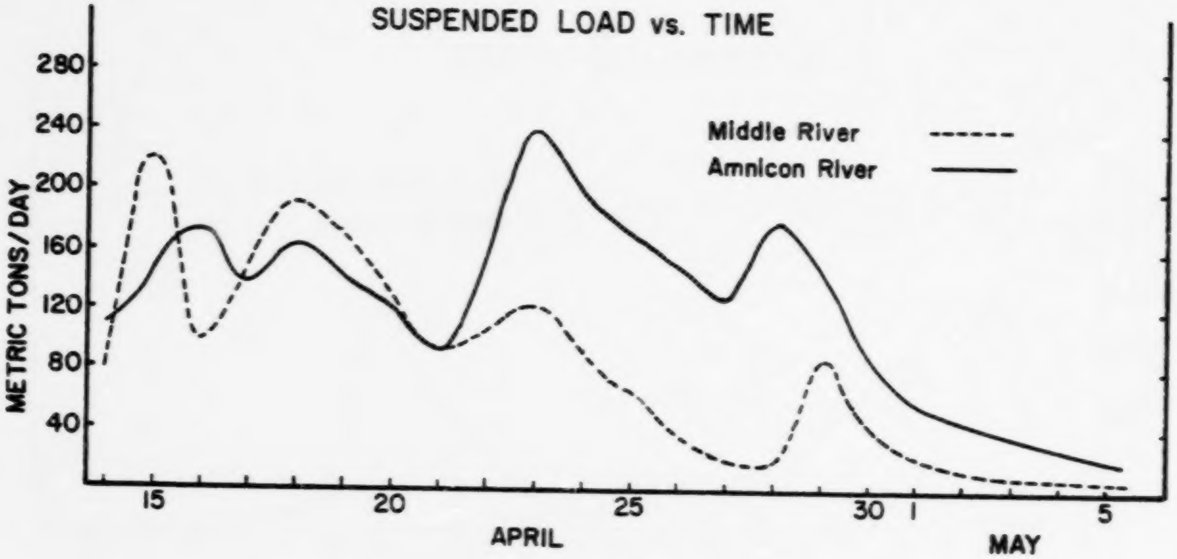

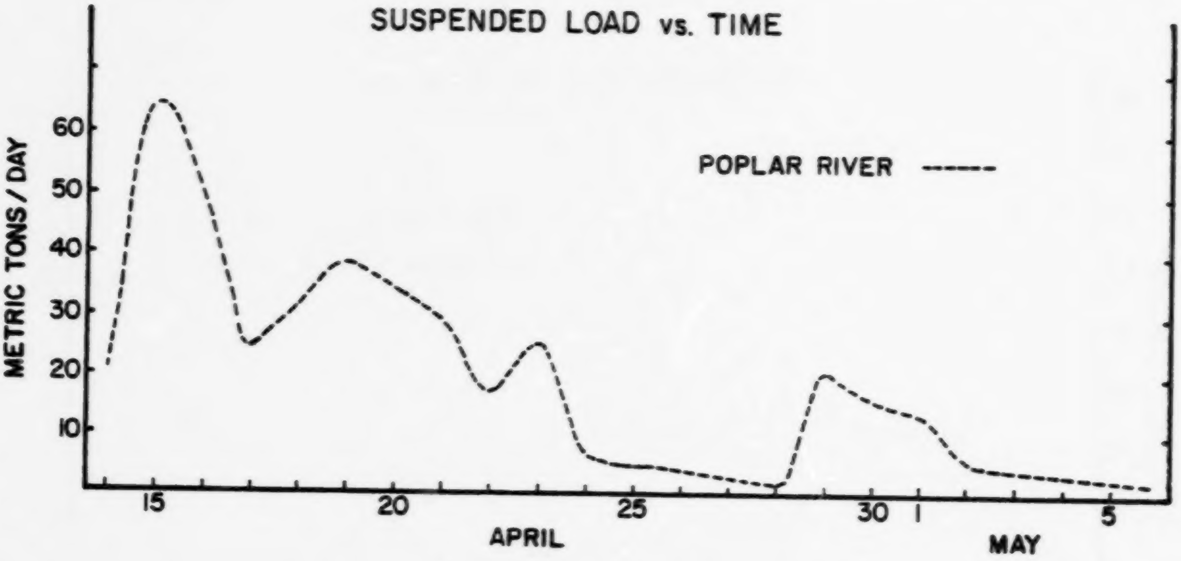

Figure 9. (continued)

Because of the uniform nature of the clay deposits responsible for much of the eroded load, it was hoped at the onset of this study that the suspended solids and turbidity data could be correlated in order to obtain a reasonably accurate estimate of suspended solids content of a sample by turbidity measurements alone. At low concentrations this is quite feasible and has been used extensively in lake turbidity analysis using remote sensing data, Figure 10. However, for high concentrations, the changes in suspended solids are gross for small turbidity changes. This precludes linear interpolation beyond turbidity levels higher than 100. This nonlinearity in turbidity measured for high concentrations is due to turbidity generally being a measurement of fines, rather than the large particles present in high concentration loads. An exponential curve for turbidity above 100 is also shown in Figure 10.

The total suspended load transported for all rivers and the individual stream loads for the runoff period appears in Table 1. A breakdown of the

TABLE 1

LOAD TRANSPORTED DURING APRIL 1975

River	Load (metric tons)
Nemadji	106,892
Dutchman	458
Morrison	341
Amnicon	3,157
Ten	431
Wagner	296
Hanson	148
Middle	2,008
Poplar	1,637
Bardon	544
Pearson	842
Unnamed #1 - #15	553
Total	117,307

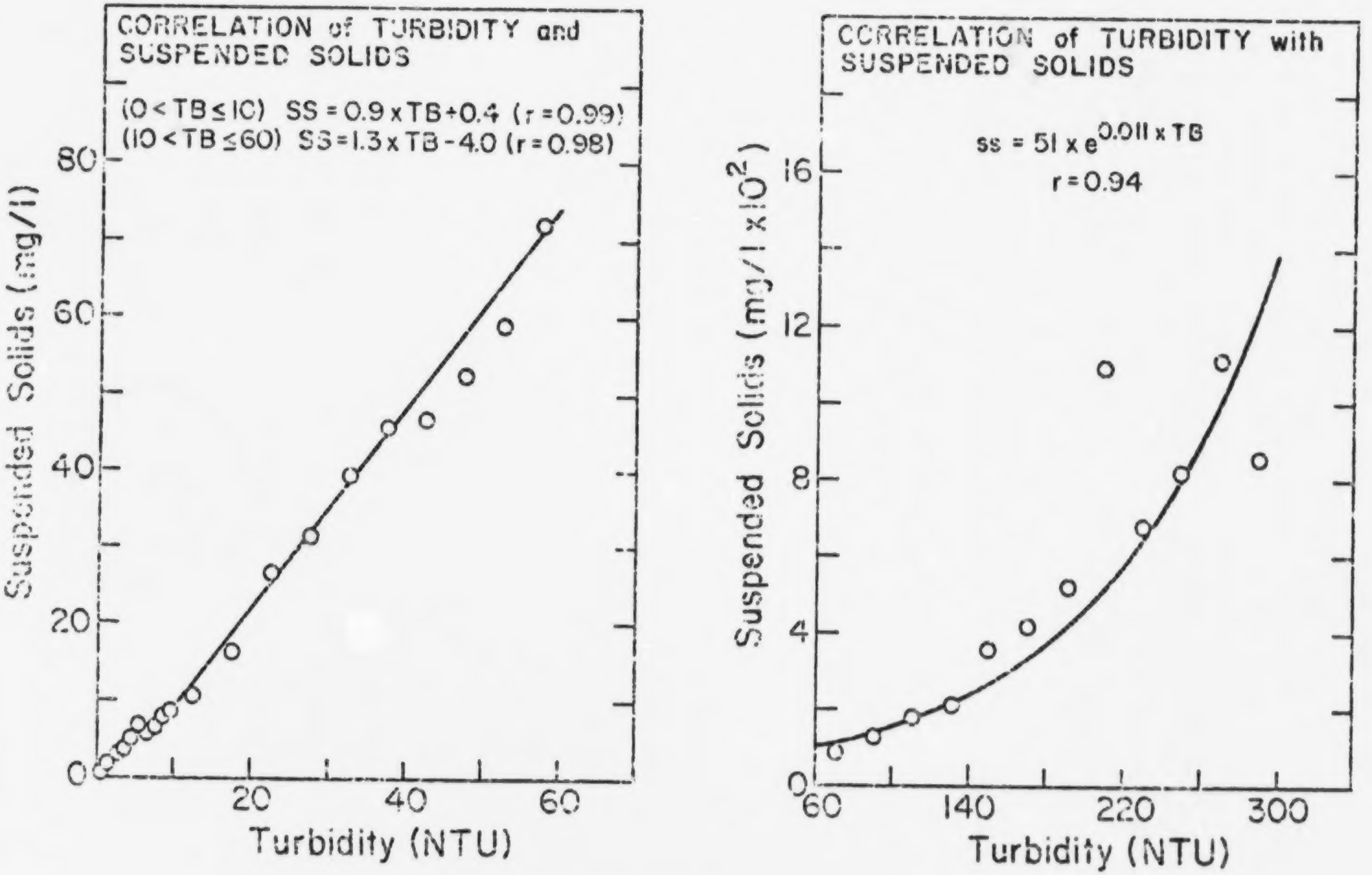

Figure 10. Turbidity and suspended solids correlation.

runoff load for each stream as a function of stream length and drainage area is shown in Appendix A. It is interesting to note that the total load transported during the snow runoff and the April rain event by the Nemadji is roughly ten times the load of all the other streams combined, yet the total discharge of the Nemadji is less than twice the total discharge of the other streams. This difference suggests that a nonlinear relationship exists between discharge and suspended load. Assuming an equivalence for the streams because of similar geologic and geographic boundaries, the total discharge vs. total load are shown in Figure 11. Although there are not enough large streams in the study area for conclusive results, the logarithmic plot of discharge vs. suspended load for the Nemadji, Amnicon, and Middle Rivers appearing in Figure 11 suggests that an exponential behavior exists between the load and the discharge.

Loads transported per km of stream length and per square km of basin area are shown in Table 2. The uniformity of eroded load per km in Table 2 suggests correlation between the suspended load and stream length, rather than the suspended load vs. basin area, particularly if the figure for the stream length comprises the main stream plus a fixed percentage of the intermittent stream tributaries. This suggests that the erosion is mainly due to immediate bank erosion rather than to surface runoff area. This further indicates that an excellent relationship between suspended load transported and stream length could be obtained by uniformly mapping each stream into main trunk, main branches, and tributary branches, and then deriving a total stream length figure based upon the sum of the entire main trunk plus a fixed percentage of the intermittent branches. The difficulty of this system lies in the fact that USGS maps are not consistent enough for uniform detailed mapping. The nature of each stream should be based on long-term observation. Continual, detailed aerial photography would be sufficient for this purpose.

RAIN RUNOFF

To monitor the runoff during the summer, five stations including rain gauges were set up: one on the Nemadji at the Golf Course Bridge, one each at Hwy 2 and Hwy 13 on the Amnicon River, and one each on the Poplar River at a county road 3 km south of Hwy 13 and a county road 4 km north of Hwy 13.

The necessity for measurement of rainfall rates and distribution becomes evident from examination of the runoff data obtained at the rivers in comparison to the rainfall recorded at Duluth during the same period. The Duluth precipitation measurements are completely inadequate for this purpose, although those are generally the only data readily available.

There are no significant rain runoff events from early July through October 20, 1975; on two occasions 1.25 cm (0.5 inch) rainfall was recorded at various stations, but the ground was so dry that the rainfall did not alter the suspended load appreciably.

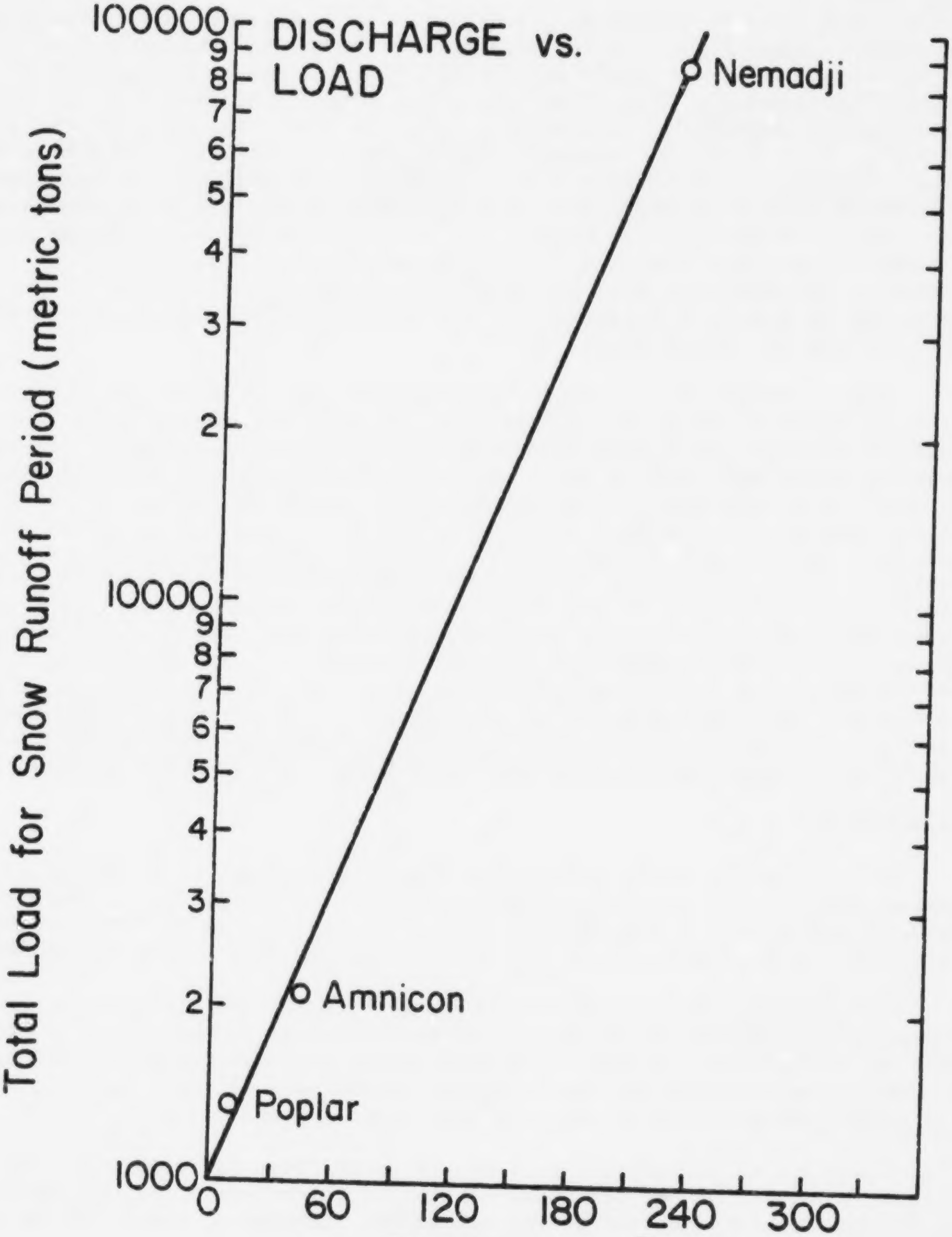

Figure 11. Total load vs. total discharge for the large streams.

TABLE 2

SNOW RUNOFF PER LINEAR KM OF STREAM LENGTH AND PER SQUARE KM OF BASIN AREA FOR THE PERIOD APRIL 10 - 27

RIVER	% INTERMITTENT STREAMS INCLUDED IN STREAM LENGTH	TOTAL RUNOFF LOAD PER LINEAR KM	TOTAL RUNOFF LOAD PER SQUARE KM AREA
		METRIC TONS	METRIC TONS
DUTCHMAN (south of Hwy 13)	50%	9.1	16.3
TEN (south of Hwy 13)	50%	10.1	19.3
POPLAR (south of Hwy 13)	50%	8.0	15.2
+ POPLAR (between stations)	100%	17.4	29.6
* BARDON (south of Hwy 13)	50%	7.0	9.4
* PEARSON (south of Hwy 13)	50%	12.7	18.8
* PEARSON (between stations)	50%	13.9	26.8

+ 100% intermittents included because the stretch between the station does not include the source area, which always includes a large number of intermittents.

* USGS map indicates entire stream to be intermittent, which is not correct in comparison with similar streams.

Thus the general monitoring of summer rain events was unsuccessful. However, a rainfall event in the spring at the end of April was well established for the entire area, as was a late June and early July rainfall event for the Nemadji, Figure 12, which is the most important runoff source. The ratio of suspended load in the Nemadji to the total load of the other Douglas County streams observed during the snow runoff was preserved for the rain runoff in the spring. This was largely because the soil conditions at that time were the same as those during the spring runoff. The summer vegetation may alter this ratio.

Based on the runoff characteristics of the Nemadji River, and assuming that the load ratio for the Nemadji and the Douglas County streams was the same as in the spring runoff, the output due to rain runoff for the past few years is estimated in Table 3 and total yearly runoff due to all streams is estimated in Table 4. Not included in the total in Table 4 is the contribution from Bluff and Bear Creeks, which flow into Allouez Bay, and contributions from streams such as the Pokegama River, which flows into the St. Louis River.

TABLE 3

SUMMER RAIN RUNOFF FOR NEMADJI RIVER (1970-1974)

(metric tons)

	1970	1971	1972	1973	1974
May	35,545	58,959	23,165	89,455	20,050
June	19,396	34,305	90,914	37,182	46,191
July	60,109	75,765	135,909	25,682	81,364
Aug.	4,991	71,991	196,636	147,664	64,727
Sept.	30,245	51,618	88,127	93,464	5,359
Oct.	128,237	87,173	8,895	74,223	5,982
Nov. 1-15	44,500	23,182	21,818	809	31,300
Total	323,023	402,993	565,464	468,479	254,973

An important question is how much of the Nemadji's load contributes to Lake Superior turbidity. This is not known and has not been included in the

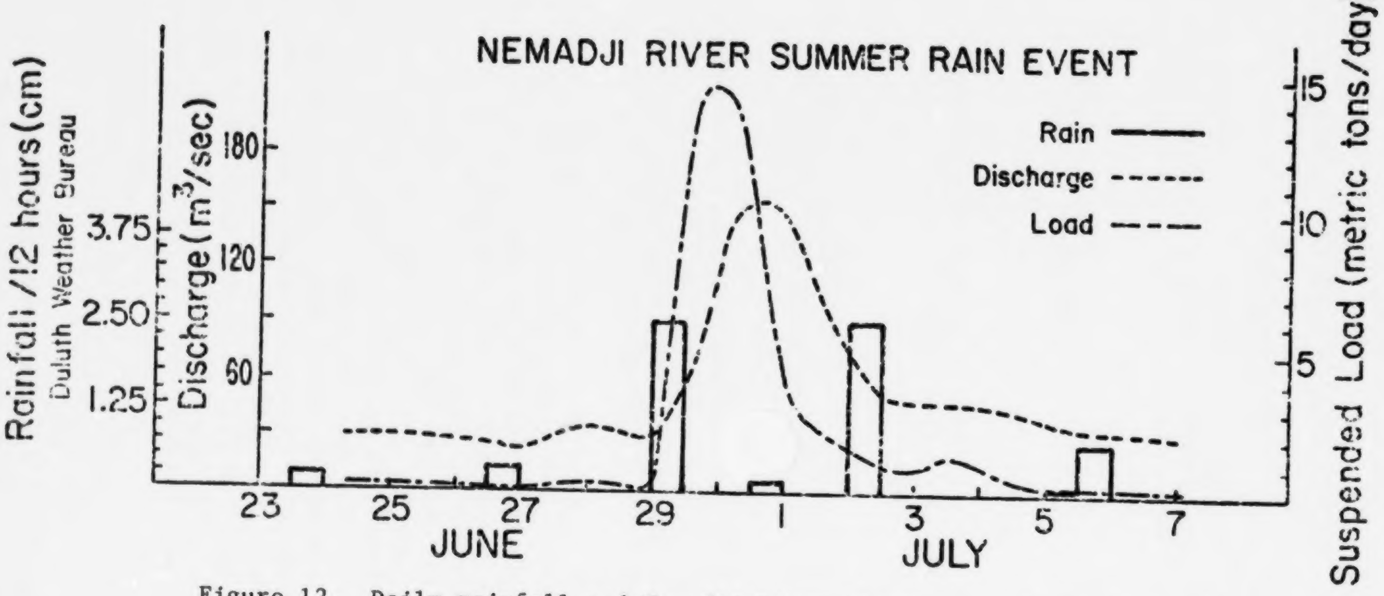

Figure 12. Daily rainfall and Nemadji River discharge and suspended-load data for a summer rain event.

TABLE 4

YEARLY INPUT OF SUSPENDED LOAD

(metric tons)

	Nemadji	Doug. Co.	Bay. Co.	Total
Average yearly rain runoff	402,986	40,298	23,210*	466,494
Spring runoff	106,892	10,415	6,000*	123,307
Total	509,878	50,713	29,210	589,801

* Based upon University of Wisconsin, Superior data for spring runoff for Bayfield County Streams (EPA R-005169-01).

measurements. Such measurements would have to account for the seiche actions affecting the transports in Duluth-Superior Harbor and would require continuous monitoring of the turbidity in the Nemadji and along the Superior entry. A rough estimate can, however, be obtained from two approaches.

Soil analysis of samples from red clay banks off rivers and the lakeshore by the University of Wisconsin, Superior (Bahnick et al., 1972) show roughly that 30% of the material is less than 4 μ in size. It is anticipated that at least 25% of the Nemadji's load would wash out into the lake. A comparison of the relative-size distribution of the particles in the lake and in the Nemadji, Table 5, indicates that roughly 60% of the load finds its way into the lake. This estimate of the fraction of load from the Nemadji entering the lake directly is in agreement with a rough order approximation obtained from the satellite data for June 14, 1975, which show 14,000 tons of material in the lake due to runoff while the output for that event in the Nemadji totaled about 27,000 tons. Accounting for the output of the Douglas County streams, this indicates roughly 50% output into the lake from the Nemadji River. Based on the assumption that 90% of the particles 3 μ and less flow out into the lake, the estimate obtained from the particle-size data indicates that nearly 40% of the coarser particles also flow out into the lake.

CONCLUSIONS

The 1975 spring runoff for the rivers is estimated to be 117,000 metric tons for Douglas County rivers and the Nemadji River, with the exclusion of Bluff and Bear Creeks flowing into Allouez Bay. The Nemadji is responsible

TABLE 5

PERCENT ABUNDANCE OF PARTICLE SIZES BY NUMBER

	Particle Size				
	0-2 μ	2-3 μ	3-4 μ	4-6 μ	6-20 μ
Nemadji	12	10	24	47	7
Lake Near Shore	21	15	24	35	7
Lake Intermediate	30	17	23	27	3
Lake Deepwater	30	16	23	29	2
Dutchman Creek	19	13	22	41	5

for 90% of the total runoff load in the spring. An estimated 75% of the contribution to lake turbidity due to runoff comes from the Nemadji River Basin. This contrasts with the total discharge of the Nemadji, which is approximately twice the runoff for the Douglas County streams. These numbers may be accounted for by the fact that the erosion rate appears to increase exponentially with the discharge rate.

The eroded load correlates better with river length as opposed to drainage area, indicating that immediate bank erosion is primarily responsible for the load rather than the area of the drainage basin. The erosion per km of stream length is roughly 10 tons for the spring runoff, and an estimated 0.7 tons/km per cm of precipitation runoff.

5. SOURCES AND TRANSPORTS OF TURBIDITY IN WESTERN LAKE SUPERIOR

ESTIMATION OF SEDIMENT RESUSPENSION AND TOTAL LOADING

A measure of shore erosion and sediment resuspension can be obtained from Landsat remote sensing and ground truth data. Reliable correlations between satellite imagery data and measurements of turbidity and suspended solids concentrations have made possible reasonable estimates of the total suspended load in the lake and its distribution on satellite-overpass days. This method of estimating lake loading has several advantages. Since only a representative number of stations must be sampled on satellite-overpass days, manpower and field-sampling requirements are limited. Furthermore, this method measures primarily the fine particulates which remain in suspension for prolonged periods and hence pose an environmental problem. This method also provides a better understanding of the transports of the loaded material and subsequent resuspension processes as a function of meteorological and lake conditions.

Analysis of Landsat Imagery

To be useful, remote sensing data must be correlated to ground truth data. Numerous samples were taken on Landsat-overpass days. Satellite imagery was analyzed in the vicinity of these sampling stations. A reliable correlation was established between surface turbidity and relative Band 5 intensity, Figure 13. Relative-band intensity is defined as the difference between the signal at a given site and the minimum signal observed in clean sections of the lake. Turbidity is in turn correlated with suspended-solids concentrations, Figure 10. Since suspended red clay particulates from shore erosion, sediment resuspension, and river runoff are fairly uniform and are similar in nature, the correlations shown in Figure 10 and Figure 13 are valid for the entire load of suspended red clay. These correlations make possible the delineation of various levels of suspended-solids concentrations directly from Landsat imagery, Figure 14.

In analysis of the Landsat data, 70 mm positive transparencies were viewed on an optical density slicer. Band 5 intensities were determined by comparison with the calibration step wedge provided on each transparency. The study area of the lake bordered by Douglas County, Wisconsin, and St. Louis, Minnesota, shores was subdivided into 77, three-kilometer-square grid spaces, Figure 15. For each satellite image several readings were taken in each grid square and averaged. The data was then processed on a computer. The grid allowed for a comparison of the turbidities at various points to the insitu measurements at those points. On a few days Landsat computer compatible tapes were available. The Landsat tape data is more accurate and allowed for a check of the optical data reduction methods. The tape data was used in effluent tracing, to distinguish red clay from other particles in low

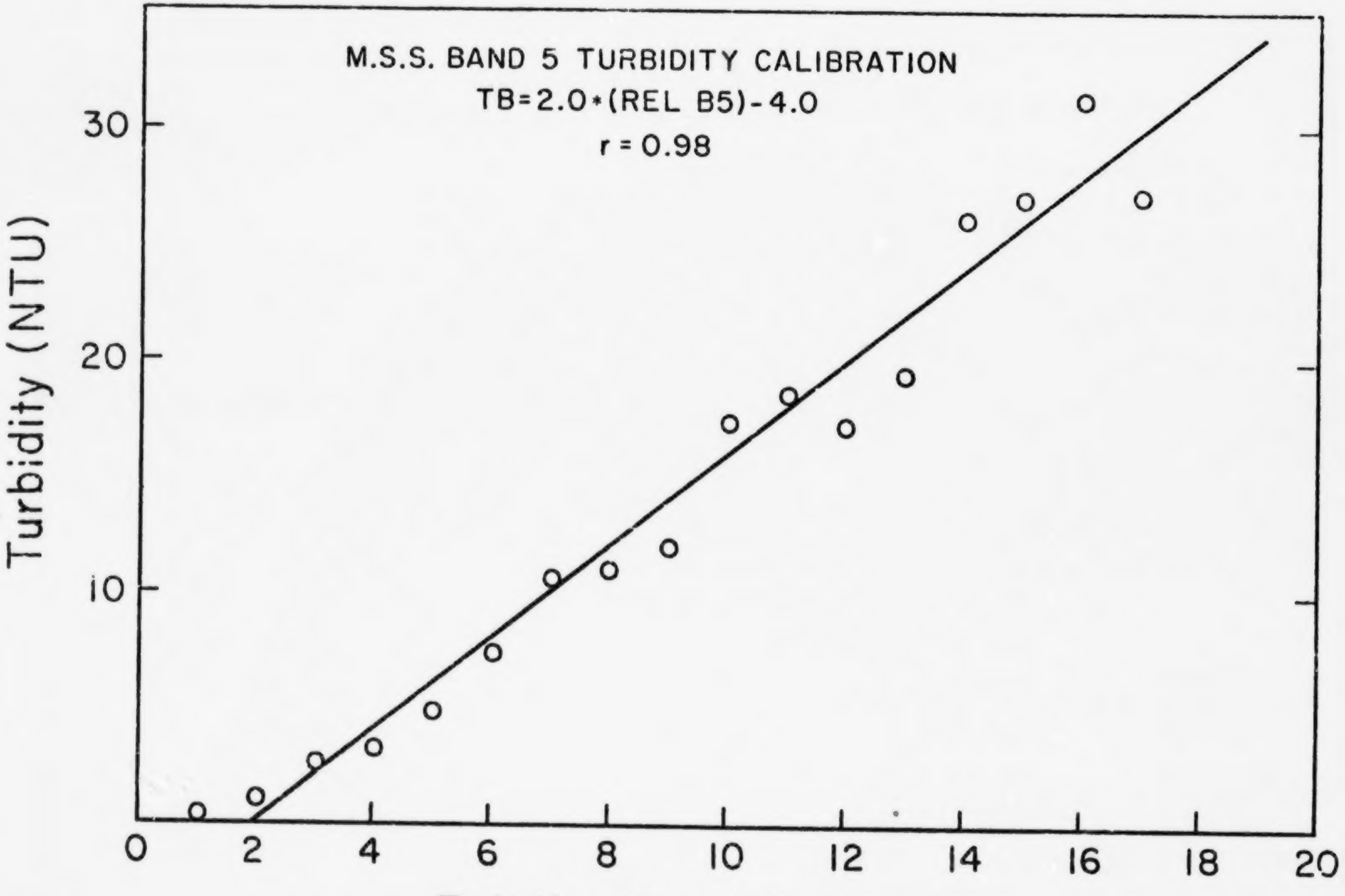

Figure 13. Turbidity calibration of Landsat image.

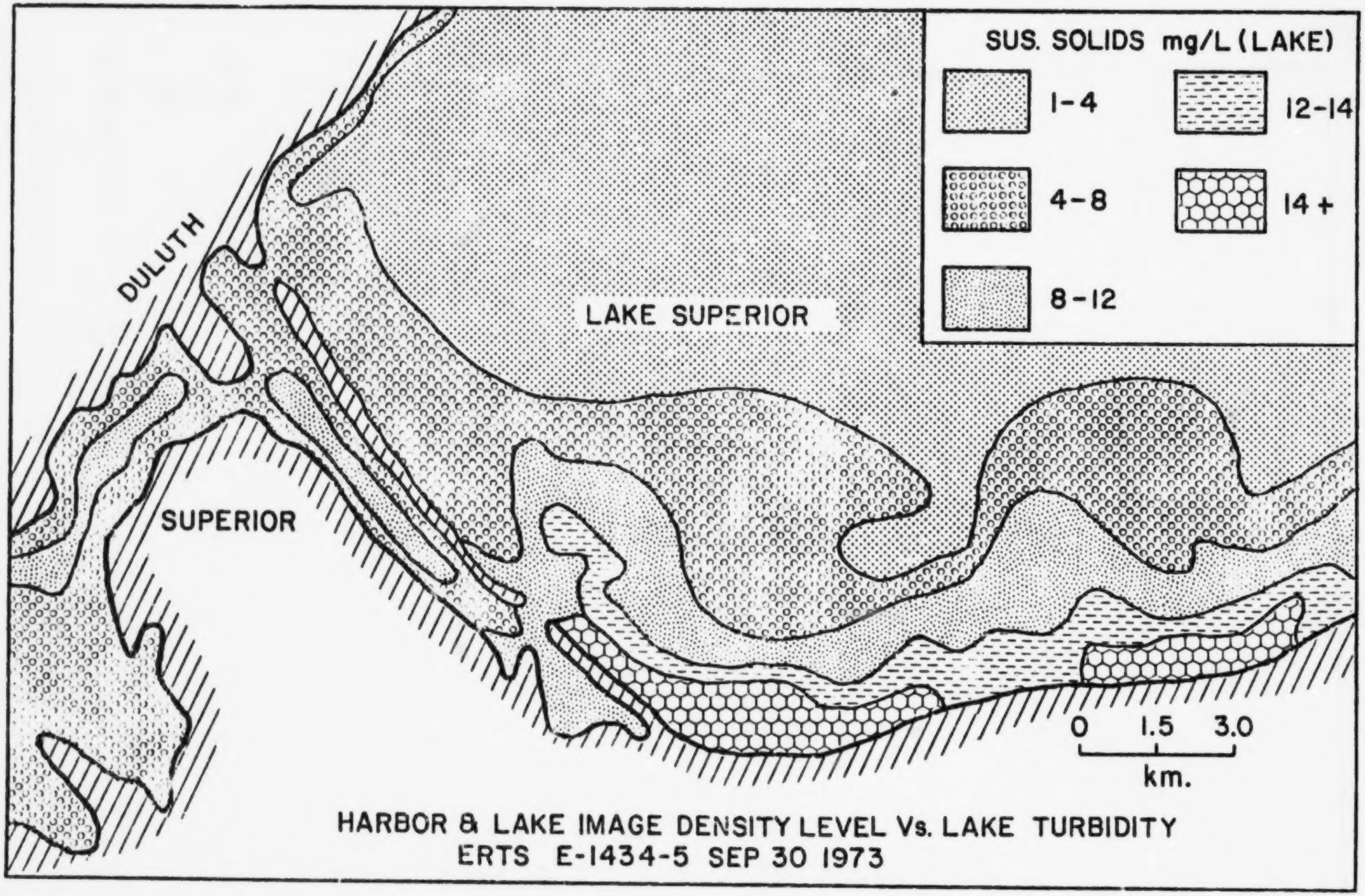
SUS. SOLIDS mg/L (LAKE)
1-4
4-8
8-12
12-14
14 +
LAKE SUPERIOR
DULUTH
SUPERIOR
0 1.5 3.0
km.
HARBOR & LAKE IMAGE DENSITY LEVEL Vs. LAKE TURBIDITY
ERTS E-1434-5 SEP 30 1973

Figure 14. Representative suspended-solids distribution produced from Landsat data.

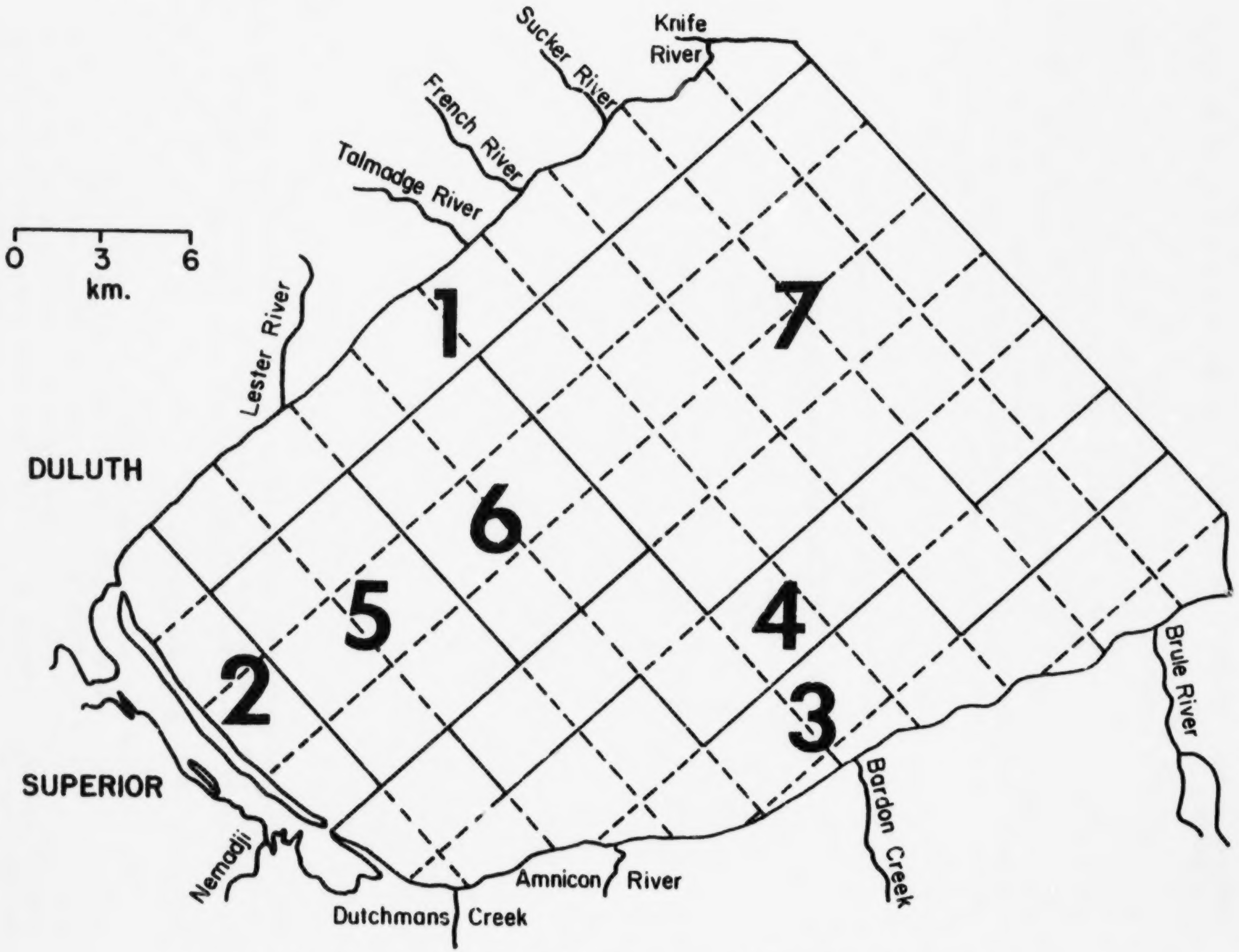
0
3
6
km.
DULUTH
SUPERIOR
Lester River
Talmadge River
French River
Sucker River
Knife River
Brule River
Bardon Creek
Amnicon River
Dutchmans Creek
Nemadji
1
2
3
4
5
6
7

Figure 15. Lake grid spaces and regions used in Landsat-image analysis.

density plumes. However, because tape data was expensive, it was not used exclusively.

Using the optical methods described above, the distribution of surface turbidity was determined on each image analyzed. To derive total suspended loads from surface turbidities, vertical profiles of suspended solids concentrations had to be estimated. The study area was divided into seven regions Figure 15. Measurement indicated turbidity profiles in these regions were uniform throughout each region and remained more or less constant throughout the year. Average ratios of surface suspended solids to average suspended solids in each of these regions are shown in Table 6. Using the values in this table, the surface turbidities derived from satellite data, and the calibration between turbidity and suspended solids, the total suspended loads shown in Table 7 and their distributions were derived.

TABLE 6

RATIO OF AVERAGE TURBIDITY TO SURFACE TURBIDITY

FOR WESTERN LAKE SUPERIOR

Region	Ratio
1	1.0
2	1.1
3	1.2
4	1.1
5	1.5
6	1.2
7	1.2

Estimation of Sediment Resuspension

To determine the relative contribution to lake turbidity due to erosion, sediment resuspension, and runoff, the data was examined in light of weather records of winds and precipitation. The observed plumes were categorized to distinguish between events which show predominant input from one source and events displaying a mixture of contributions from various turbidity sources. For instance, spring events yield a measure of the magnitude of the sediment

TABLE 7

TOTAL SUSPENDED LOAD IN WESTERN LAKE SUPERIOR

(metric tons)

12AUG72	88,000
06OCT72	58,000
29NOV72	50,000
16DEC72	32,000
28MAY73	115,000
03JUL73	61,000
12SEP73	28,000
30SEP73	46,000
18OCT73	32,000
19OCT73	29,000
06NOV73	36,000
23NOV73	34,000
22MAY74	59,000
27JUN74	77,000
28JUN74	53,000
15JUL74	94,000
25SEP74	38,000
26SEP74	36,000
18NOV74	27,000
15MAR75	31.000
03APR75	198,000
11APR75	412,000
12APR75	338,000
09MAY75	94,000
18MAY75	58,000
27MAY75	58,000
14JUN75	61,000
23JUN75	64,000
19JUL75	38,000
06AUG75	51,000
02SEP75	51,000
11SEP75	39,000
08OCT75	27,000
17OCT75	54,000
18OCT75	56,000
04NOV75	34,000
14NOV75	90,000
21FEB76	30,000
05APR76	78,000
06APR76	61,000
03MAY76	56,000
11MAY76	36,000
12MAY76	41,000
20MAY76	38,000

resuspension term. The fact that the turbidity during spring events is attributable to resuspension only is justified from the observation of the lakeshores and the simultaneous monitoring of river runoff. For example, examination of the photograph in Figure 16, which was taken on April 12, 1975, shows that even in the absence of the lake ice cover, a substantial ice ledge 1 - 3 meters thick at the shore and 30 - 60 meters wide protected the south shore from direct removal of the material from the clay bank. This ice shelf left resuspension as the only major source of red clay turbidity until the spring runoff began on April 13. Consecutive images on March 15 and 16, 1975, showed an increase of about 2 x 10^3 tons of suspended load in resuspension areas. Some of the turbidity in the March 16 image was attributable to erosion of the North Shore, which had no protective ice shelf, but the increase in the resuspension zones was probably caused by a 5 m/sec northeasterly wind on March 16. Images from April 3 and April 11, 1975, yielded observed suspended loads of 149 x 10^3 and 184 x 10^3 metric tons, respectively. Weather records show strong northeasterly winds in excess of 5 m/sec prevailed between these two satellite overpasses which resuspended on the order of 1.2 x 10^4 tons of material per storm-day. Such turbidity events occur on the average two to three times for the ice-free conditions on the lake and generally leave the early spring and late fall average turbidity much higher than the average turbidity during the months of June - November, Figure 17.

The total suspended load observed during the study period, including the resuspension term in the months when the shores were ice-covered, was 9.18 x 10^5 metric tons as compared to the load of 6.1 x 10^5 metric tons for the May - November season. Thus, at least 35% of the year-round lake turbidity was due to the sediment resuspension. Since sediment resuspension is generated by steady northeast winds in excess of 5 m/sec, it contributes up to 30% of the total turbidity for severe storms in the summer months as well. Based upon data from pure resuspension events, if winds in excess of 5 m/sec which prevail over 24 hours resuspend about 10^4 metric tons of fines per storm day, then the total contribution due to sediment resuspension for the entire year increases to about 45% of the total observed turbidity on the lake. Thus, sediment resuspension should play an important part in the consideration of the lake turbidity and its effects on the water quality and in considerations of leachate from the red clay (Bahnick, 1972).

A better estimate of the fraction of the observed load attributable to resuspension for the summer events was obtained by examination of the remote sensing data in light of weather records. Only the images for the May - November season on days when precipitation could be neglected were used. Resuspension was considered significant only after easterly winds exceeding 5 m/sec and lasting approximately 2 or more days. These criteria were met in about 35% of the events. Since the summer wind storms are usually mild and short in duration, the resulting plumes usually are not transported far from their sources. Thus, the suspended load in a series of source points which extended from Amnicon River to Bardon Creek was considered a good measure of erosion. These source points were in the middle of the south shore erosion belt along a uniform red clay bank far away from known resuspension areas. Since the near-shore zone accumulates only a thin veneer of red clay, which is quickly removed by succeeding storms, the turbidity in

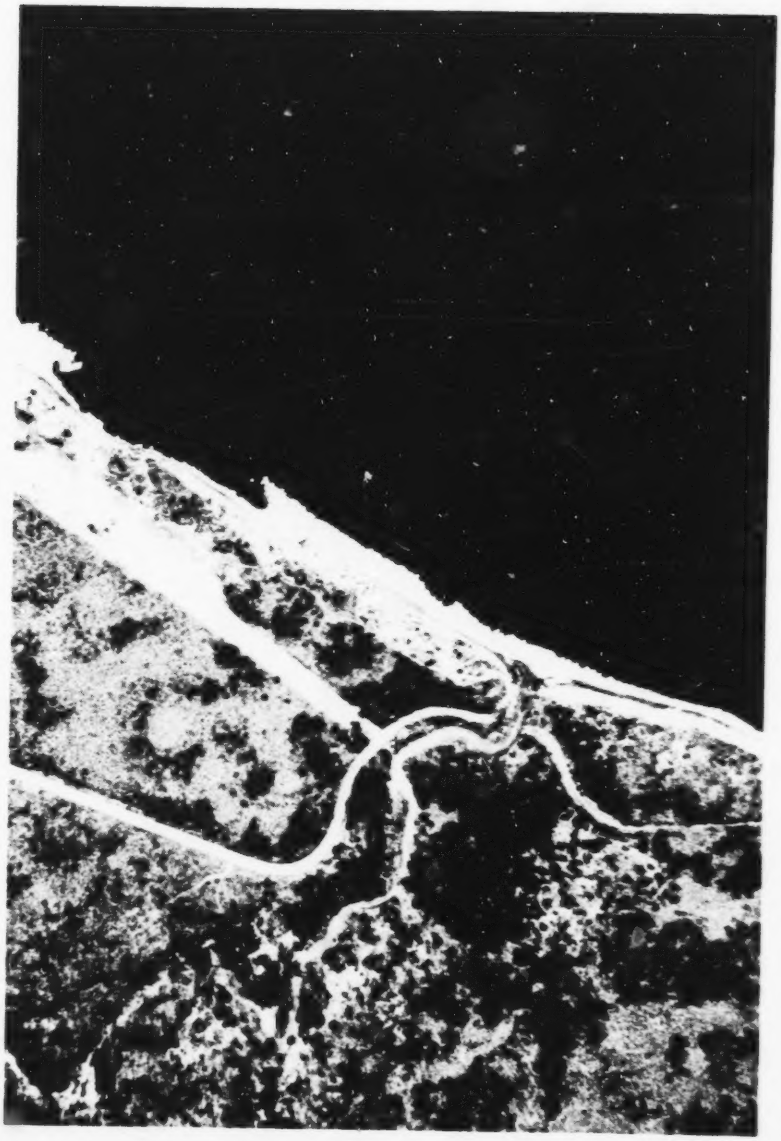

Figure 16. Spring ice shelf near Amnicon River (1 - 3 meters thick).

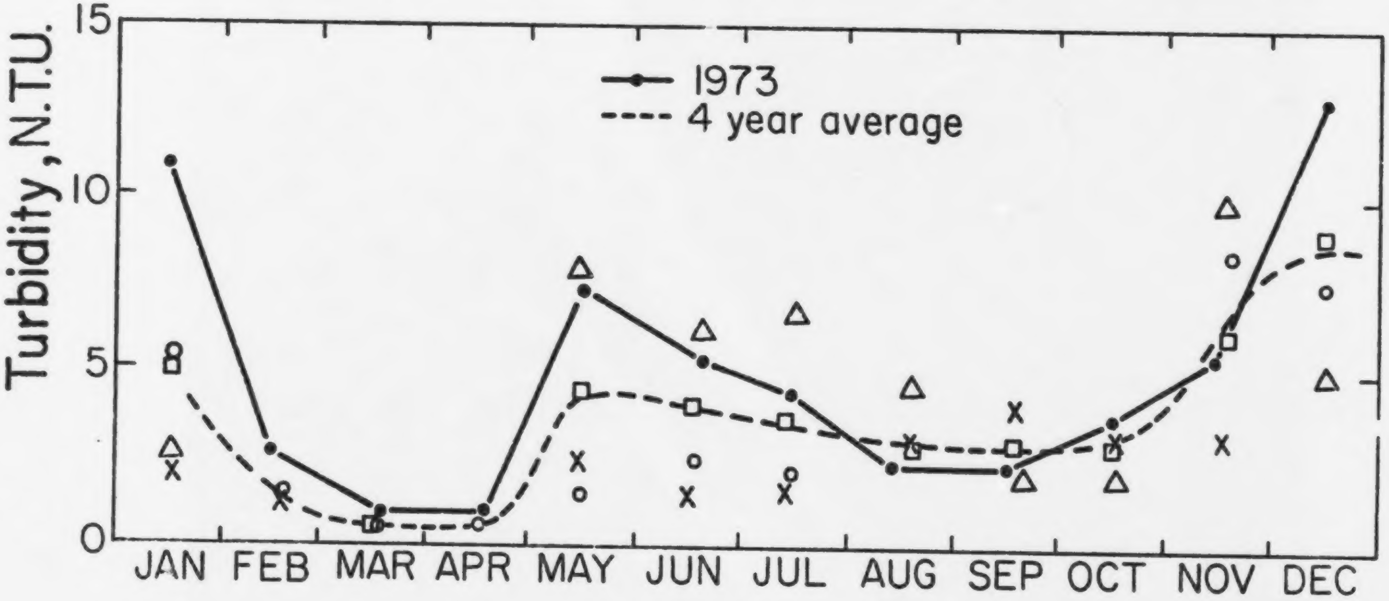

Figure 17. Average lake turbidity near Duluth.

these source points was attributable almost entirely to erosion.

The fraction of the total turbidity due to resuspension was obtained by comparing the total suspended load above background for resuspension and pure erosion events. Assuming no other sources of turbidity were present, the total load (T) was found by summing the contributions of erosion (E) and resuspension (R). Letting the subscripts "r" and "e" denote resuspension and pure erosion events the equations become:

$$T_r = E_r + R_r \qquad T_e = E_e \tag{1}$$

The contribution of erosion was assumed proportional to the suspended load (S) in the erosion source points. Letting α denote the constant of proportionality, equation (1) becomes:

$$T_r = \alpha S_r + R_r \qquad T_e = \alpha S_e \tag{2}$$

Summing overall observed events and eliminating α, the fraction (f) of observed turbidity attributable to resuspension was found:

$$F = \frac{\Sigma R_r}{\sum_r T_r + \sum_r T_e} = \frac{(\sum_r T_r - \sum_e T_e \cdot \sum_r S_r)}{\sum_r T_r + \sum_e T_e} \tag{3}$$

Calculations using equation (3) indicated about 16% or about 10^5 tons of the observed turbidity for the May - November seasons was due to resuspension. This value is close to the one obtained from the resuspension rate per storm day derived from observations of pure resuspension events.

Estimation of Shore Erosion

The actual eroded load throughout the year in its relation to the observed suspended load depends on the total number of storms, the dispersion-settling factor, and the cloudiness. These factors must be taken into consideration in the determination of total shore erosion. The erosion process takes place throughout the time when the shores are ice-free. Generally, as will be pointed out in the numerical model, northeasterly winds raise the lake level and produce waves which directly abrade the red clay bank toe. Many times, large chunks of clay fall into the water, where they are rolled around in the sand slurry and produce large round balls of red clay which dissipate rapidly and give rise to high turbidity in the near-shore area. Many areas of the beach have a veneer of sand covering the red clay which is subject to erosion by the wave action. The erosion takes place in a season roughly 210 days long.

To determine the total eroded load from the data in Table 7, the statistical nature of the problem was considered. If the events occurred randomly, then the observed turbidity should be directly related to the total turbidity input through the dispersion and settling rate and the probability that an event was observed. This is true provided the overlap of the events was reasonably small and the time for the decay of the event to the background turbidity values was short compared to the period between observations. Both of these conditions are satisfied when images for successive days are considered as a single observation. If "t" is the time after a storm, f(t) the dissipation function, p(t) the probability density that a storm was observed at time t given that the storm was observed, and S_o the total initial suspended load, then the total observed load (T) is given by equation (4):

$$T = S_o \int_o^{t_o} f(t) \cdot p(t)\, dt = S_o \overline{f(t)} \qquad (4)$$

Using equation (4), the average suspended load of observed storms can be calculated. Assuming all storms regardless of magnitude are equally likely to be observed by satellite, the total load of all storms can then be obtained by multiplying average load by the total number of storms.

Measurements of turbidity dissipation for easterly and westerly wind storms, Figure 18, indicate that turbidity for a typical storm remains above background for approximately 8 days. The turbidity dissipation for a large storm in early November 1974 is shown in Figure 19. Assuming the dissipation rates for other storms were similar, one obtains the typical dissipation curve shown in Figure 20 using the relationship between turbidity and suspended solids, Figure 10.

The two functions, f(t) and p(t), are not independent. The storm build-up times for high easterly wind storms have a low probability of being observed since they are almost always accompanied by cloudiness. This consideration is important because the settling rate for the first day is very high. Cloudiness is not the only obstacle in the successful observation of turbidity. At the peak of the storm, concentrations of suspended solids often exceeded 100 mg/ℓ, the point at which the Landsat optical signal saturates. Because of the nature of the sources and currents, very high concentrations of suspended solids are often confined at the beginning of a storm to a small area near shore which is susceptible to blockage by partial cloud cover and the limits of spatial resolution of the satellite. Since the tail of the storm is highly observable, the total observed load is a small fraction of the initial or total load.

The function p(t) was approximated using weather records and the above considerations, Figure 20. For most of the time during the storm decay, p(t) assumed nearly a constant value. Numerical calculations give the average observed storm intensity p(t) a value .11. Since most of the turbidity observed was "fines," on the order of 11% of the total load was

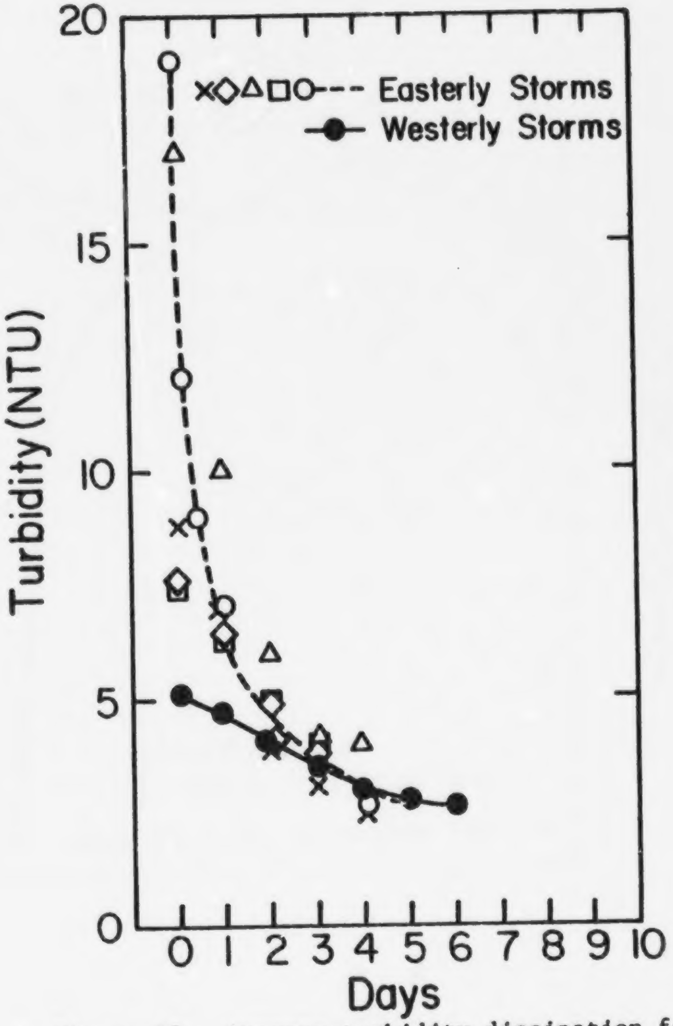

Figure 18. Average turbidity dissipation for easterly and westerly wind storms.

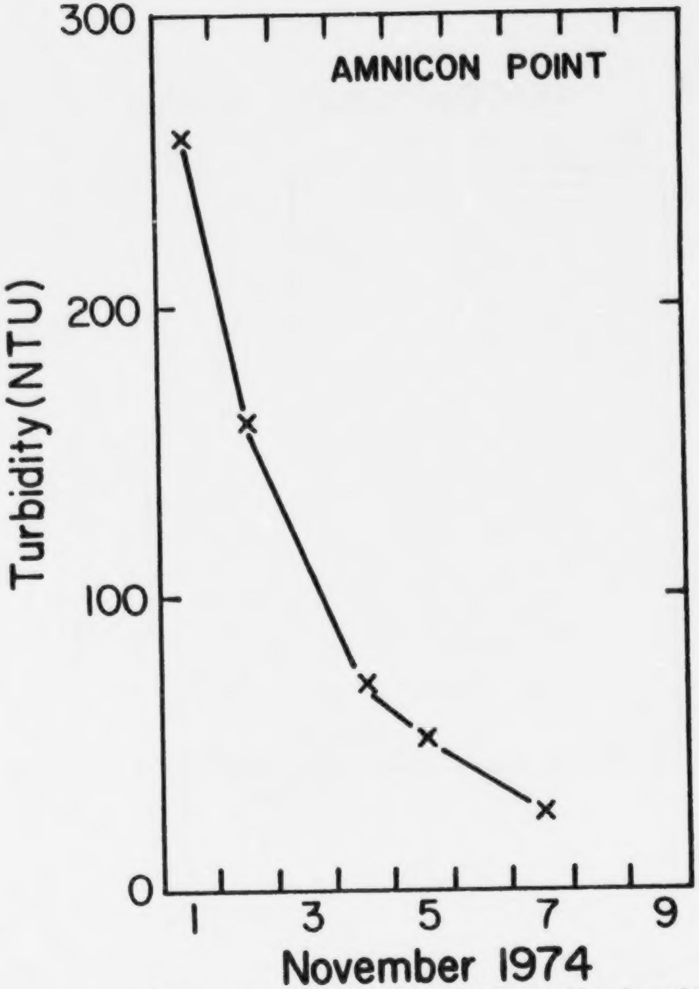

Figure 19. Actual turbidity dissipation for a large easterly storm.

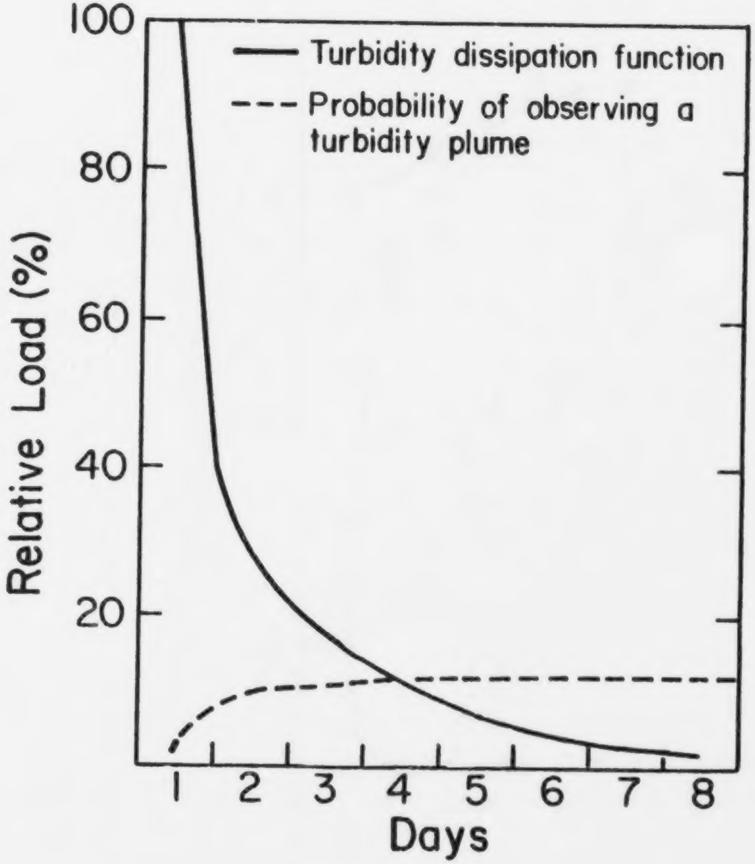

Figure 20. Average storm characteristics.

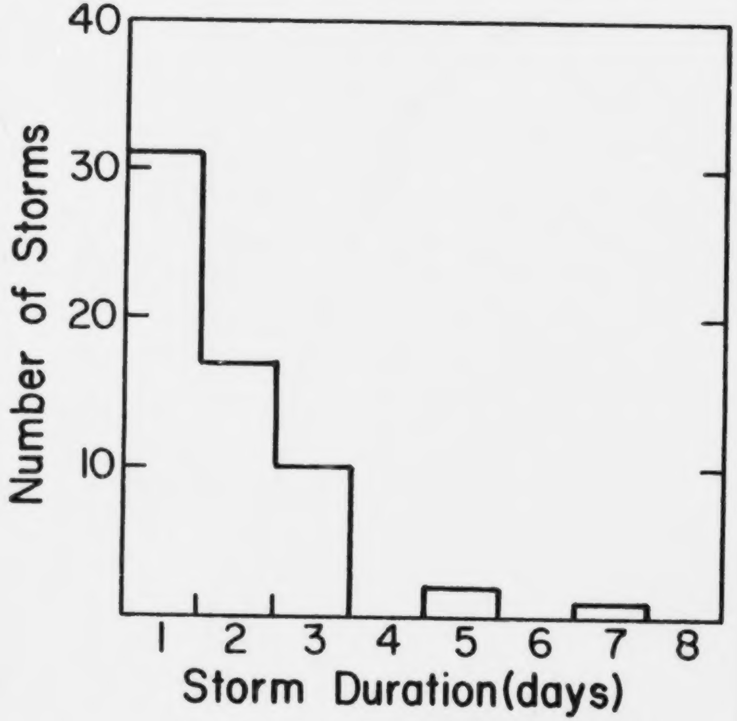

Figure 21. Distribution of storm duration.

attributable to the fines. Particle-size data for lake samples and river samples indicated that fines consist primarily of particles less than 4 μ. (See Section 4.)

Wind data for western Lake Superior was analyzed for days showing steady easterly and northeasterly winds in excess of 5 m/sec. Records of storms in the past few years and insitu measurements have shown easterly wind storms give rise to high turbidity in western Lake Superior. The distribution of storms for the ice-free season from August 1972 - August 1975 is shown in Figure 21. The category of storm depended on the duration and sequence of wind; thus single-day events, double-day events, etc., were derived from successive days of dominant high winds. The total number of events was 63. Subtracting estimated contributions of resuspension and runoff, the total observed load attributable to erosion is 4.37×10^5 metric tons. Since 20 images showed turbidity above background, the average observed eroded load was 2.19×10^4 metric tons. The total initial eroded load (S_o) for an average storm can be obtained by dividing by $\overline{f(t)}$. This gives S_o a value of 2.0×10^5. Assuming all storms were equally likely to be observed, the total eroded load over the three-year year period, 1.26×10^7 metric tons, was found by multiplying by the number of storms. Thus, about 4.0×10^6 metric tons of eroded material is loaded into the lake per year.

Table 8 summarizes the estimated magnitudes of the various sources of red

TABLE 8

SOURCES OF LAKE TURBIDITY

	Average Rate/Season (May - November) Metric Tons	% Contribution (Rounded off)
Lakeshore erosion for Douglas County, Wisconsin	4.0×10^6	75%
Sediment resuspension (May - November) in extreme western Lake Superior	1.0×10^6	20%
River runoff contribution to lake turbidity	$.32 \times 10^6$	5%
Sediment resuspension for winter conditions (Dec., Jan., Apr.)	2×10^6	

clay turbidity in western Lake Superior. As was established by insitu measurements, the runoff comes principally from the Nemadji. Since runoff sources were relatively small in magnitude and infrequent, insitu measurements provided a good estimate of their magnitude. Shore erosion and resuspension contribute much greater loads. In addition, their contribution is continual and geographically more extensive. Landsat remote-sensing data were ideally suited for estimating the contribution of these sources.

TURBIDITY TRANSPORT AND THE DISTRIBUTION OF TURBIDITY SOURCES

Statistical analysis of turbidity distributions for various wind conditions yields information on turbidity transports and the nature of the turbidity sources. Images were examined in light of weather records and classified according to the kind of storm that gave rise to the observed turbidity. The relative turbidity taken directly from the density slices indicated that for an easterly wind storm, turbidity from red clay banks along the Wisconsin shore is transported toward Wisconsin Point, where it is subsequently taken out in a return path along the axis of the lake, Figure 22. This transport pattern was also established by a numerical model of currents in Lake Superior. (See Section 6.) Similarly the transports for westerly winds, derived from statistical analysis of the plume shapes, yields transport paths shown in Figure 23 and 24. Variable winds tend to produce circulation eddies, and periodically trap the degraded water from the St. Louis River in the areas near Duluth, Figure 25. The range of transport of red clay particles can be assessed from the analysis of the Landsat image for April 11, 1975, where a resuspension plume traveled in high concentrations for about 135 km between Grand Marais and the Apostle Islands, where it had a concentration of 2 mg/ℓ.

The distribution of turbidity sources can also be obtained from Landsat data. The average turbidity for the ice-free season is shown in Figure 26. Using this figure one obtains the map of relative erosion rate shown in Figure 27. Thus the 4.0 x 10^6 metric tons of material eroded along the lakeshore is distributed fairly uniformly along the shoreline, with maximum rate just west of the Amnicon River and near Middle River to roughly half the rate west of the Brule River. For high northeasterly winds, sediment resuspension takes place. Examination of the relative distribution of turbidity for such storms, Figure 22, in comparison to turbidity distribution for other events, Figures 23 - 26, indicates that the resuspension area exists north of Dutchman Creek, which enters the lake at the southern most part of the lakeshore in Douglas County, Figure 28. Intermediate depth areas along the Douglas County shore are also subject to sediment resuspension after periodic accumulation of material in those places during the quiescent times. The determination of the resuspension areas are, however, quite difficult since for high northeasterly winds, considerable erosion takes place, the transports are rapid, and the probability of observing a storm at the peak moment is low because of the accompanying cloud cover. A good verification of the suspected resuspension areas can be obtained from the early spring events which occur before runoff and during the time when there is a protective ice shelf along the shore to inhibit direct lakeshore erosion. These indicate that the south shore and Dutchman Creek areas and the waters off Minnesota Point are the major resuspension areas, in agreement with Figure 28. The area off Minnesota Point

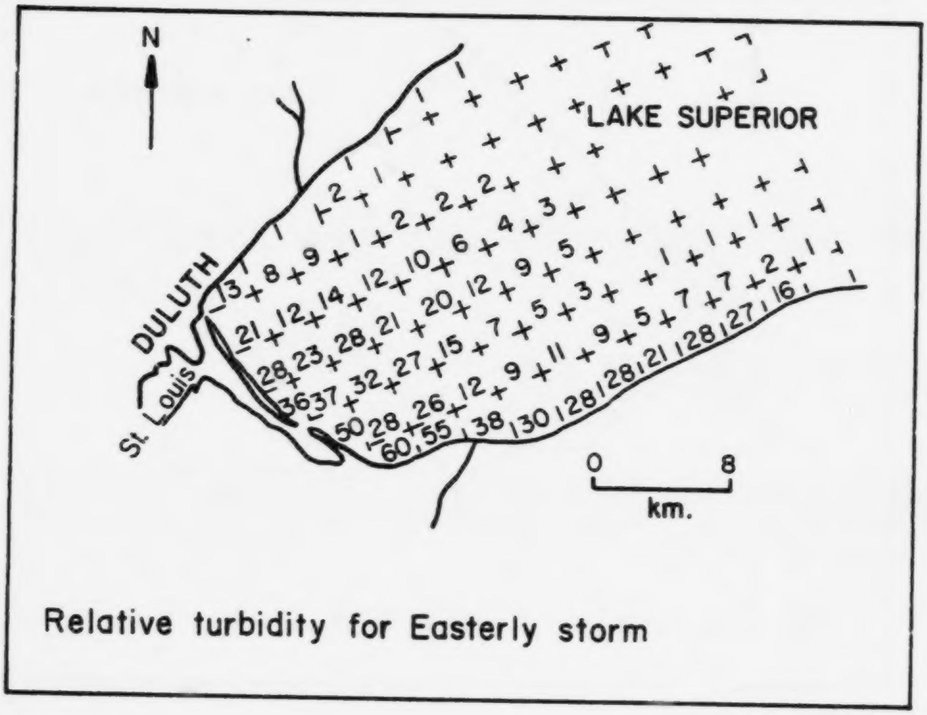
N
LAKE SUPERIOR
DULUTH
St. Louis
13 8 9 1 2 2
21 12 14 12 10 6 4 3
28 23 28 21 20 12 9 5
36 37 32 27 15 7 5 3 1 1 1
50 28 26 12 9 11 9 5 7 7 2 1
60 55 38 30 28 28 21 28 27 16 1
0
8
km.

Relative turbidity for Easterly storm

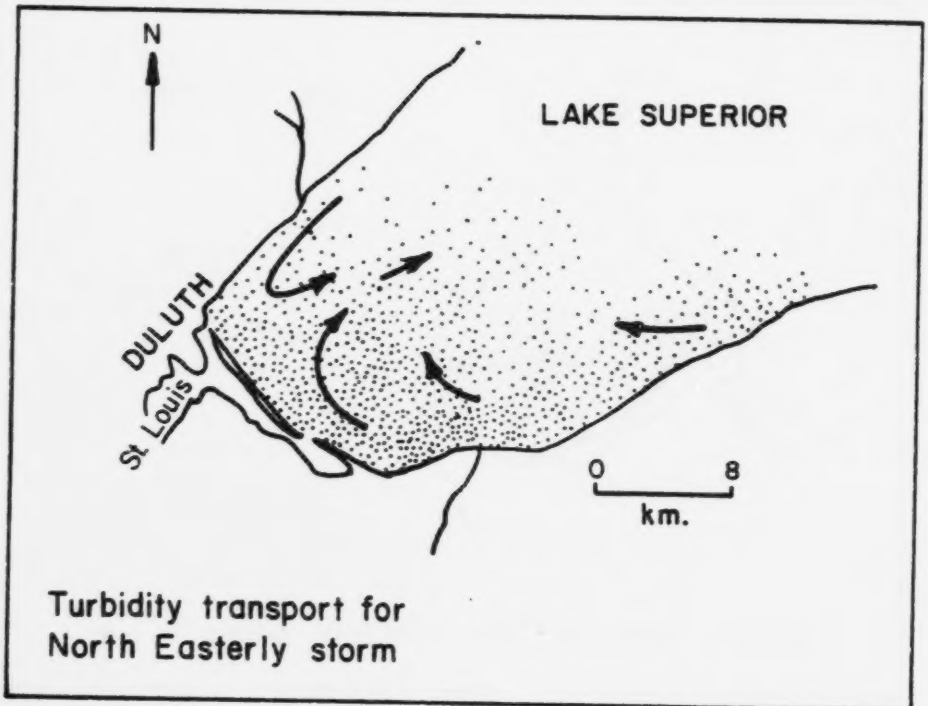
N
LAKE SUPERIOR
DULUTH
St. Louis
0
8
km.

Turbidity transport for North Easterly storm

Figure 22. Average turbidity distribution and transport for an easterly storm.

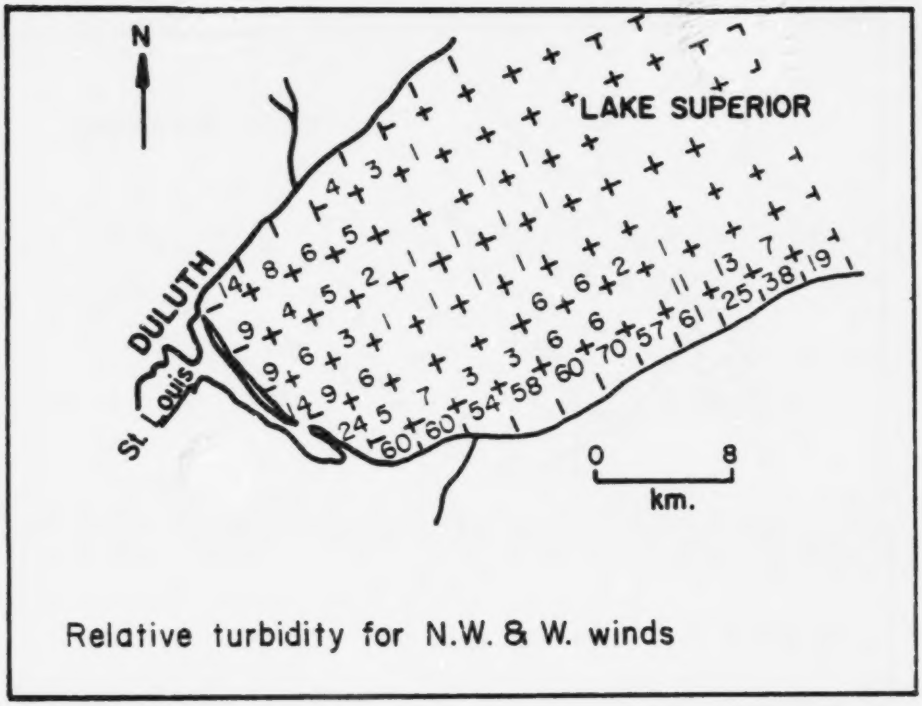
N
LAKE SUPERIOR
DULUTH
St Louis
4 3
14 8 6 5
9 4 5 2 1 1 1 6 6 2 1 13 7 19
9 6 3 1 1 6 6 11 61 25 38
14 9 6 3 3 6 70 57
24 5 7 54 58 60
60 60
0 8
km.

Relative turbidity for N.W. & W. winds

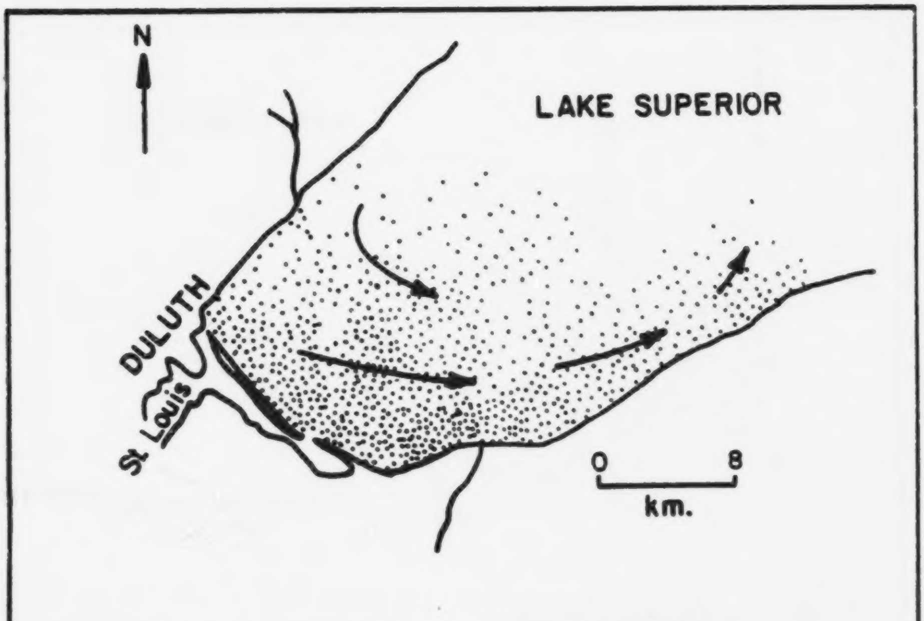
N
LAKE SUPERIOR
DULUTH
St Louis
0 8
km.

Turbidity transport for N.W. & W. winds

Figure 23. Average turbidity distribution and transport for a westerly storm.

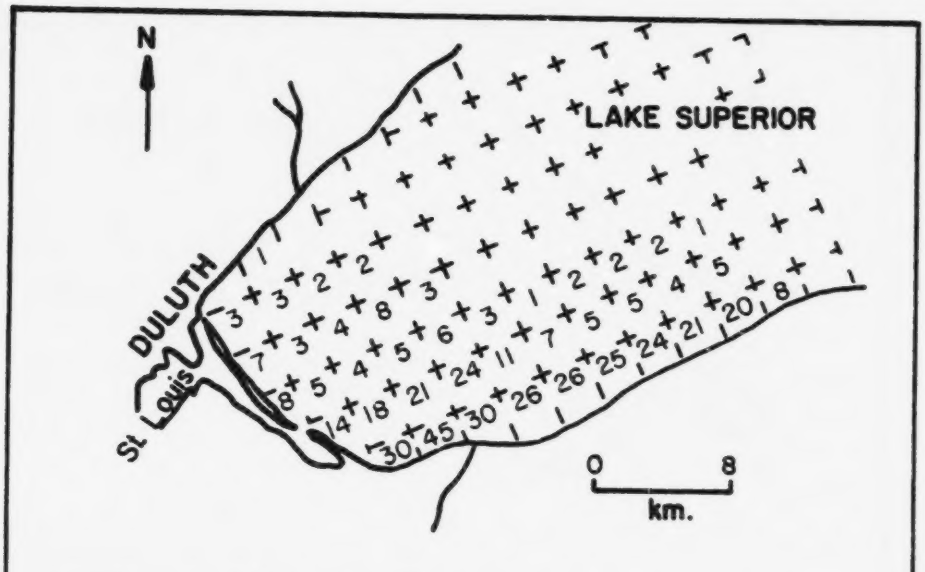
N
LAKE SUPERIOR
DULUTH
St. Louis
3 3 2 2
7 3 4 8 3
8 5 4 5 6 3 1 2 2 1
14 18 21 24 11 7 5 5 4 5
30 45 30 26 26 25 24 21 20 8
0
8
km.

Relative turbidity for Easterly storm followed by westerly dispersion

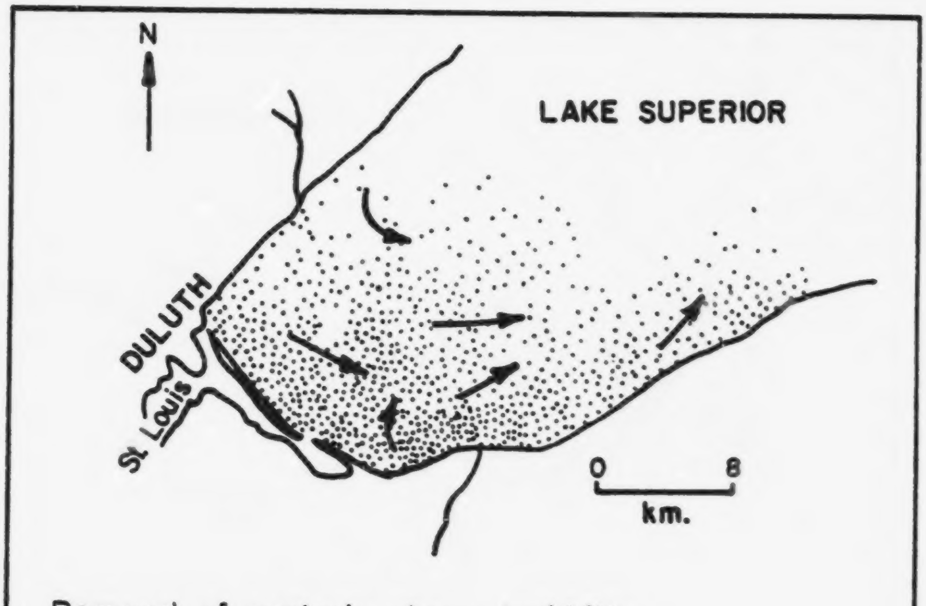
N
LAKE SUPERIOR
DULUTH
St. Louis
0
8
km.

Removal of easterly storm turbidity by N.W. & W. winds

Figure 24. Average turbidity distribution and transport by westerly winds.

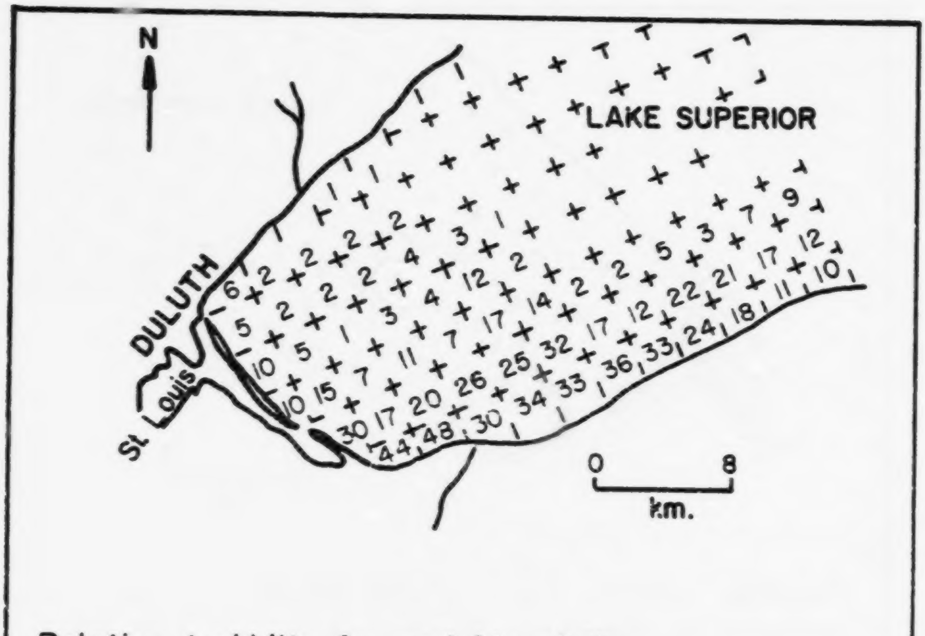
N
LAKE SUPERIOR
DULUTH
St Louis
9
7
3 1
2 2 2 2
6 2 2 2 4 3 5 3 17 12
5 2 2 4 12 2 2 21 10
10 5 1 3 17 14 12 22 11
10 15 7 11 7 25 32 17 24 18
30 17 20 26 34 33 36 33
44 48 30
0
8
km.

Relative turbidity for variable winds

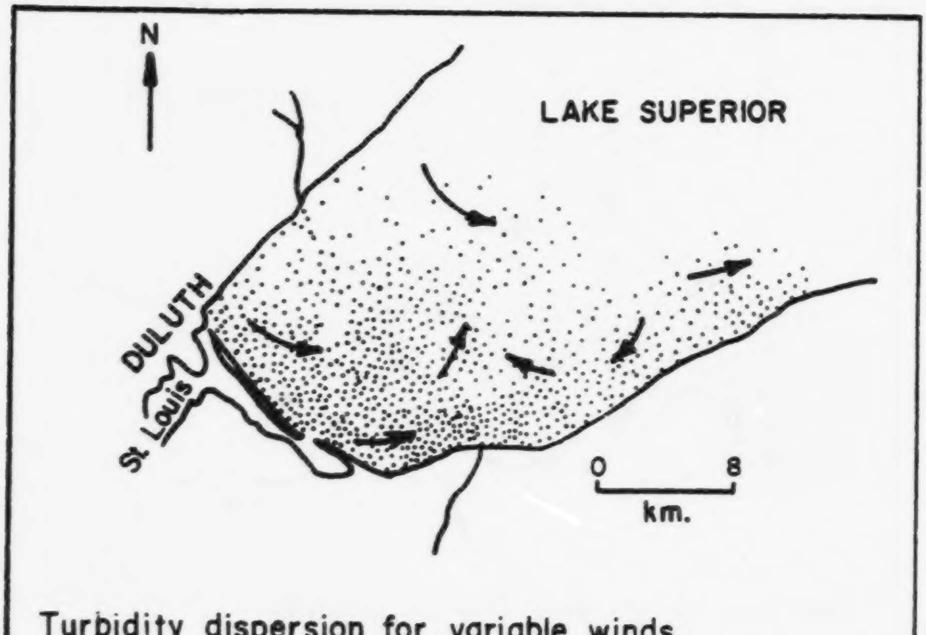
N
LAKE SUPERIOR
DULUTH
St Louis
0
8
km.

Turbidity dispersion for variable winds

Figure 25. Average turbidity distribution and transport for variable winds.

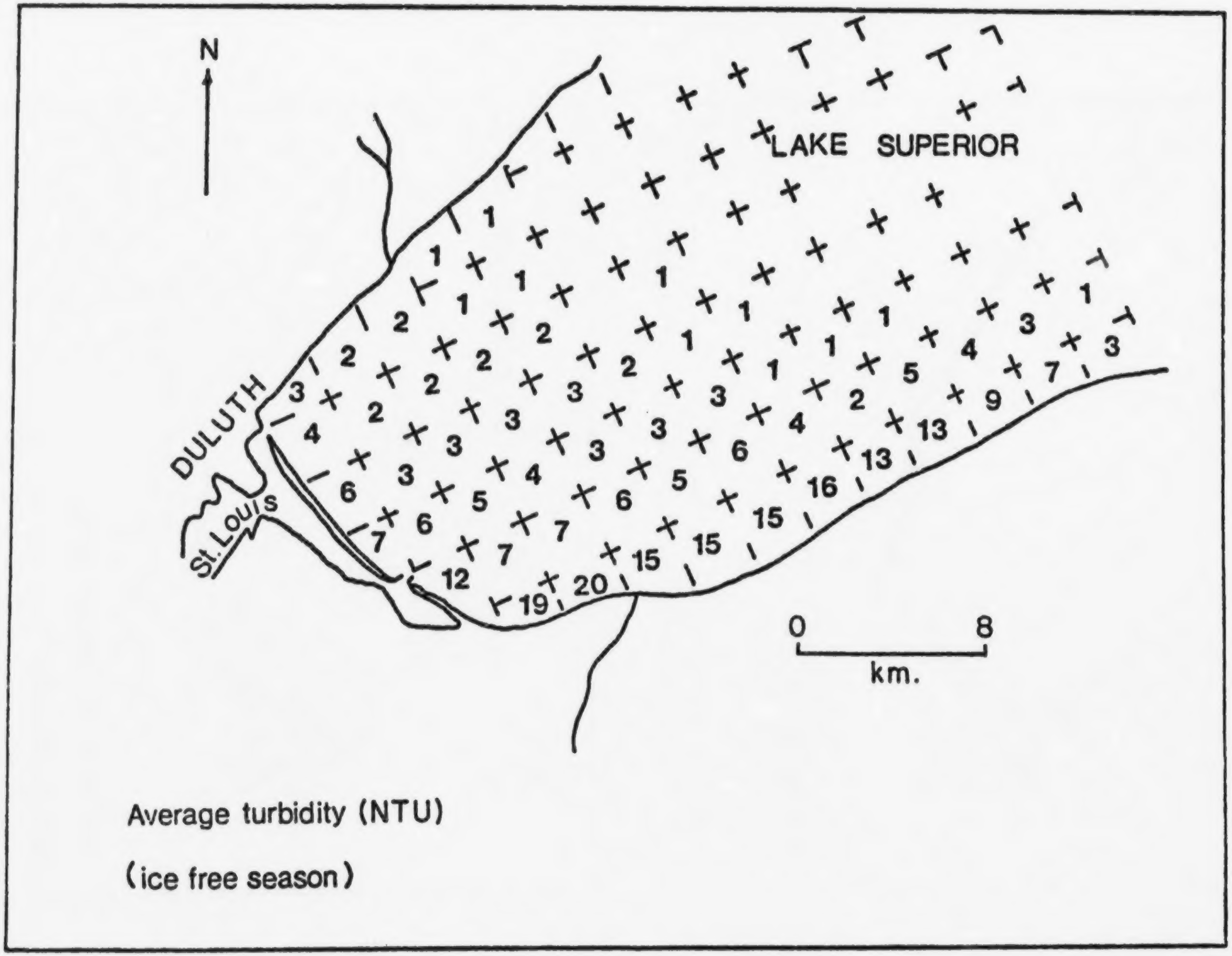
N
LAKE SUPERIOR
DULUTH
St. Louis
0
8
km.
Average turbidity (NTU)
(ice free season)

Figure 26. Average turbidity distribution for the ice-free season.

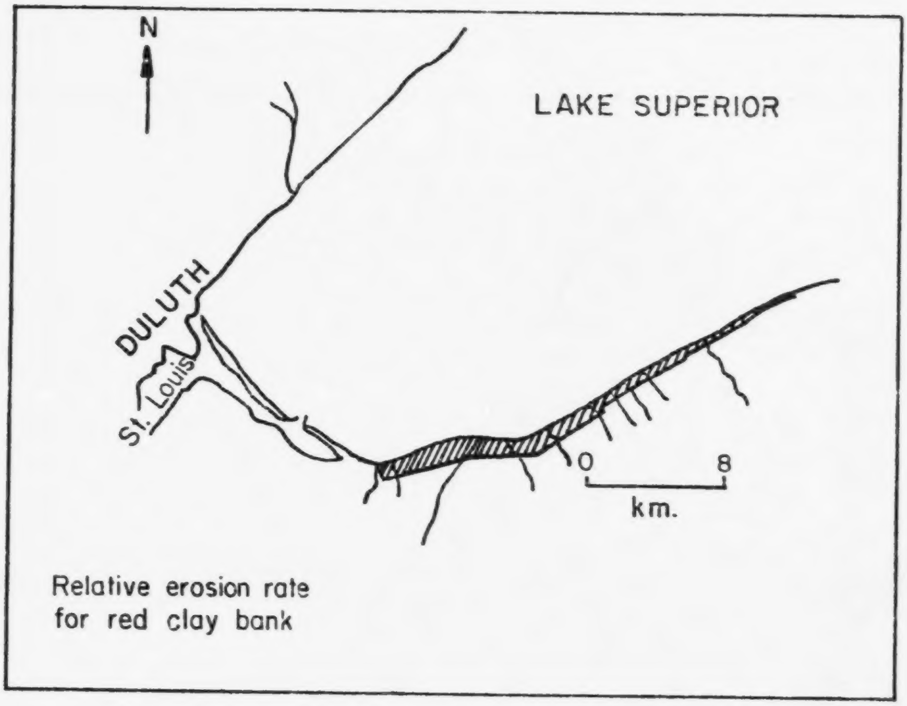
N
LAKE SUPERIOR
DULUTH
St. Louis
0
8
km.
Relative erosion rate for red clay bank

Figure 27. Relative south shore erosion rate.

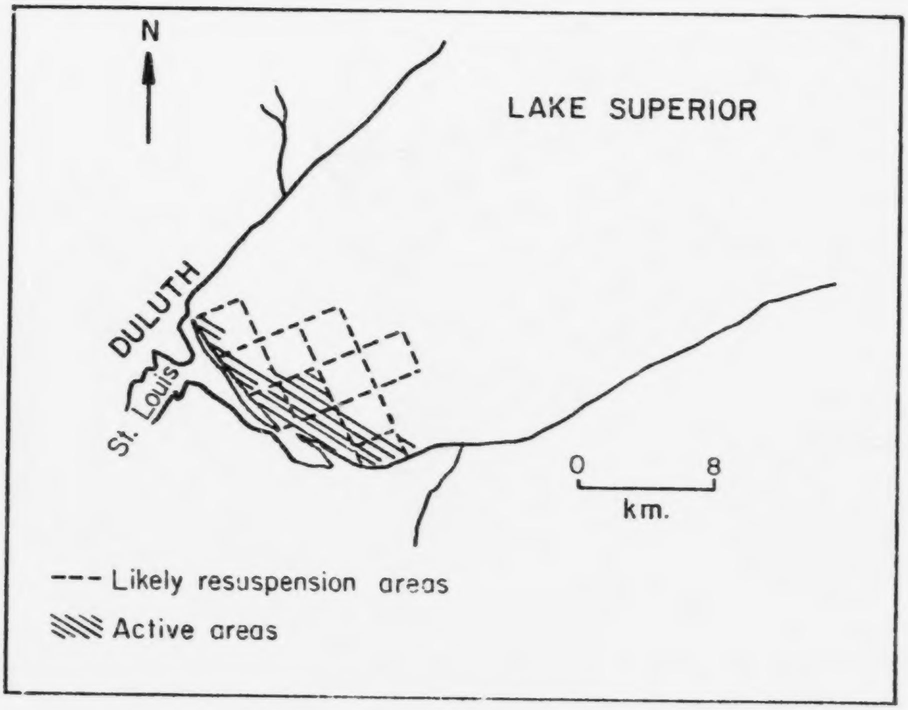
N
LAKE SUPERIOR
DULUTH
St. Louis
0
8
km.
--- Likely resuspension areas
▨ Active areas

Figure 28. Resuspension areas in Lake Superior.

should be particularly subject to periodic scouring since it lies between two major river turbidity outputs, the St. Louis and the Nemadji **rivers.** At the same time the area midway off the Minnesota Point is the place where major near-shore currents meet for the easterly storm conditions.

6. A NUMERICAL MODEL OF TRANSPORTS IN LAKE SUPERIOR

DESCRIPTION OF THE MODEL

Transport patterns of suspended material in Lake Superior have been rather controversial. Drift-bottle studies (Ruschmeyer et al., 1961) indicate an average overall counterclockwise summer circulation. Studies of currents and turbidity transport through insitu measurements and remote sensing studies in the extreme western arm of Lake Superior show that the currents have complex patterns near Duluth (Sydor, 1973). These localized currents give rise to an eddy circulation off Minnesota and Wisconsin Points which transports red clay turbidity to the area of the Duluth water intake and accounts for the general turbidity of the water near Duluth. Numerical modeling provided a means of studying lake circulation. However, to investigate transports in western Lake Superior--that is, roughly from Duluth to the Apostle Islands--it was necessary to develop a numerical model for the entire lake.

The two-dimensional, time-dependent mathematical model used for the present study is based on a tidal simulation model developed by Leendertse (1967) for the Rand Corporation. The model has several features which make it an attractive choice for predicting water levels:

1) The nonlinear convective-inertia terms are retained in the equations of motion resulting in higher accuracy in regions where the land-water boundaries are complicated.

2) The space-staggered grid has the advantage that there are centrally located spatial derivatives available for the linear terms of the partial differential equations.

3) The multi-operational method used in the solution of the partial differential equations is accurate to 2nd order in time, yet requires only two successive arrays to be stored for the water-level field and each of the velocity fields. Furthermore, the method is unconditionally stable, with no upper limit on the number of time steps. Numerical experiments conducted by the Rand Corporation, as well as tests in this study, showed that moderate variations in the time step size had a negligible effect on the predicted water levels, which are needed later by the current profile model. In order to model wind-induced water levels and transports for Lake Superior, the effects of wind stress were incorporated into the tidal model.

Mathematical Formulation

Consider a cartesian coordinate system in which z is increasing upward. The equations of motion for a viscous fluid are given by

$$\frac{\partial u}{\partial t} + u\frac{\partial u}{\partial x} + v\frac{\partial u}{\partial y} + w\frac{\partial u}{\partial z} - fv + \frac{1}{\rho}\frac{\partial p}{\partial x} = \nu_h\left[\frac{\partial^2 u}{\partial x^2} + \frac{\partial^2 u}{\partial y^2}\right] + \nu_v\frac{\partial^2 u}{\partial z^2} \qquad (5)$$

$$\frac{\partial v}{\partial t} + \frac{\partial v}{\partial x} + \frac{\partial v}{\partial y} + \frac{\partial v}{\partial z} + fu + \frac{1}{\rho}\frac{\partial p}{\partial y} = \nu_h\left[\frac{\partial^2 v}{\partial x^2} + \frac{\partial^2 v}{\partial y^2}\right] + \nu_v\frac{\partial^2 v}{\partial z^2} \qquad (6)$$

$$\frac{\partial w}{\partial t} + u\frac{\partial w}{\partial x} + v\frac{\partial w}{\partial y} + w\frac{\partial w}{\partial z} + fv_\varepsilon + \frac{1}{\rho}\frac{\partial p}{\partial z} = \nu_h\left[\frac{\partial^2 w}{\partial x^2} + \frac{\partial^2 w}{\partial y^2}\right] + \nu_v\frac{\partial^2 w}{\partial z^2} + g \qquad (7)$$

where u, v and w are the x, y and z components of the water velocity, ν_h and ν_v are the horizontal and vertical eddy viscosity coefficients, ρ is the fluid density and p is the pressure. The coriolis parameter f is equal to $2\omega \sin \phi$, where ω is the angular velocity of the earth's rotation and ϕ is the latitude. The eastward component of the water velocity is denoted by v_ε.

In studies of long-period water waves, the vertical accelerations and velocities are generally assumed small enough to be ignored. The vertical component of the coriolis acceleration is also quite small compared to g and is dropped from eq. (7). The terms containing horizontal-eddy viscosity are very small compared to the vertical-eddy viscosity term and are neglected in this model. With these assumptions, the equations of motion become:

$$\frac{\partial u}{\partial t} + u\frac{\partial u}{\partial x} + v\frac{\partial u}{\partial y} - fv + \frac{1}{\rho}\frac{\partial p}{\partial x} = \nu\frac{\partial^2 u}{\partial z^2} \qquad (8)$$

$$\frac{\partial v}{\partial t} + u\frac{\partial v}{\partial x} + v\frac{\partial v}{\partial y} + fu + \frac{1}{\rho}\frac{\partial p}{\partial y} = \nu\frac{\partial^2 v}{\partial z^2} \qquad (9)$$

$$\frac{1}{\rho}\frac{\partial p}{\partial z} = g \qquad (10)$$

A uniform density is assumed so that pressure becomes a linear function of depth. Consequently, the model is suitable for predicting flows only when the water is well mixed. Since, in a typical year, stratification does not develop until August and disappears by October, Lake Superior can be considered well mixed during the times of significant loading of red clay, i.e., the spring runoff and late fall storm surges. With the assumption of hydrostatic pressure, the horizontal derivatives of fluid pressure become functions of the water slope:

$$p(z) = \rho g[h-z]$$

$$\frac{1}{\rho}\frac{\partial p}{\partial x} = g\frac{\partial h}{\partial x} \qquad \frac{1}{\rho}\frac{\partial p}{\partial y} = g\frac{\partial h}{\partial y}$$

where h is the displacement of the water surface from the undisturbed level. Because they generate only weak currents, the atmospheric pressure gradients have been ignored.

Vertically averaged velocities are introduced

$$U = \frac{1}{(H+h)}\int_{-H}^{h} u\,dz \qquad V = \frac{1}{(H+h)}\int_{-H}^{h} v\,dz$$

where H is the depth of the undisturbed water. Vertically integrating the simplified equations of motion from -H to h, and dividing through by H + h gives:

$$\frac{\partial U}{\partial t} + U\frac{\partial U}{\partial x} + V\frac{\partial U}{\partial y} - fV + g\frac{\partial h}{\partial x} = \frac{\nu}{(H+h)}\frac{\partial U}{\partial z}\Big|_{z=h} - \frac{\nu}{(H+h)}\frac{\partial U}{\partial z}\Big|_{z=-H}$$

$$\frac{\partial V}{\partial t} + U\frac{\partial V}{\partial x} + V\frac{\partial V}{\partial y} + fU + g\frac{\partial h}{\partial x} = \frac{\nu}{(H+h)}\frac{\partial V}{\partial z}\Big|_{z=h} - \frac{\nu}{(H+h)}\frac{\partial V}{\partial z}\Big|_{z=-H}$$

The integrals of the non-linear terms are only approximate, but since these are small, only slight inaccuracies result. The integration causes terms containing the surface and bottom shear stress to appear on the right-hand side, corresponding to the wind stress and bottom friction respectively. The components of the bottom friction are taken proportional to the square of the vertically averaged water velocity

$$\nu\frac{\partial U}{\partial z}\Big|_{z=-H} = gC^{-2}U(U^2 + V^2)^{\frac{1}{2}} \qquad \nu\frac{\partial V}{\partial z}\Big|_{z=-H} = gC^{-2}V(U^2 + V^2)^{\frac{1}{2}}$$

where C is the de Chézy coefficient. In general, the value of C depends upon the roughness of the bottom, the bottom material,and the depth, and should be determined by experiment. Tsai and Chang (1974) found that the water levels predicted by the Rand model were relatively insensitive to the bottom frictior used. Therefore, the values of C were calculated for Lake Superior according to the following formula which is based on table of de Chézy values versus depth for lakes and rivers (Hutchinson, 1957):

$$C = 25 \times h^{.168745}$$

The Chézy coefficients obtained were somewhat lower but still comparable to those found experimentally by Leendertse in modeling an estuary of the Rhine River.

In its original form, the Rand model contained no wind-forcing function, relying only upon water levels as a function of time along an open water boundary as a driving force. In order to model wind-induced transports and water levels in Lake Superior, the wind-forcing terms (Wilson, 1960)

$$\frac{\nu}{(H+h)} \frac{\partial U}{\partial z}\bigg|_{z=h} = \frac{k}{H} Wx(Wx^2+Wy^2)^{\frac{1}{2}} \qquad \frac{\nu}{(H+h)} \frac{\partial V}{\partial z}\bigg|_{z=h} = \frac{k}{H} Wy(Wx^2+Wy^2)^{\frac{1}{2}}$$

were added to the vertically integrated equations of motion, where Wx and Wy are the x and y components of the wind velocity and k is the wind-stress coefficient. Following Tsai and Chang (1974), who did an extensive study of wind-stress coefficients, k was taken as

$$k = 1.25 \times 10^{-6} \qquad \text{for } W < W_1$$

$$k = 1.25 \times 10^{-6} + 1.75 \times 10^{-6} \sin\left(\frac{W-W_1}{W_2-W_1}\frac{\pi}{2}\right) \quad \text{for } W_1 \leq W \; W_2$$

$$k = 3.0 \times 10^{-6} \quad \text{for } W_2 \leq W$$

where W_1 = 5.1 m/sec, W_2 = 15.4 m/sec and W is the wind speed. In their final form, the vertically integrated equations for the horizontal motion are:

$$\frac{\partial U}{\partial t} + U\frac{\partial U}{\partial x} + V\frac{\partial U}{\partial y} - fV + g\frac{\partial h}{\partial x} + g\frac{U(U^2+V^2)^{\frac{1}{2}}}{C^2(H+h)} = \frac{k}{H} Wx(Wx^2+Wy^2)^{\frac{1}{2}} \tag{11}$$

$$\frac{\partial V}{\partial t} + U\frac{\partial V}{\partial x} + V\frac{\partial V}{\partial y} + fU + g\frac{\partial h}{\partial y} + g\frac{V(U^2+V^2)^{\frac{1}{2}}}{C^2(H+h)} = \frac{k}{H} Wy(Wx^2+Wy^2)^{\frac{1}{2}} \tag{12}$$

For an incompressible fluid, the continuity equation is written

$$\frac{\partial u}{\partial x} + \frac{\partial v}{\partial y} + \frac{\partial w}{\partial z} = 0$$

After vertically integrating, and applying the boundary conditions:

$$w(h) = \frac{dh}{dt} = \frac{\partial h}{\partial t} + u\frac{\partial h}{\partial x} + v\frac{dh}{y} \qquad \text{at the surface, and}$$

$$w(-H) = -u\frac{\partial H}{\partial x} - v\frac{\partial H}{\partial y} = 0 \qquad \text{at the bottom,}$$

the continuity equation becomes

$$\frac{\partial h}{\partial t} + \frac{\partial}{\partial x}[U(H+h)] + \frac{\partial}{\partial y}[V(H+h)] = 0 \tag{13}$$

Numerical Procedure

The vertically integrated equations of motion and continuity must be replaced by finite difference approximations which can be solved at points on a spatial grid such that

$U(j\Delta x,\ k\Delta y,\ n\Delta t) = U(x,y,t)$ where $\Delta x = \Delta y = \Delta s$

$j = 0,\ \pm \tfrac{1}{2},\ \pm 1,\ \pm 3/2,\ \ldots$

$k = 0,\ \pm \tfrac{1}{2},\ \pm 1,\ \pm 3/2,\ \ldots$

$n = 0,\ \tfrac{1}{2},\ 1,\ 3/2,\ \ldots$

A space-staggered grid is used in which the x and y components of velocity, water levels, and depths are located at separate points.

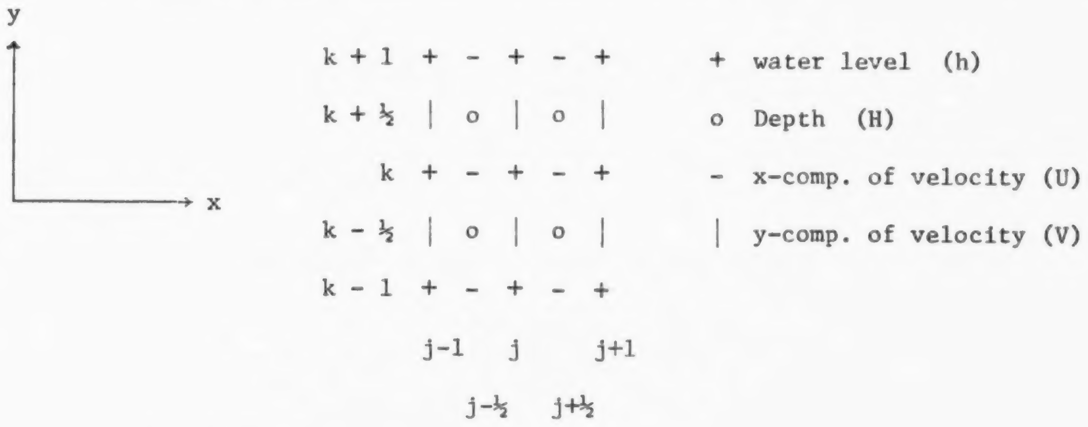

The advantage of such a grid is that centrally located spatial derivatives across only one grid space are available for the linear terms of the partial differential equations. The land-water boundaries are fitted through the depth locations, and the perpendicular component of velocity at the boundary is fixed at zero.

In order to see how the numerical integration might be performed, $h(t + \Delta t)$ is expanded about $h(t)$ in a Taylor's series:

$$h(t + \Delta t) = h(t) + \Delta t \frac{\partial h(t)}{\partial t} + \frac{\Delta t^2}{2} \cdot \frac{\partial^2 h(t)}{\partial t^2} + \ldots$$

To first order in Δt, the new h is found in a single time step where $h^{(n+1)} \simeq h^{(n)} + \Delta t \frac{\partial h^{(n)}}{\partial t}$ is found by evaluating the continuity equation using finite differences on the grid. This is the simplest scheme, however it has the disadvantage that errors tend to build rapidly in time because of the low order of accuracy.

In the Rand Model, a double time step operation is used to perform the numerical integration. Each step has two time levels associated with it, the first from time n to $n + \frac{1}{2}$, and the second from time $n + \frac{1}{2}$ to $n + 1$. The spatial derivative and coriolis force terms alternate between the old and new time levels in each step such that over the two successive steps of the time interval, these terms are either central or averaged in time. By using a combination of central and time-averaged terms, the resulting integration is accurate to second order in time while requiring only two successive fields of information to be stored at any given time. During the first operation, the fields of $h(n+\frac{1}{2})$, $U(n+\frac{1}{2})$, and $V(n+\frac{1}{2})$ are computed from the fields of $h(n)$, $U(n)$, and $V(n)$. Since the solution for $h(n+\frac{1}{2})$ involves $U(n+\frac{1}{2})$ while the solution of $U(n+\frac{1}{2})$ requires knowledge of $h(n+\frac{1}{2})$, the equations for an entire row are written in matrix form and solved simultaneously to develop recursion factors which enable the computation of $h(n+\frac{1}{2})$ and $U(n+\frac{1}{2})$ to be carried out implicitly. Once these fields are known, $V(n+\frac{1}{2})$ can be solved explicitly. Similarly, in the second operation, the fields of $h(n+1)$, $U(n+1)$, and $V(n+1)$ are computed from the fields of $h(n+\frac{1}{2})$, $U(n+\frac{1}{2})$, and $V(n+\frac{1}{2})$. In this case, $h(n+1)$ and $V(n+1)$ require each other for solution so they are solved implicitly using a recursive scheme, and finally $U(n+1)$ is solved explicitly. Some of the nonlinear terms had to be approximated at a lower time level in order to avoid an iterative procedure which would require excessive computation time.

RESULTS OF TRANSPORT MODEL

Lake-Level Oscillations

Because of their observed importance in the transport of suspended materials in western Lake Superior, two main types of wind stresses were modeled, an easterly and a westerly. Both wind functions were constructed from the composite of a large number of weather observations and thus represent "typical" weather patterns. For example, the northeast wind becomes out of the southeast as one moves toward the east end of the lake, as though a low-pressure area with its counterclockwise air circulation were centered south of the lake. Similarly, the westerly wind represents a low-pressure center north of the lake.

The transport model was verified by comparing observed water levels for easterly and westerly wind stresses with that obtained from the model. Fourier analyses for both wind stresses are shown in Figures 29 and 30. Notice that the 7.8-hour mode is dominant in both cases. A series of high-frequency modes appear at the general frequencies reported by Rao and Schwab (1976) and found from experimental data by Mortimer and Fee (1976), Table 9. The model also appears to exhibit a 5.6-hour mode, which was also occasionally observed in the lake-oscillation data taken at Duluth. Similarly the model exhibits a 2-hour mode which was observed in the lake data at Duluth. This mode plays an important role in the mass transport in Duluth Harbor. The transports from the model were also verified by comparing them to the transports of turbidity obtained from statistical analysis of the Landsat data (described in the section on Turbidity Transport), and the general shape of the turbidity plumes observed in Landsat images.

Predicted Transports in Western Lake Superior

The results of transport calculations for northeasterly winds are given in Figure 31. It is seen that for northeasterly winds which present a large fetch at Duluth, there is a strong current along the North Shore from Silver Bay to Duluth; Figures 31A - 31C. This generally accounts for the transport of large concentrations of taconite fines to the Duluth intake area for high easterly winds (Baumgartner, et al., 1973). For northeasterly winds, the transport along the south shore is due west. This transport and the one coming down the North Shore appear to turn and meet at Minnesota Point and then return out in the middle of the lake along an axis running parallel to the North Shore. This transport pattern is consistent with that obtained from statistical analysis of Landsat images. Figure 32 shows a resuspension plume after an extended northeasterly wind. Red clay from south shore erosion and from sediment resuspension moved along the Wisconsin and Minnesota Points, then abruptly turned out along the axis of the lake. The turbidity on that date at Minnesota Point Airport was 50 mg/ℓ and dropped to 8 mg/ℓ 1.5 km farther towards Duluth, where it generally reflects the near-shore turbidities of the water coming in from the North Shore and from the St. Louis River out of the Duluth entry.

As the northeast wind slackens, Figure 31E, the transports in extreme western Lake Superior begin to subside and scramble. A large clockwise circulation cell appears to form northwest off the Apostle Islands. The plume moving out along the axis of the lake becomes unstable, and disperses. Thus, for high-turbidity events, the Duluth intake becomes contaminated by red clay, Figure 33. Figure 31F shows the transport pattern 14 hours after the northeast wind was completely relaxed. A counterclockwise cell off Two Harbors and a clockwise cell off Silver Bay have developed. The turbidity plume off Silver Bay due to dumping of taconite tailings from iron ore processing is shown in Figure 34. This image strongly suggests such a circulation pattern. The currents near Duluth at the time of Figure 31E show the characteristic

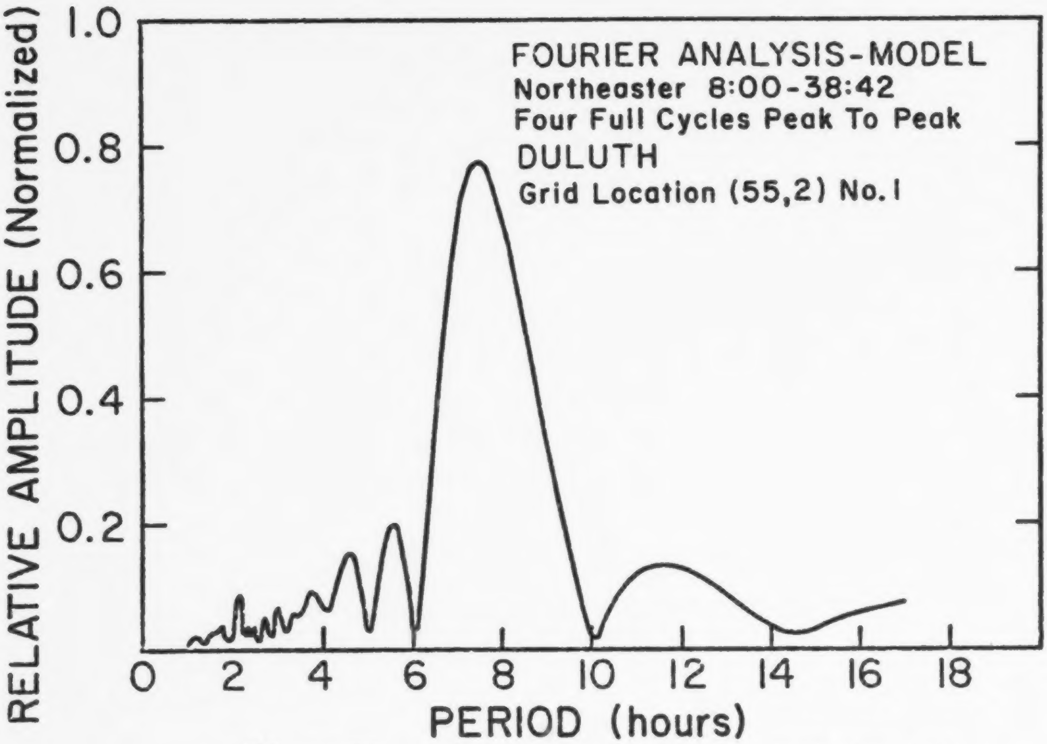

Figure 29. Duluth water levels for easterly wind.

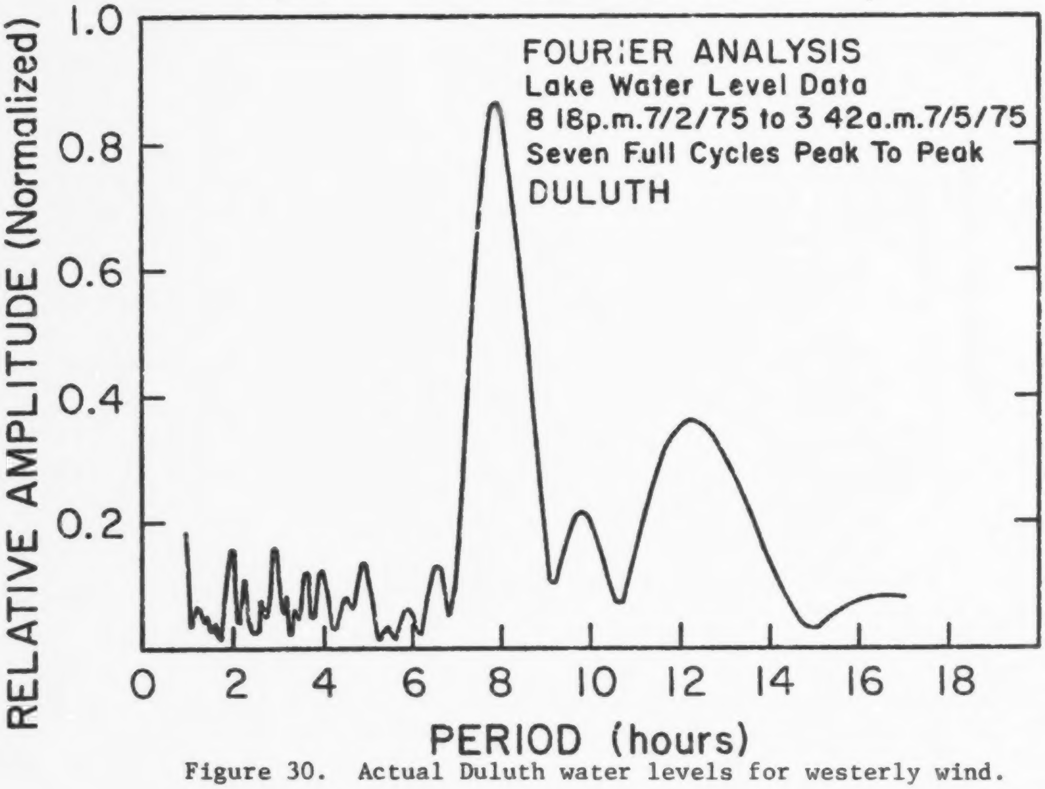

Figure 30. Actual Duluth water levels for westerly wind.

TABLE 9

COMPARISON OF PERIODS IN HOURS OF GRAVITATIONAL MODES IN LAKE SUPERIOR

Mode (As Identified by Rao & Schwab)	Observed (Mortimer & Fee)	Calculated (Rao & Schwab)	Observed at Duluth (Sydor)	Calculated Model Values at Duluth
1	7.89	7.86	7.88	7.53
	- -	- -	- -	5.56
2	4.84	4.45	4.88	4.62
3	3.80	3.76	3.96	3.73
4	3.37	3.17	3.58	3.33
5	3.02	2.94	2.93	2.97
	- -	- -	1.98	2.13

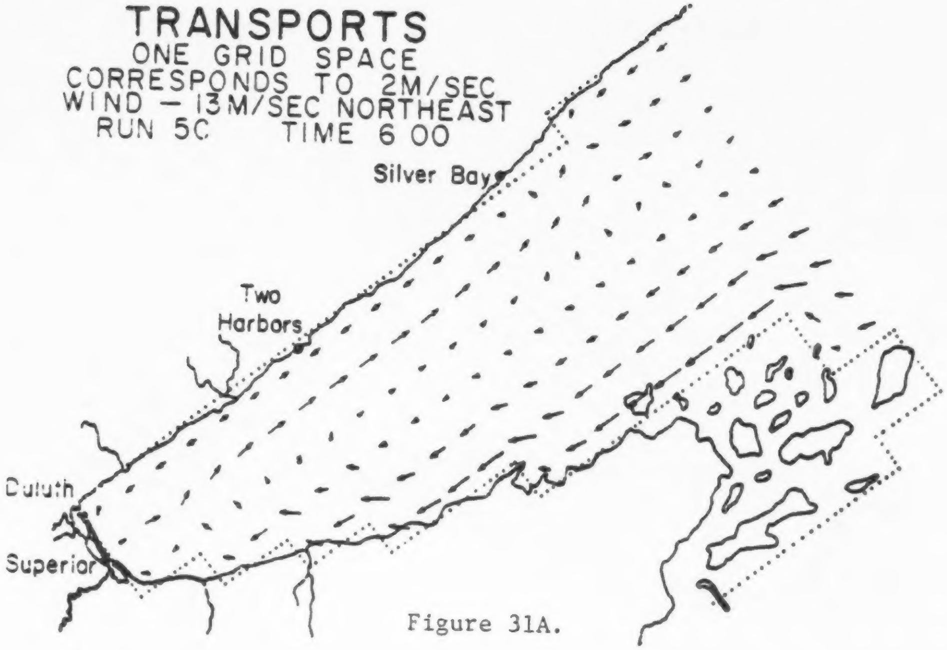
TRANSPORTS
ONE GRID SPACE
CORRESPONDS TO 2M/SEC
WIND — 13M/SEC NORTHEAST
RUN 5C TIME 6 00
Silver Bay
Two Harbors
Duluth
Superior

Figure 31A.

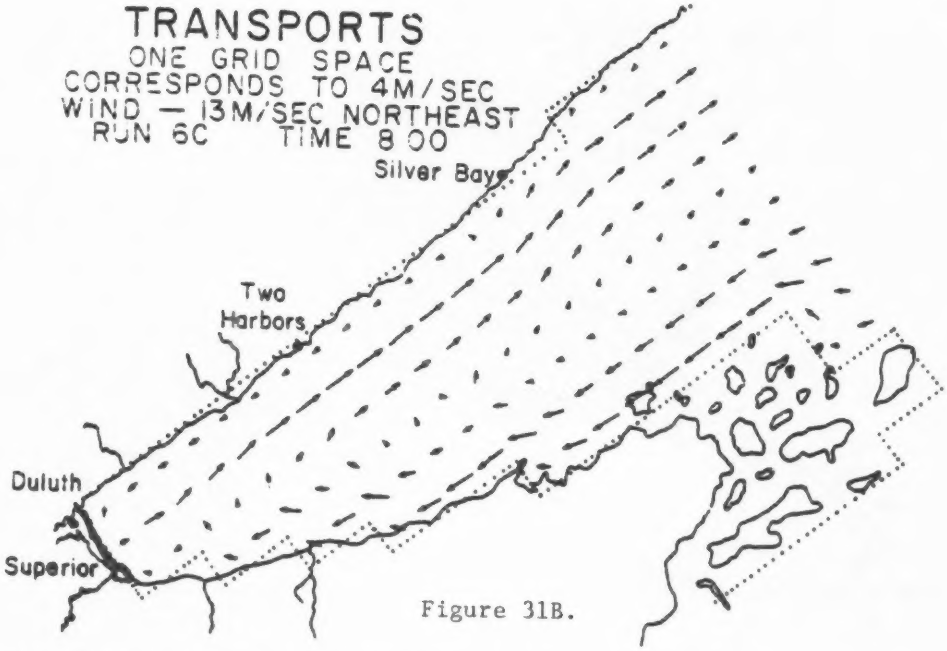
TRANSPORTS
ONE GRID SPACE
CORRESPONDS TO 4M/SEC
WIND — 13M/SEC NORTHEAST
RUN 6C TIME 8 00
Silver Bay
Two Harbors
Duluth
Superior

Figure 31B.

Figure 31. Western Lake Superior transports for easterly storm.

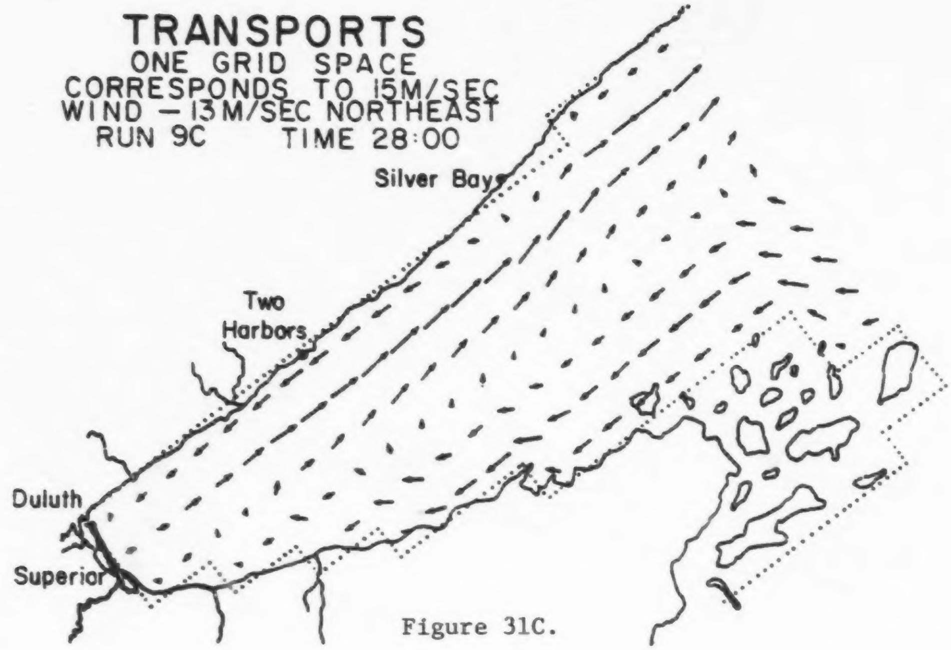
TRANSPORTS
ONE GRID SPACE
CORRESPONDS TO 15M/SEC
WIND — 13M/SEC NORTHEAST
RUN 9C TIME 28:00
Silver Bay
Two Harbors
Duluth
Superior

Figure 31C.

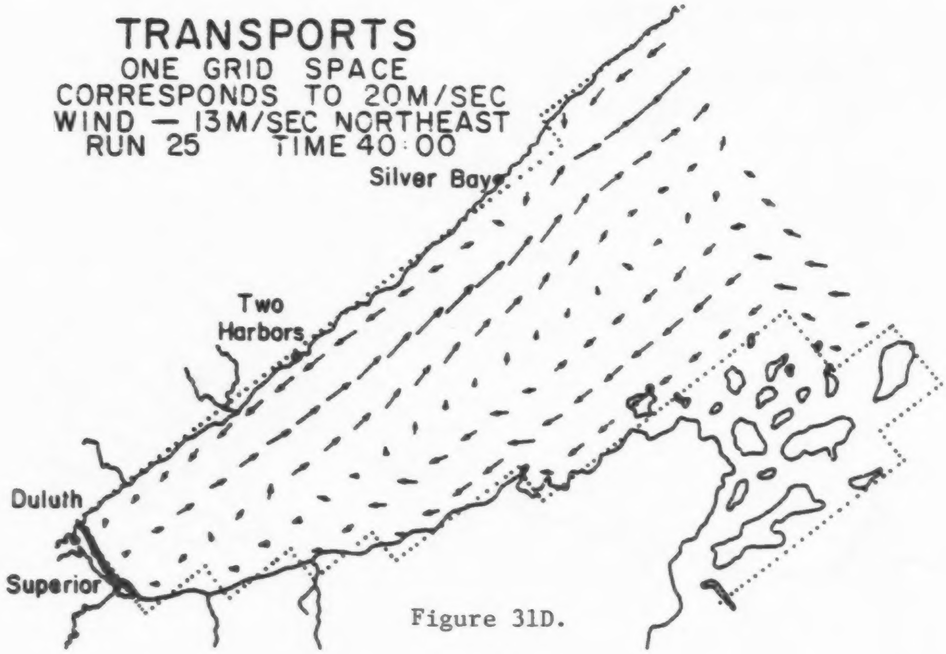
TRANSPORTS
ONE GRID SPACE
CORRESPONDS TO 20M/SEC
WIND — 13M/SEC NORTHEAST
RUN 25 TIME 40:00
Silver Bay
Two Harbors
Duluth
Superior

Figure 31D.

Figure 31. (continued)

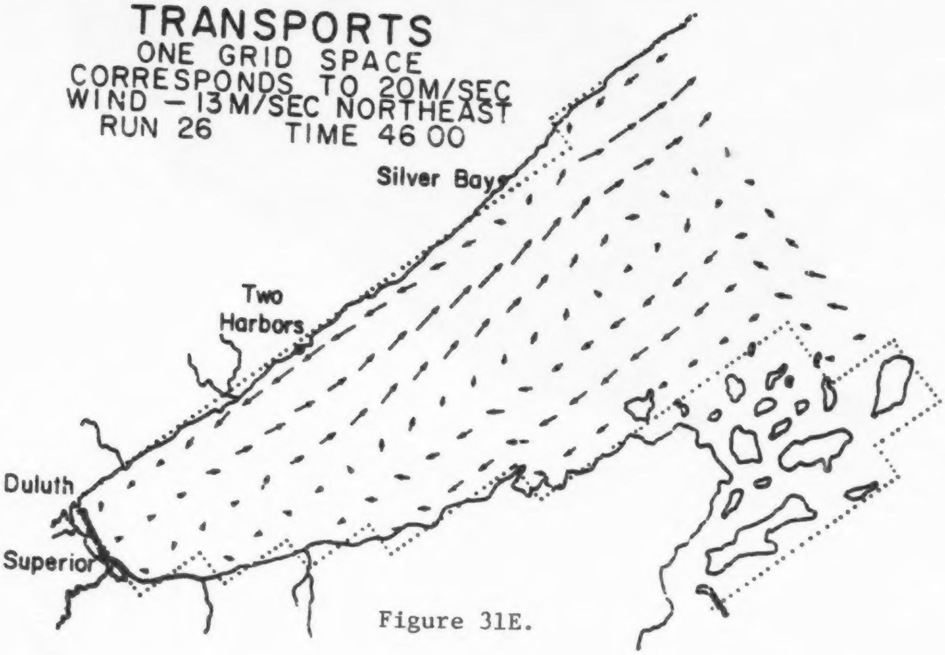
TRANSPORTS
ONE GRID SPACE
CORRESPONDS TO 20M/SEC
WIND — 13M/SEC NORTHEAST
RUN 26 TIME 46 00
Silver Bay
Two Harbors
Duluth
Superior

Figure 31E.

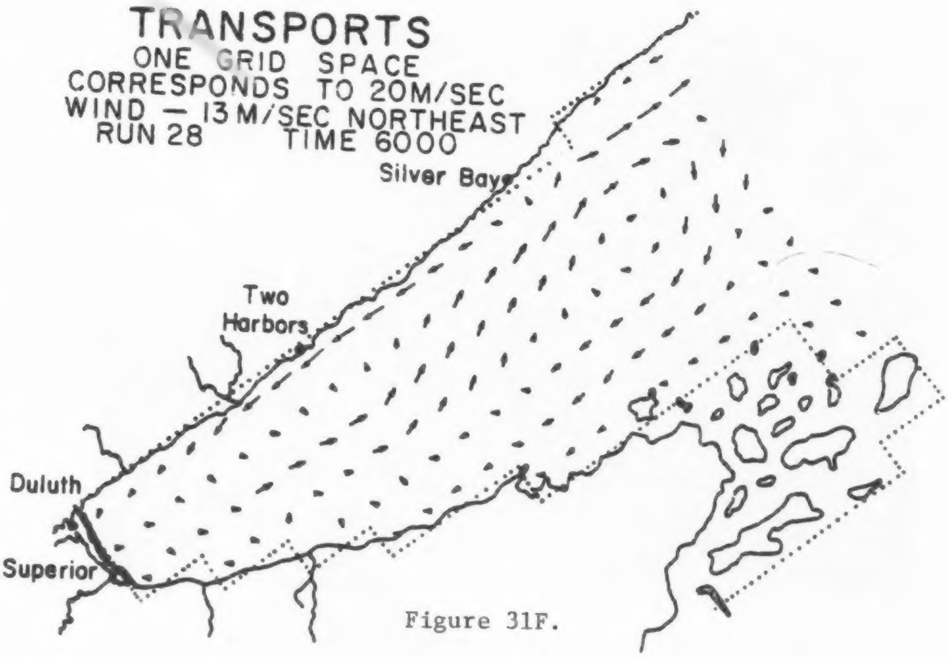
TRANSPORTS
ONE GRID SPACE
CORRESPONDS TO 20M/SEC
WIND — 13M/SEC NORTHEAST
RUN 28 TIME 6000
Silver Bay
Two Harbors
Duluth
Superior

Figure 31F.

Figure 31. (continued)

Figure 32. Landsat image for 11APR75 showing resuspension plume caused by northeasterly winds.

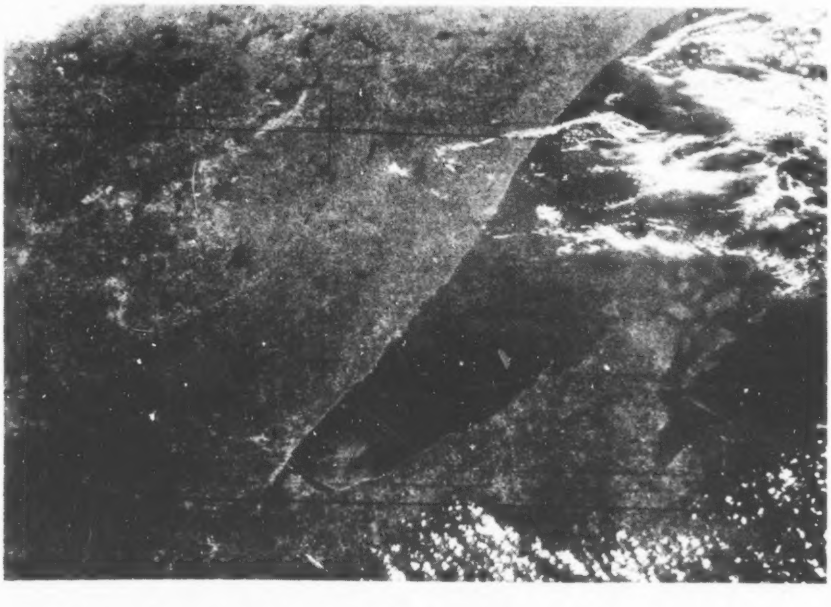

Figure 33. Skylab image showing turbidity entrapment near Duluth.

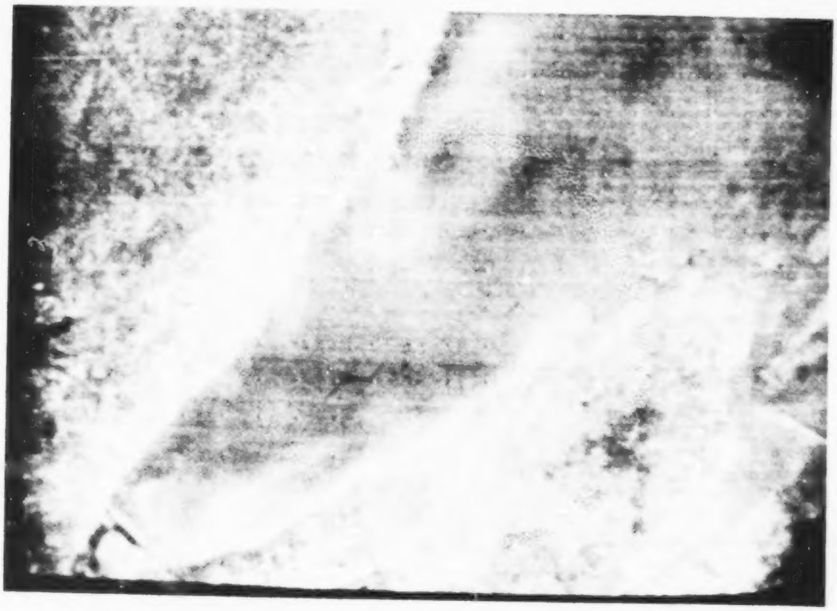

Figure 34. Landsat image for 23NOV73 showing taconite tailings plume off Silver Bay.

eddy circulation off Wisconsin Point where large amounts of sediment settle and can be subsequently resuspended.

The transports for westerly winds, Figure 35, are quite different. The Silver Bay area shows transports away from the shore, while the transport of the red clay is confined to the south shore and is taken out along an easterly direction past Bark Point, towards the Apostle Islands, where a large counterclockwise cell is established, Figure 35B. As seen in Figure 35A, the transports along the North Shore bring in water from the center of the lake towards Duluth, where the transports disperse, and show a return path up along the North Shore. This generally accounts for the lack of red clay turbidity at the Cloquet intake for such winds, the generally lower taconite tailing concentration at the Duluth intake, and the flushing of the turbid water out of the Duluth area. However, as pointed out earlier, variable winds often tend to cause an entrapment of the turbid waters and harbor effluents in the Duluth area. The summer transports near Duluth are somewhat complicated by the presence of a warm-water cell near Duluth. This generally tends to shield the Duluth intake in the summer from the influx of tailing fines even for easterly winds. A fine-grid model for extreme western Lake Superior, together with measurements of water levels necessary for the mathematical description of an open boundary where the warm-water cell ends in the lake, together with application of water quality models to the area, will be the subject of subsequent investigation.

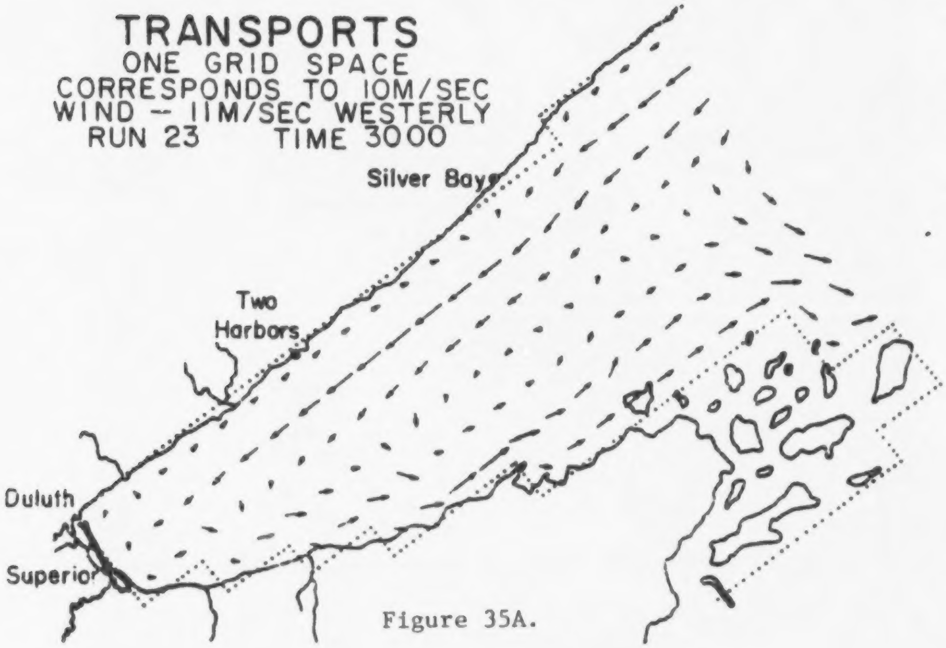
TRANSPORTS
ONE GRID SPACE
CORRESPONDS TO 10M/SEC
WIND — 11M/SEC WESTERLY
RUN 23 TIME 3000
Silver Bay
Two Harbors
Duluth
Superior

Figure 35A.

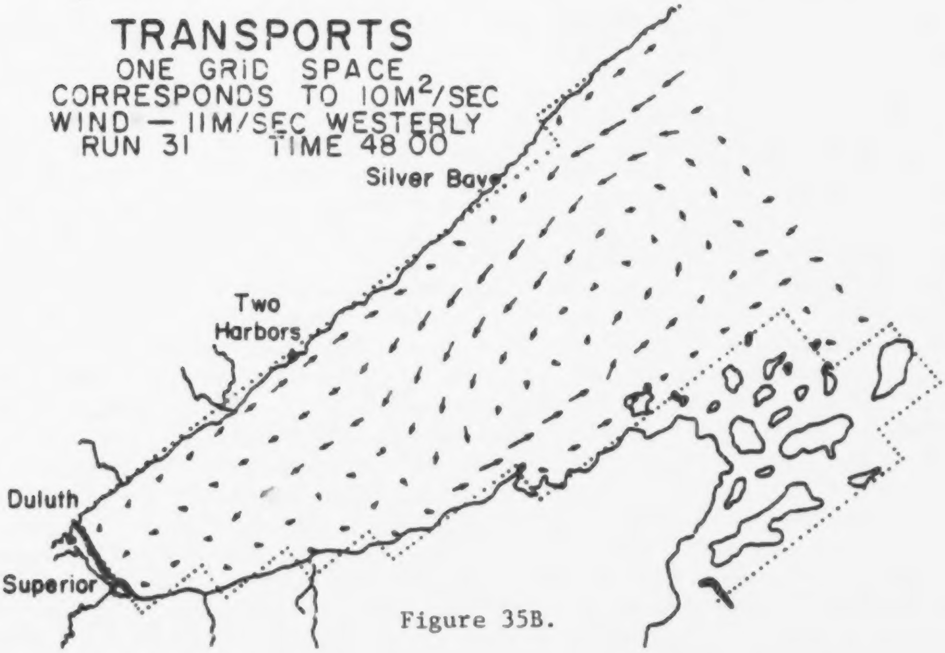
TRANSPORTS
ONE GRID SPACE
CORRESPONDS TO 10M^2/SEC
WIND — 11M/SEC WESTERLY
RUN 31 TIME 48 00
Silver Bay
Two Harbors
Duluth
Superior

Figure 35B.

Figure 35. Western Lake Superior transports for westerly storm.

Water Levels Due to Storm Surge

Water levels from the model for a northeasterly and westerly wind storm are shown in Figures 36 - 38. High water levels are evident at the base of Wisconsin Point and Minnesota Point. The water levels at the shore are actually higher than those indicated in Figure 37 which reflects the water height at points 3 km off shore. Thus the surge at Wisconsin Point and Minnesota Point should be between 15 and 30 cm. A water-level distribution for a model by Forristall (1970) is shown in Figure 39. It demonstrates more vividly the near-shore water pileup, although this method of calculation was discarded because of other shortcomings. The Leendertse model generally predicts a pileup of water in the corners of the grid which is quite real and not a mathematical contrivance. Wisconsin Point was breached on November 1, 1974, while the area at the base of Minnesota Point sustained substantial property damage during the northeasterly storm of January, 1975.

It is difficult, however, to attribute the damage directly to the water surge, without comparing it to the wave height for such storms. Significant wave heights for a 13 m/sec (30 mph) northeasterly over the long fetch would run 2 - 3 meters at Minnesota Point with about a 6-second period, and the anticipated disturbance would reach a depth of 20 - 25 meters. It should also be noted that the transport velocities due to storm surges are high; thus,if one considers the dissipation of energy as proportional to the square of the velocity, then significant damage can be assigned to the transport velocities directly, say $\sim$ 15 - 25% in comparison to the potential energy due to wave height.

The importance of water level may also be assessed from the remote sensing for Douglas County, which shows a greater erosion for mild northeasterlies than severe westerly winds producing comparable wave action. The westerly winds depress the water level along the Douglas County shore.

Transports for the Entire Lake

One of the concerns with regard to fine particles which remain in suspension for a period of months is the possibility of direct transport of these particles in high concentrations across the international boundary. The possibility of such an incident was reported in April, 1975, when asbestiform fibers were observed in the water supply of Thunder Bay, Canada.

Predicted transports for the entire lake are shown in Figure 40 for northeasterly and Figure 41 for westerly winds. Due to space limitations, only the vectors for alternate grid points are shown, and therefore only the gross features of the transport patterns are visible. At the height of the northeasterly storm, Figure 40D, the transport streamlines are moving away from the shore zone at Silver Bay to the Thunder Bay area. Later, the particles dispersed to areas away from the shore zone would apparently be rapidly transported to the Apostle Islands area. Streamlines peeling off the main circulation pattern, however, might carry tailings into the complex

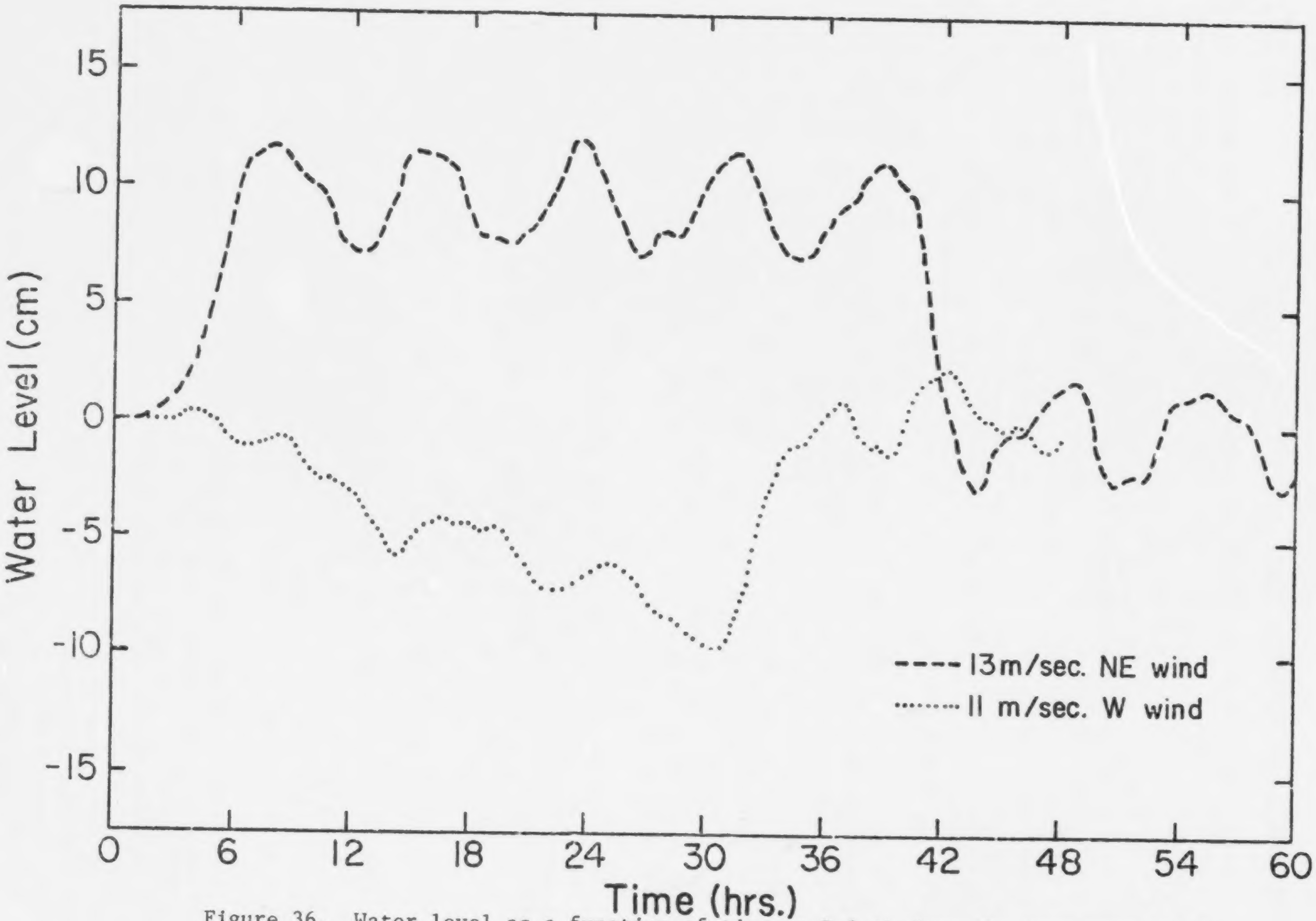

Figure 36. Water level as a function of time at Duluth from the transport model.

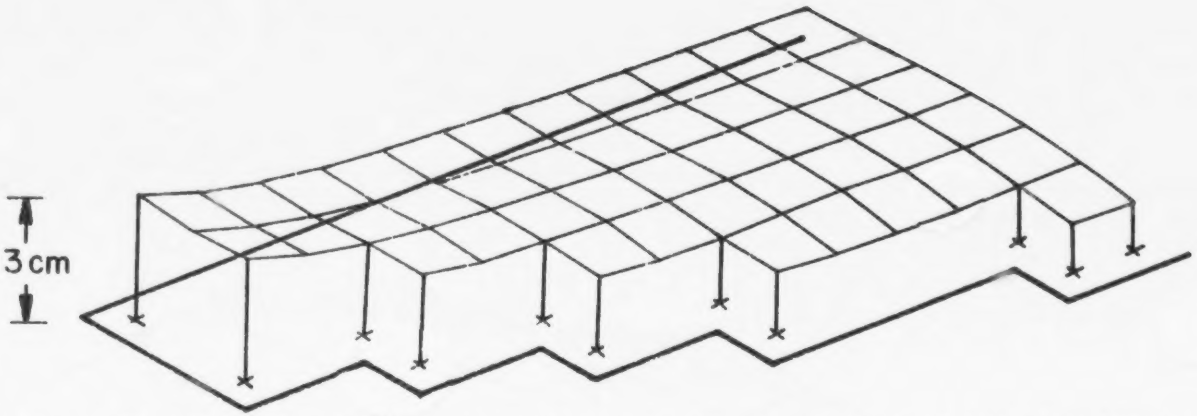

Figure 37. Water levels for western Lake Superior at one peak of the well-developed seiche caused by a 13 m/s NE wind, 31:20 hours after start of wind (Rand Corporation Model).

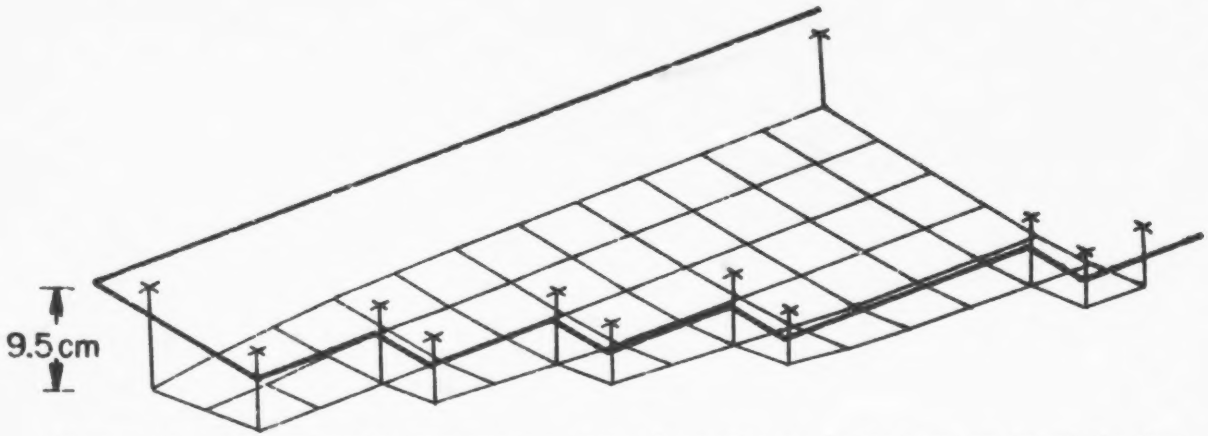

Figure 38. Water levels for western Lake Superior at lowest water level during modeled storm. Wind is 11 m/s westerly. 30 hours after start of wind (Rand Corporation Model).

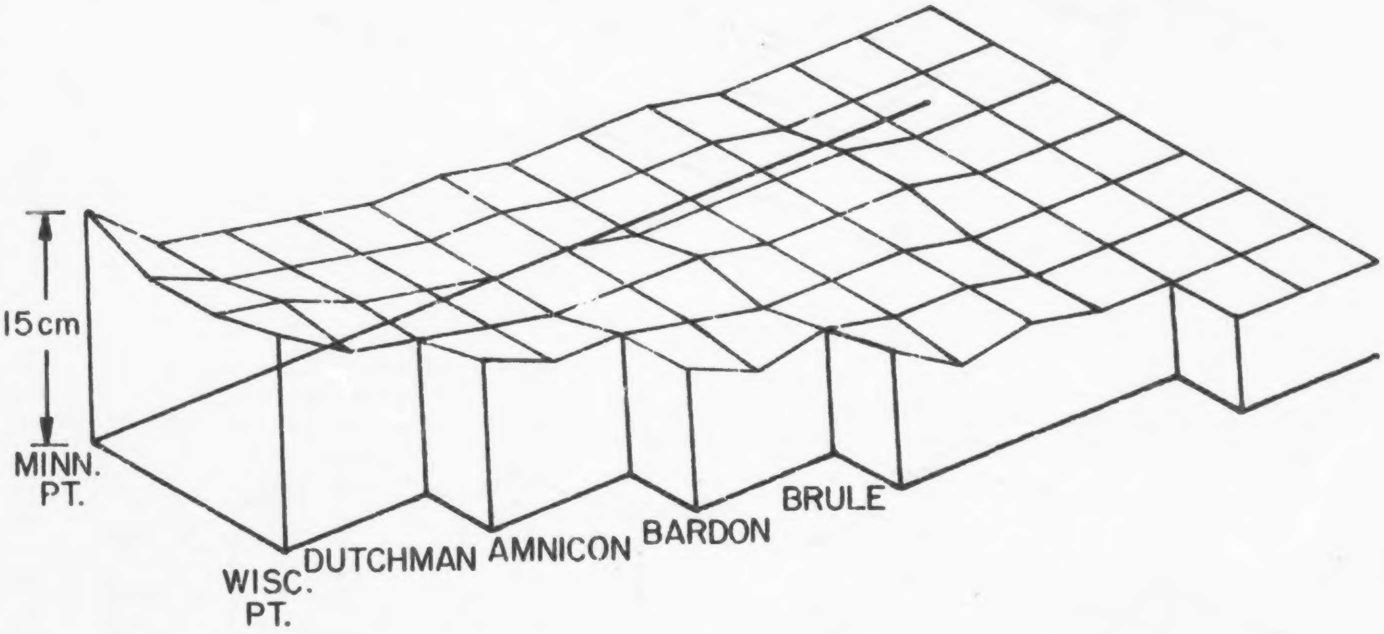

Figure 39. Water level for western Lake Superior after 15 hours of a 13 m/s NE wind. A simple transport model by Forristall was used with a time step of 60 sec and a smoothing coefficient of 0.95.

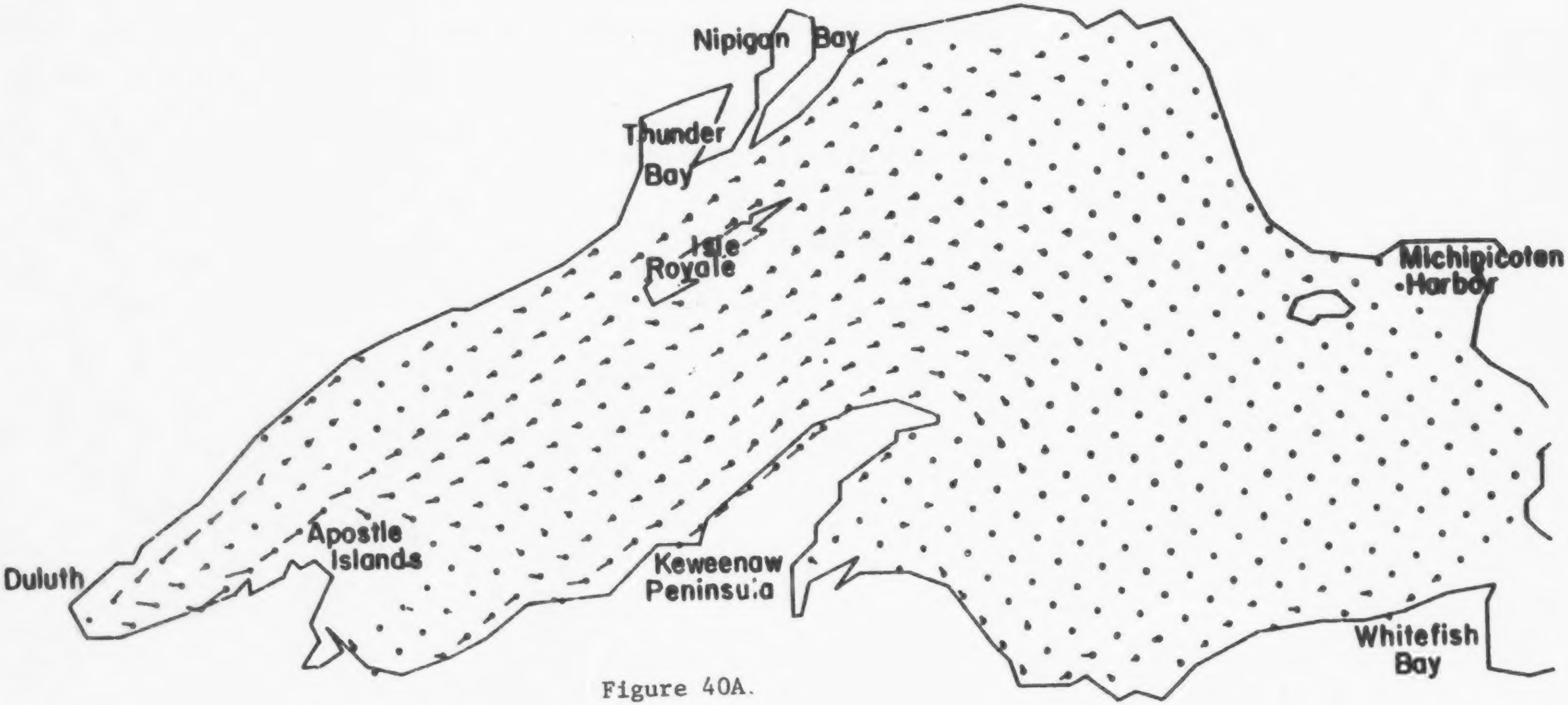
Nipigan Bay
Thunder
Bay
Isle
Royale
Michipicoten
Harbor
Duluth
Apostle
Islands
Keweenaw
Peninsula
Whitefish
Bay

Figure 40A.

LAKE SUPERIOR
13 M/SEC N.E.

TRANSPORTS FROM RUN 14
TIME = 6 6
AT = 180
SCALE 0.2 CM = .500 M^2/SEC

Figure 40. Entire Lake Superior transports from a 13 m/s NE wind.

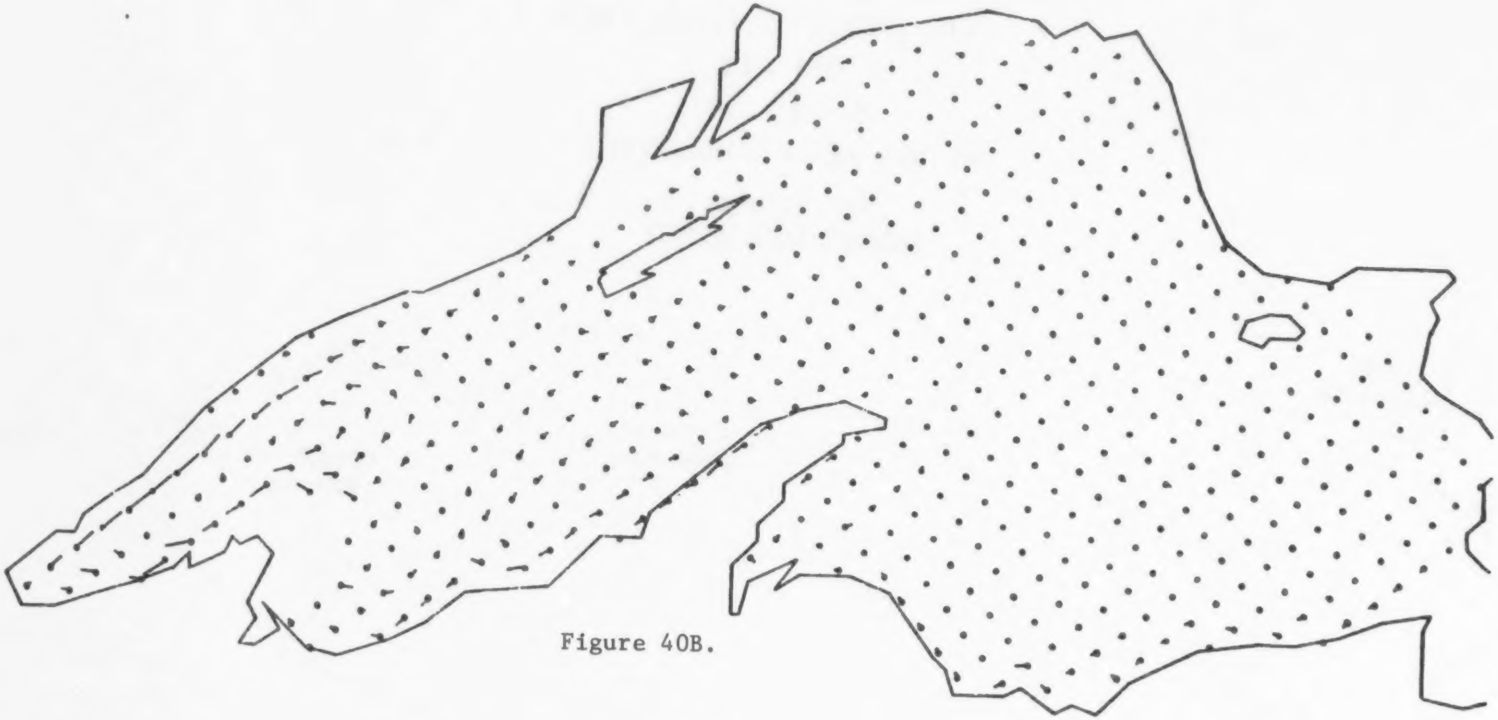

Figure 40B.

LAKE SUPERIOR

13m/sec N.E.

TRANSPORTS FROM RUN 15.

TIME = 12 12

AT = 180.

SCALE 0.2 CM = 2.000M^2/SEC

Figure 40. (continued)

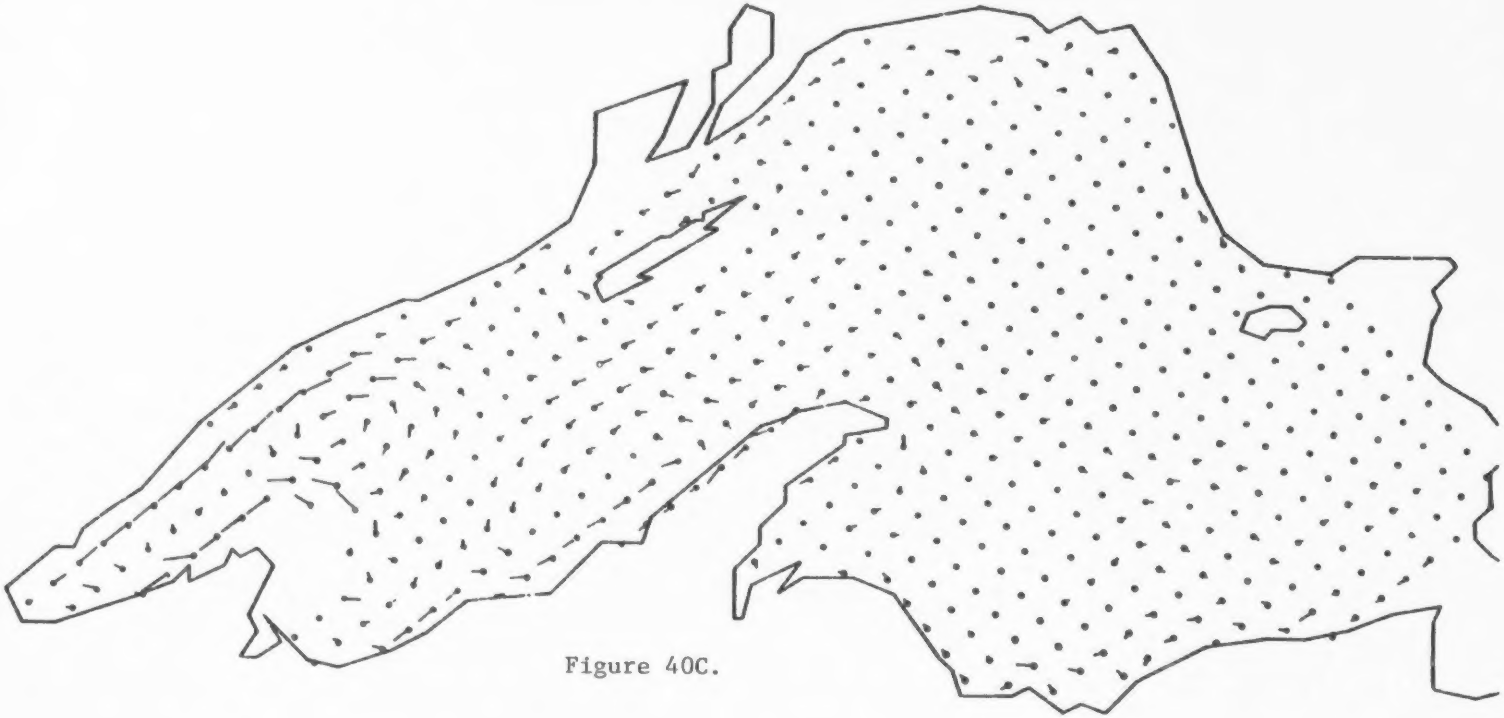

Figure 40C.

LAKE SUPERIOR
13m/sec N.E.
TRANSPORTS FROM RUN 7.
TIME = 24 24
AT = 180.
SCALE 0.2 CM = 3.003M^2/SEC

Figure 40. (continued)

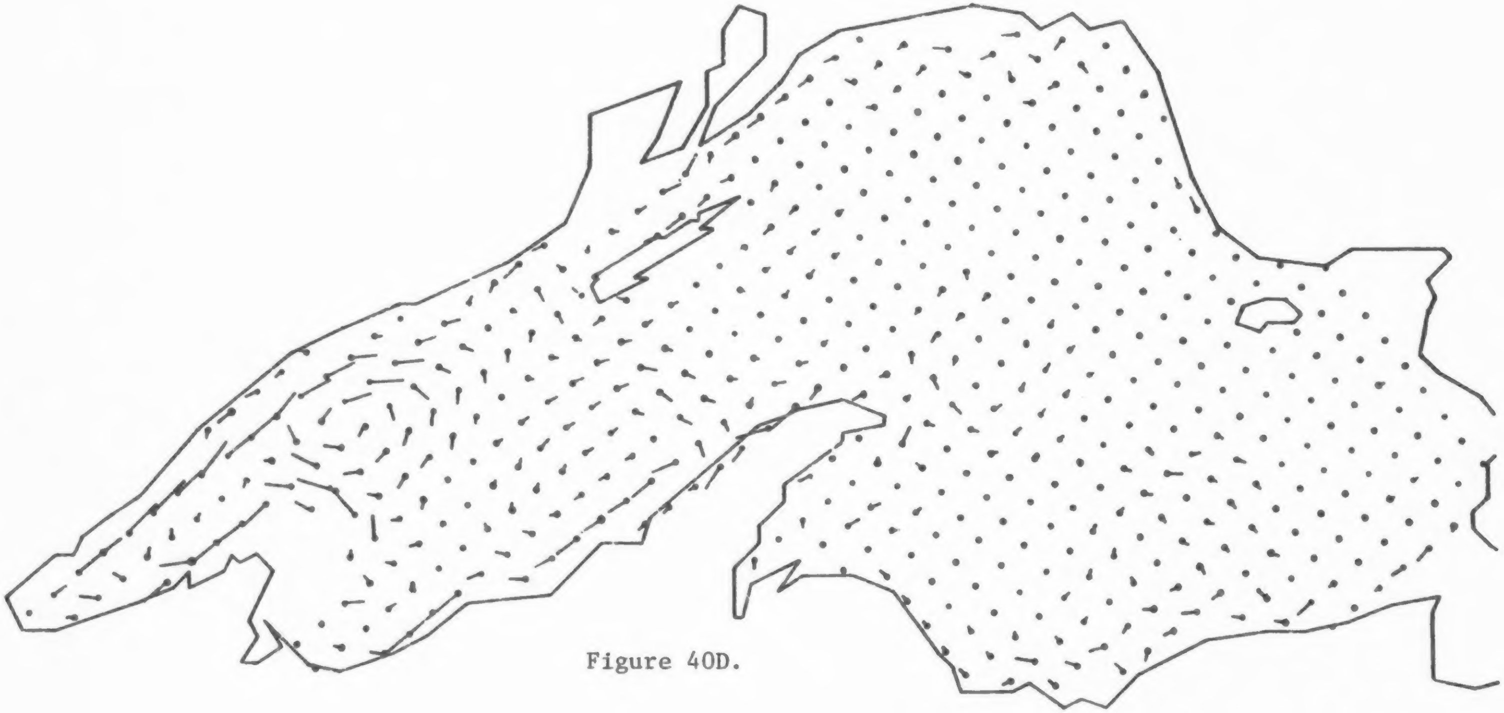

Figure 40D.

LAKE SUPERIOR
13M/SEC N.E.

TRANSPORTS FROM RUN 24
TIME = 36 6
AT = 180
SCALE 0.2 CM = 3.003M^2/SEC

Figure 40. (continued)

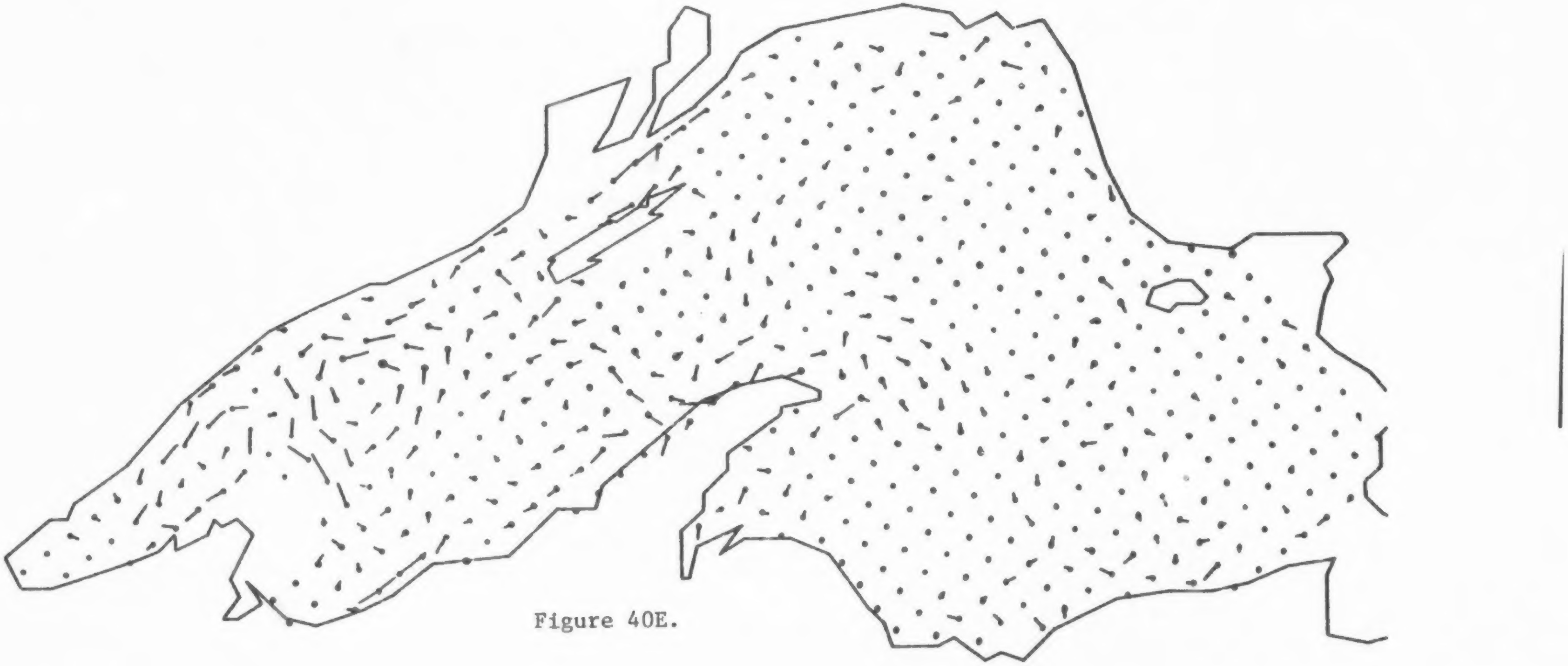

Figure 40E.

LAKE SUPERIOR
13M/SEC N.E.

TRANSPORTS FROM RUN 28
TIME = 60 6
AT = 180
SCALE 0.2 CM = 3.003M^2/SEC

Figure 40. (continued)

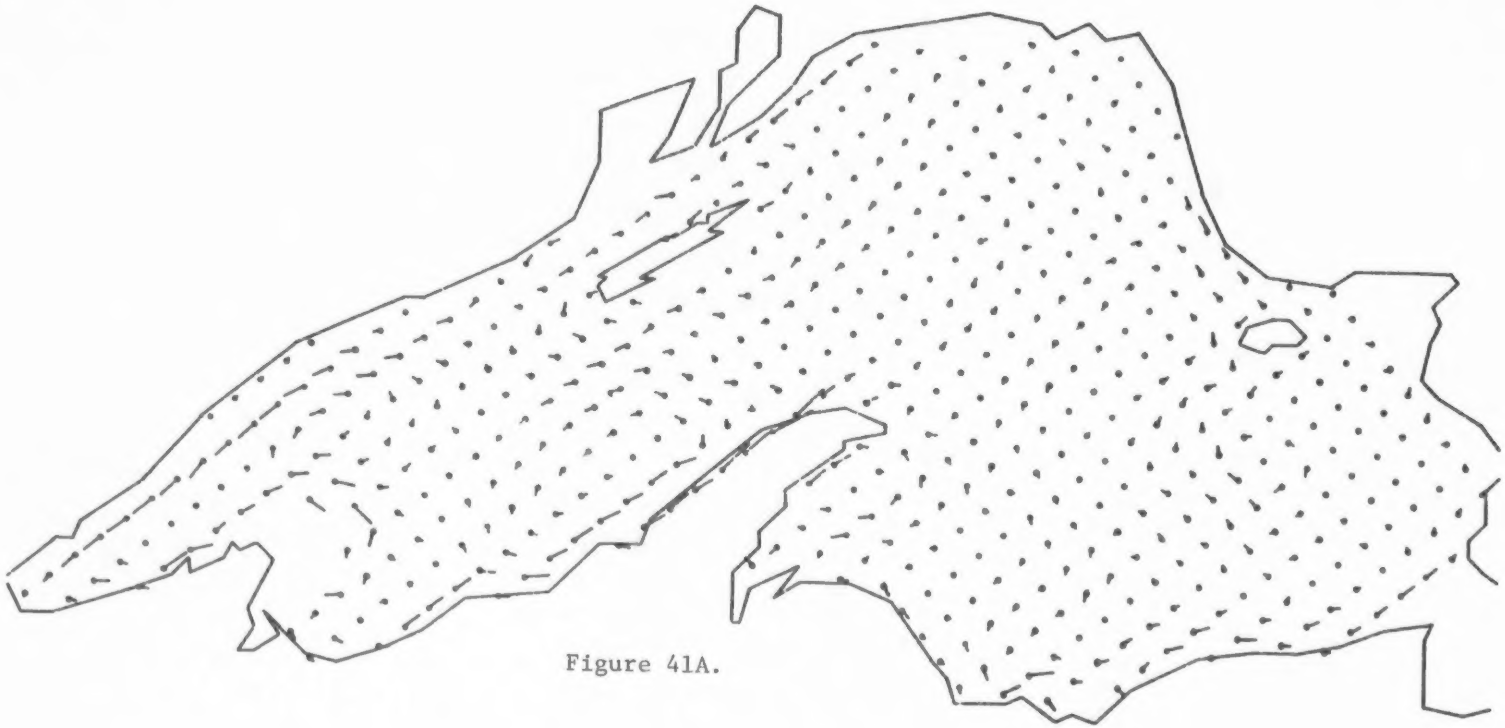

Figure 41A.

LAKE SUPERIOR
11 M/SEC W.
TRANSPORTS FROM RUN 21.
TIME = 18 18
AT = 180.
SCALE 0.2 CM = 1.000M^2/SEC

Figure 41. Entire Lake Superior transports from a 11 m/s westerly wind.

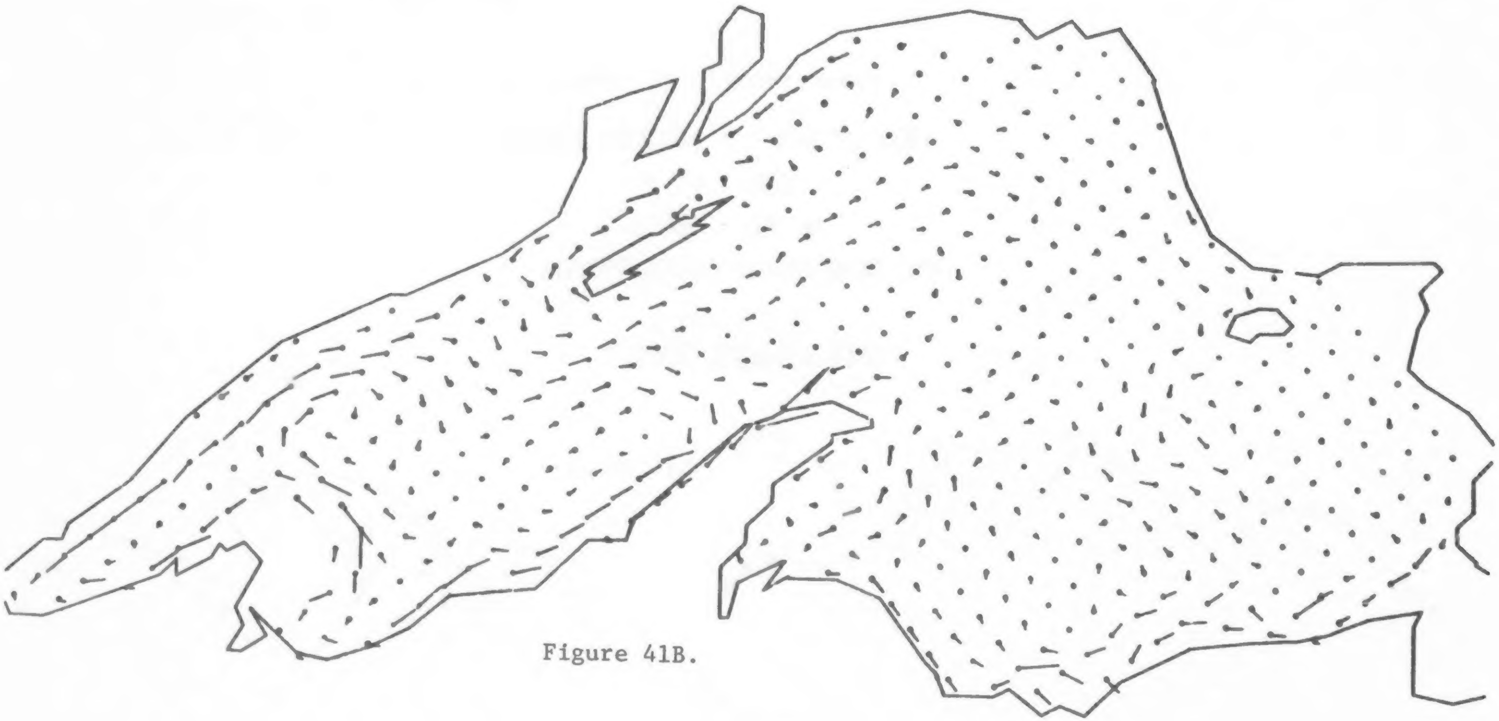

Figure 41B.

LAKE SUPERIOR
11 m/sec W.
TRANSPORTS FROM RUN 23.
TIME = 30 30
AT = 180.
SCALE 0.2CM = 2.000M^2/SEC

Figure 41. (continued)

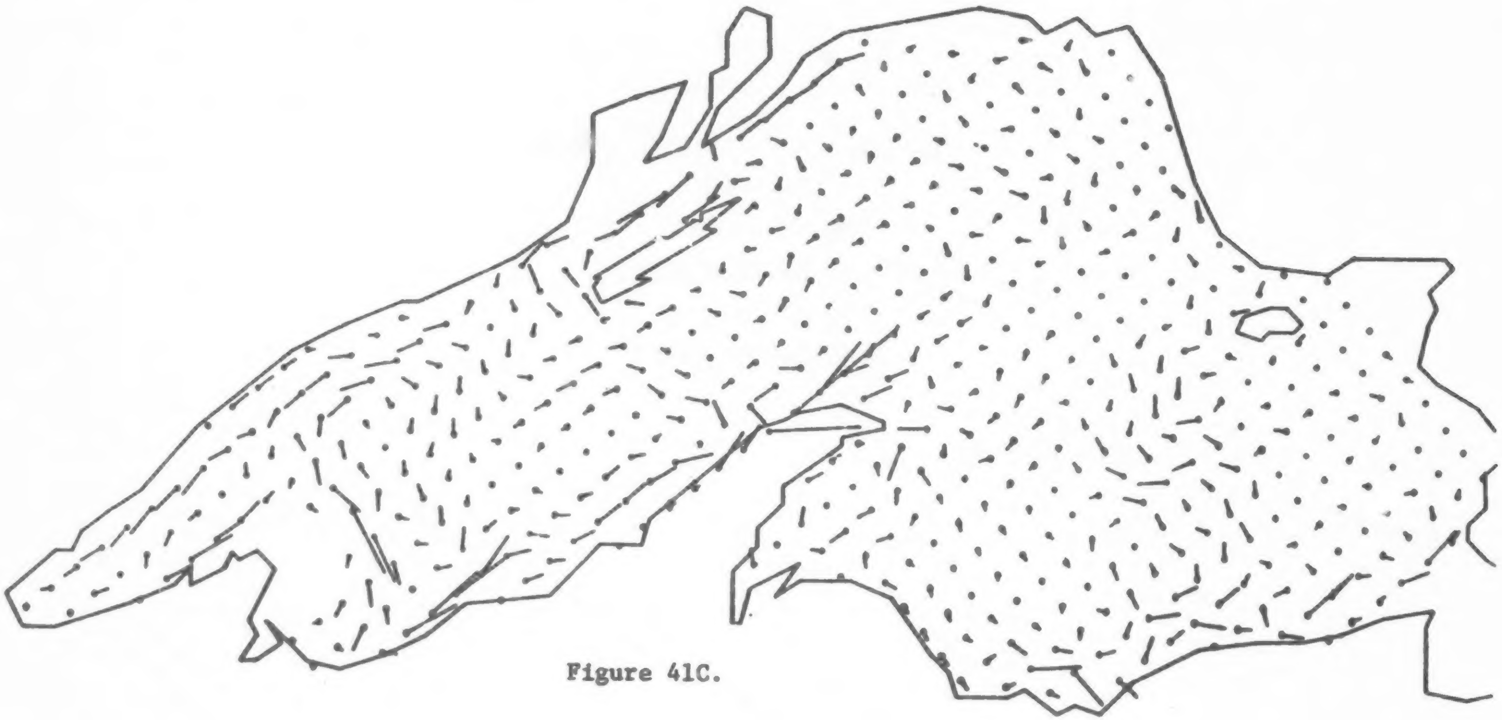

Figure 41C.

LAKE SUPERIOR
11 M/SEC W.

TRANSPORTS FROM RUN 30
TIME = 42 6
AT = 180
SCALE 0.2 CM = 1.499 M^2/SEC

Figure 41. (continued)

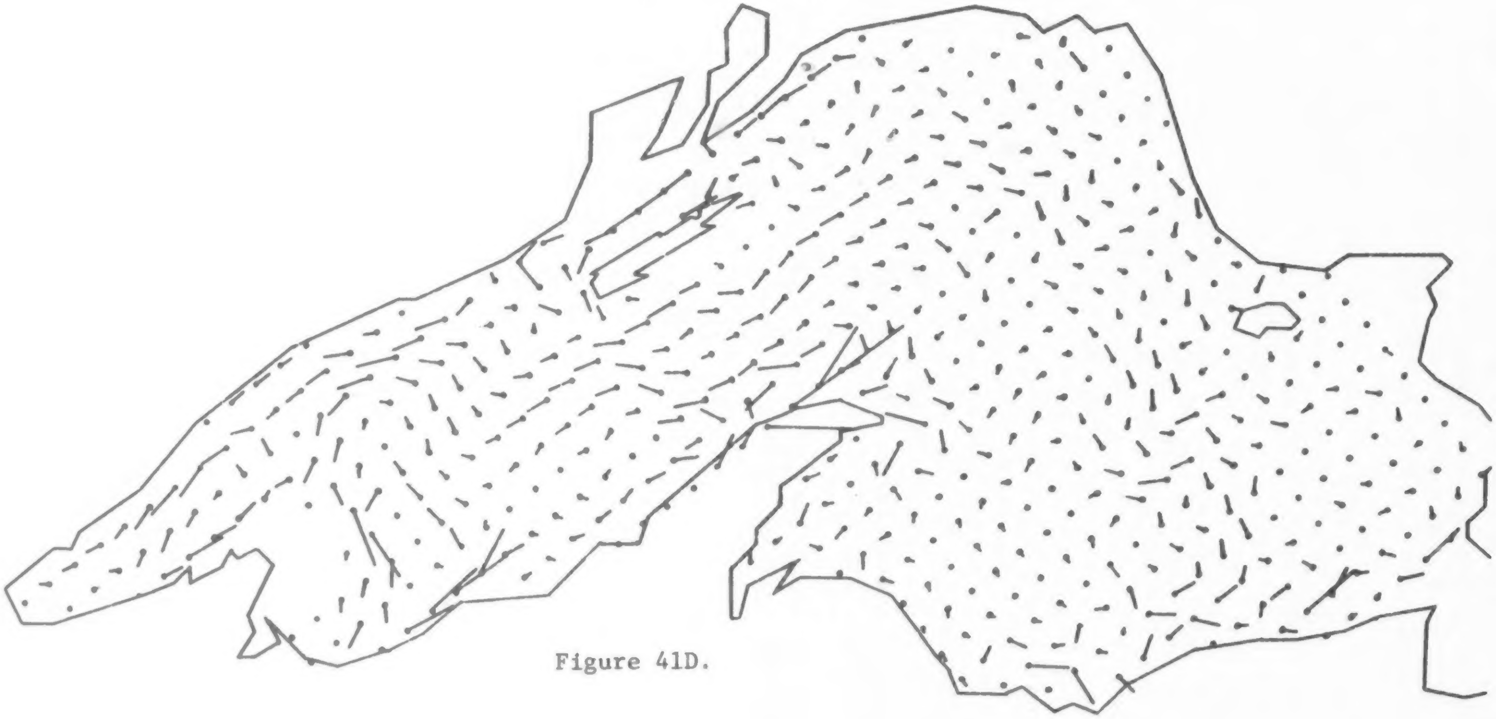

Figure 41D.

LAKE SUPERIOR
11M/SEC W.
TRANSPORTS FROM RUN 31
TIME = 48 6
AT = 180
SCALE 0.2 CM = 1.499M^2/SEC

Figure 41. (continued)

eddies seen southwest of Isle Royale, Figures 40D and 40E. Although it is difficult to say, the tailings might then work their way toward the Thunder Bay area, aided by the mixing processes and dispersion. Further studies pertaining to the distribution of currents with depth and a long-duration concentration model would shed more light on the problem.

According to the model, the rapid, well-confined transport of tailings from Silver Bay is possible only to the Duluth area and the Apostle Islands, for the wind stresses considered here. Similarly, the red clay particles tend to be confined in high concentrations to far western Lake Superior or are transported around the Apostle Islands. Thus, high concentrations of the contaminants are generally confined to western Lake Superior. Another major transport structure in the lake for the conditions modeled here is a circulation cell off the Keweenaw Peninsula, where large transport values are evident. This circulation cell for westerly winds is shown in Figure 41. Figure 41C shows a counterclockwise loop, with extremely high transports along the northern shore of the peninsula. Particles dispersing from Silver Bay could be carried around the Apostle Islands to the Keweenaw circulation cell. Comparison of currents at the south shore of the study area, where currents on the order of 20 cm/sec were measured, indicates that the currents along the Keweenaw would correspond to 40 - 60 cm/sec. Large transports are also evident in Figure 41C in the strait between the North Shore and Isle Royale but are of no direct interest here. The westerly winds in the nearshore zone show transports directly away from the shore at Silver Bay.

Lake-level data from the model for the points shown in Figure 42 are presented in Fourier Analysis form in Figures 29 and 43.

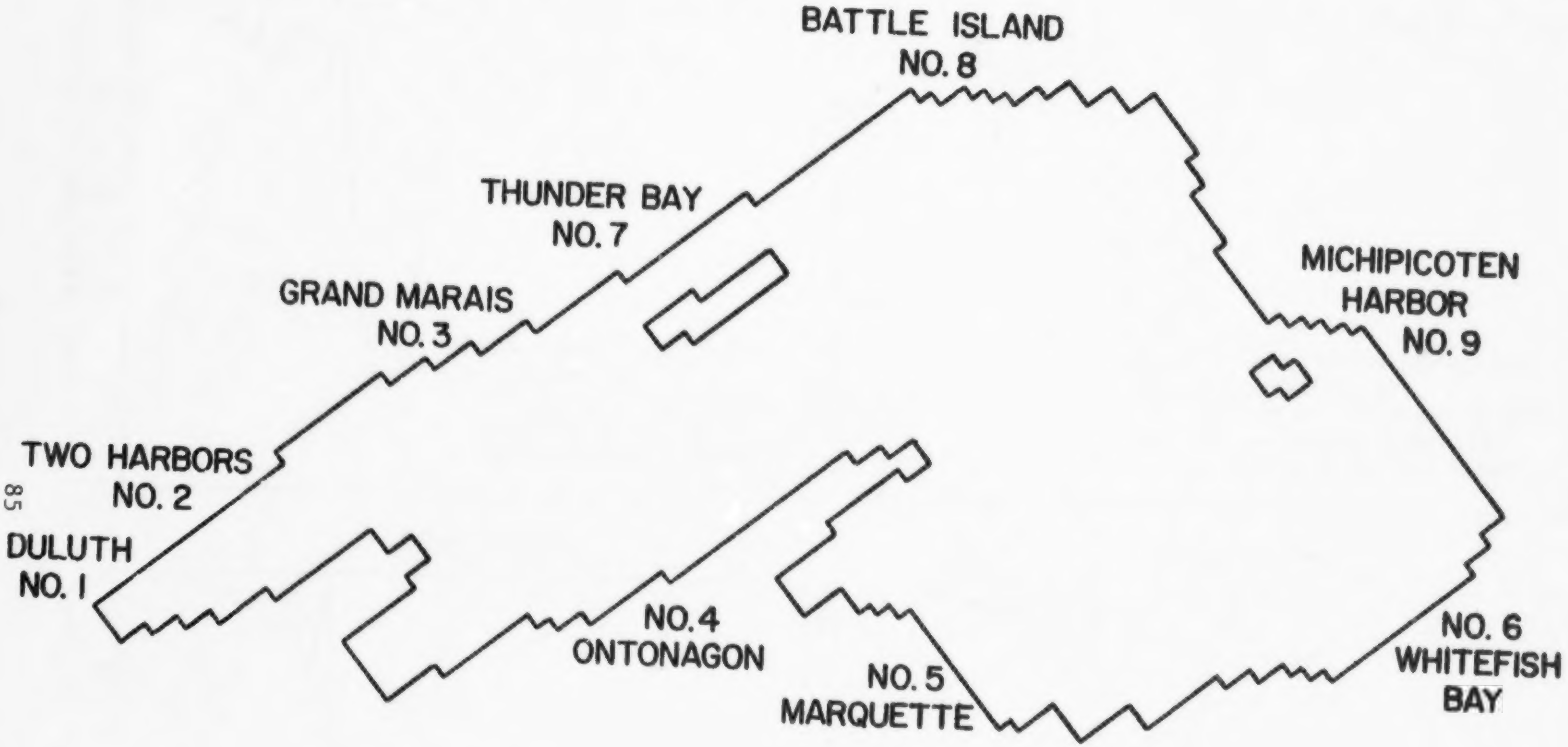
BATTLE ISLAND
NO. 8
THUNDER BAY
NO. 7
GRAND MARAIS
NO. 3
TWO HARBORS
NO. 2
DULUTH
NO. 1
MICHIPICOTEN
HARBOR
NO. 9
NO. 4
ONTONAGON
NO. 5
MARQUETTE
NO. 6
WHITEFISH
BAY

Figure 42. Lake Superior water-level station locations.

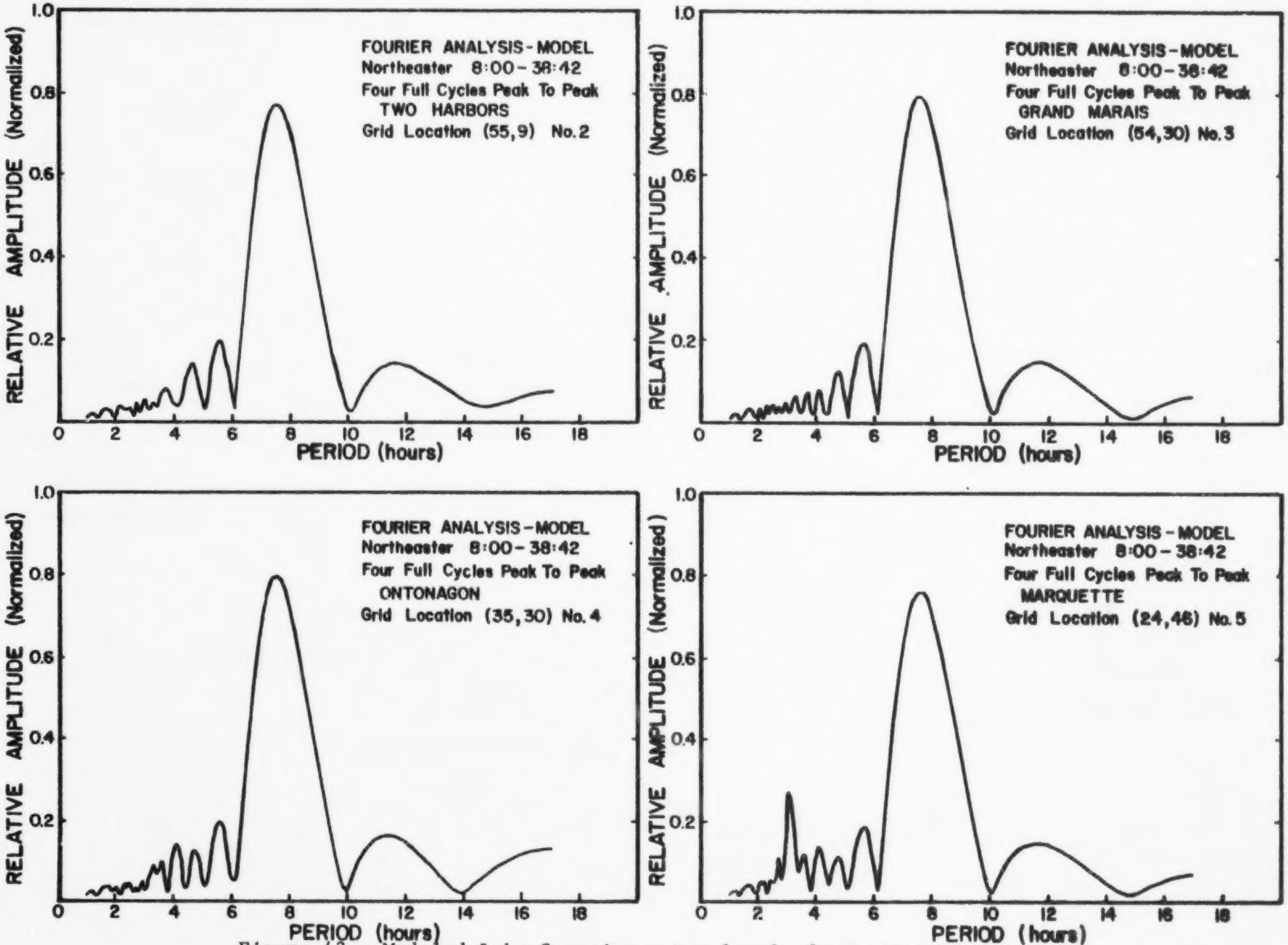

Figure 43. Modeled Lake Superior water levels from a northeast storm.

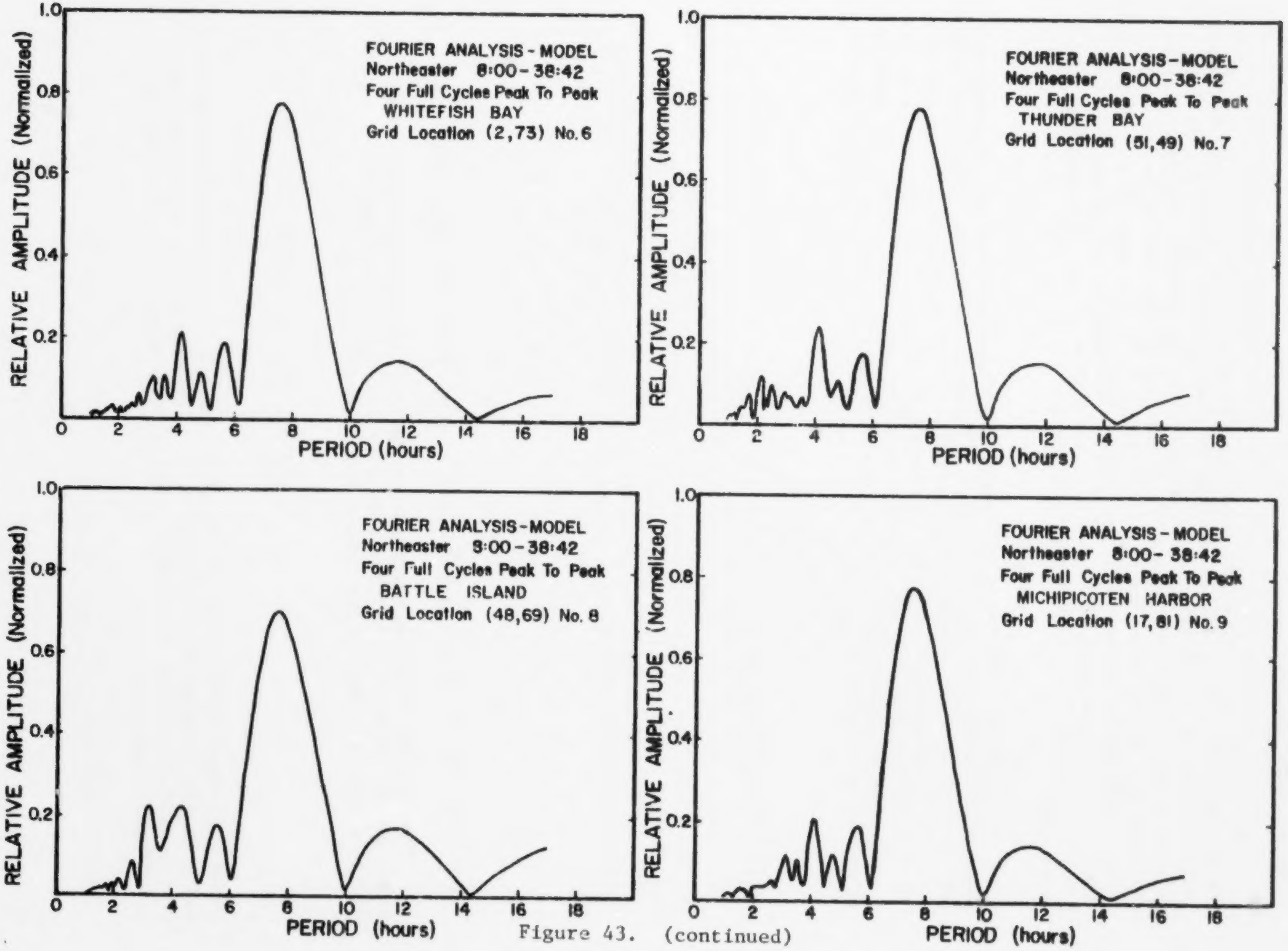

Figure 43. (continued)

CURRENT PROFILE MODEL

In the study of water circulation the vertically integrated currents, or transports, are useful in estimating general flow patterns and are a valuable aid in predicting the movement of a well-mixed sediment. However, little quantitative information about the magnitudes and directions of surface and bottom currents can be obtained from the transports. Multi-level finite difference schemes utilizing three-dimensional grids are possible, but these suffer from very large computer storage and time requirements. Also, such models lack vertical resolution due to the necessarily thick layers employed.

A different approach to the problem of finding transient, wind-driven current profiles with depth has been offered by Forristall (1974), in which the current profile at any point is evaluated by convolution integrals over the wind-stress and water-slope histories at that point. A unique solution is obtained without the use of the continuity equation. Thus, the need for a large three-dimensional grid is dispensed with and the currents need be evaluated only where desired.

Mathematical Formulation

Let the complex variable $w = u + iv$ where u and v are the x and y components of velocity in a cartesian coordinate system with $z = 0$ at the undisturbed water level and $z = H$ at the bottom. Neglecting vertical velocities and accelerations and non-linear terms, the equation for horizontal motion, which the currents are expected to satisfy, becomes

$$\frac{\partial w}{\partial t} = ifw - q + \nu\frac{\partial^2 w}{\partial z^2}$$

where f is the coriolis parameter and ν is the vertical eddy viscosity.

The complex variable q represents the horizontal pressure gradient which can be related to the surface slope through the assumption of hydrostatic pressure. Neglecting atmospheric pressure gradients

$$q = g\left(\frac{\partial h}{\partial x} + i\,\frac{\partial h}{\partial y}\right)$$

where h is the displacement of the water surface from the undisturbed level, and g is the gravitational acceleration. The solution is a superposition of the wind-driven and slope-driven contributions so that each case can be considered separately.

For the case of a pure drift current, we have

$$\frac{\partial w}{\partial t} = -ifw + \nu\frac{\partial^2 w}{\partial z^2}$$

with the boundary conditions

$$w(z = -H) = 0 \qquad \nu\frac{\partial w}{\partial z}\,(z = 0) = F(t) \qquad \frac{\partial^n w}{\partial t^n}\,(t = 0) = 0$$

where F(t) is the time-varying wind-forcing function. The solution used by Forristall is

$$w(t,z) = \frac{2}{H}\sum_{n=0}^{\infty}\cos\,[n+\tfrac{1}{2})\pi z/H]\int_0^t F(t-\tau)e^{-if\tau}e^{-(n+\frac{1}{2})^2\pi^2\nu\tau/H^2}d\tau$$

For a pure slope current

$$\frac{\partial w}{\partial t} = -ifw - q + \nu\frac{\partial^2 w}{\partial z^2}$$

with boundary conditions

$$w(z = -H) = 0 \qquad \frac{\partial w}{\partial z}\,(z = 0) = 0 \qquad \frac{\partial^n w}{\partial t^n}\,(t = 0) = 0$$

the solution is

$$w(t,z) = \frac{-2}{H}\sum_{n=o}^{\infty}\frac{(-1)^n}{[(n+\frac{1}{2})\pi/H]^2}\cos[(n+\tfrac{1}{2})\pi z/H]\int_0^t q(t-\tau)e^{-if\tau}e^{-(n+\frac{1}{2})^2\pi^2\nu\tau/H^2}d\tau$$

The solution for the pure drift current was actually found to contain three parts:

$$w(t,z) = F(t)\,\frac{sh[\gamma(H+z)]}{\nu\gamma ch[\gamma H]} \tag{i}$$

$$-\,F(t)\,\frac{1}{H\nu}\sum_{n=o}^{\infty}A_n\cos\,[(n+\tfrac{1}{2})\pi z/H] \tag{ii}$$

$$+\,\frac{2}{H}\sum_{n=o}^{\infty}\cos\,[(n+\tfrac{1}{2})\pi z/H]\int_0^t F(t-\tau)e^{-if\tau}e^{-(n+\frac{1}{2})^2\pi^2\nu\tau/H^2}d\tau \tag{iii}$$

where $$A_n = 2\frac{\beta_n^2 - \gamma^2}{\beta_n^4 + f^2/\nu^2}$$

$$\gamma = (if/\nu)^{\frac{1}{2}}$$

$$\beta_n = (n+\tfrac{1}{2})\pi/H$$

All three parts are needed to satisfy the differential equation, but parts (i) and (ii) cancel each other in the sense that part (ii) is a Fourier series for part (i). All three parts satisfy the conditions that $w(z = -H) = 0$ and $w(t = 0) = 0$. Part (i) satisfies the surface boundary condition $\nu\frac{\partial w}{\partial z}(z = 0) = F(t)$ with no contribution from parts (ii) and (iii). Part (iii) has been used alone for a good numerical approximation to the solution even though it does not match the surface boundary condition explicitly. However, numerical calculations show that the slope $\frac{\partial w}{\partial z}$ approaches the boundary value $\nu^{-1}F(t)$ a small distance δz away from $z = 0$. As seen in Figure 44, δz decreases but apparently never vanishes for increasingly large values of N, the upper limit on the series.

Treatment of Time Integral

The time integrals appearing in the solutions are uneconomical in their present form for numerical evaluation of the currents. For example, to calculate the currents at two times T_1 and T_2, where $T_2 > T_1$, the effort done in evaluating the integral from time 0 to T_1 must be repeated to do the integral from 0 to T_2. Therefore, a recursion formula was developed for the computer program which allowed the integral to be evaluated at a series of equally spaced times, without wasted computation. This was done by writing the time integral from 0 to some time $T_k = k\Delta T$ as a sum of k integrals over equally spaced intervals 0 to T_1, T_1 to T_2, etc. Making a change in the integration variable, which allowed the values of the wind function and water slopes to progress forward in time, yielded

$$C_k = \int_0^{T_k} F(T_k - \tau)e^{-\theta_n \tau}d\tau$$

$$= \int_{T_{k-1}}^{T_k} F(t)e^{-\theta_n(T_k - \tau)}dt + e^{-\theta_n \Delta T}C_{k-1}$$

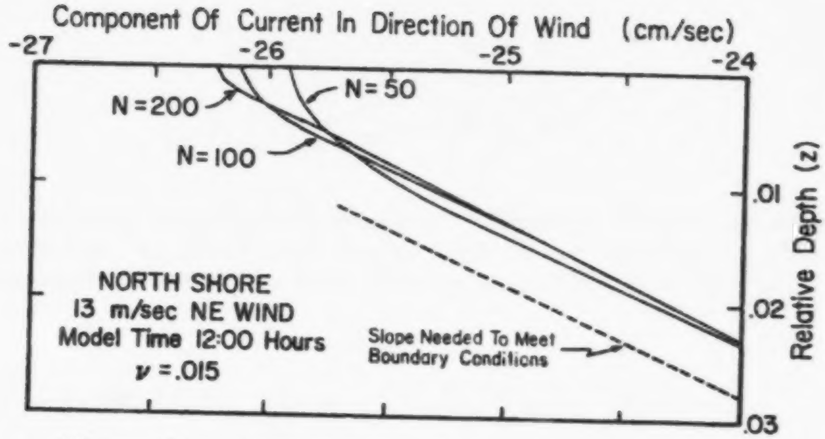

Figure 44. Current vs. relative depth near surface.

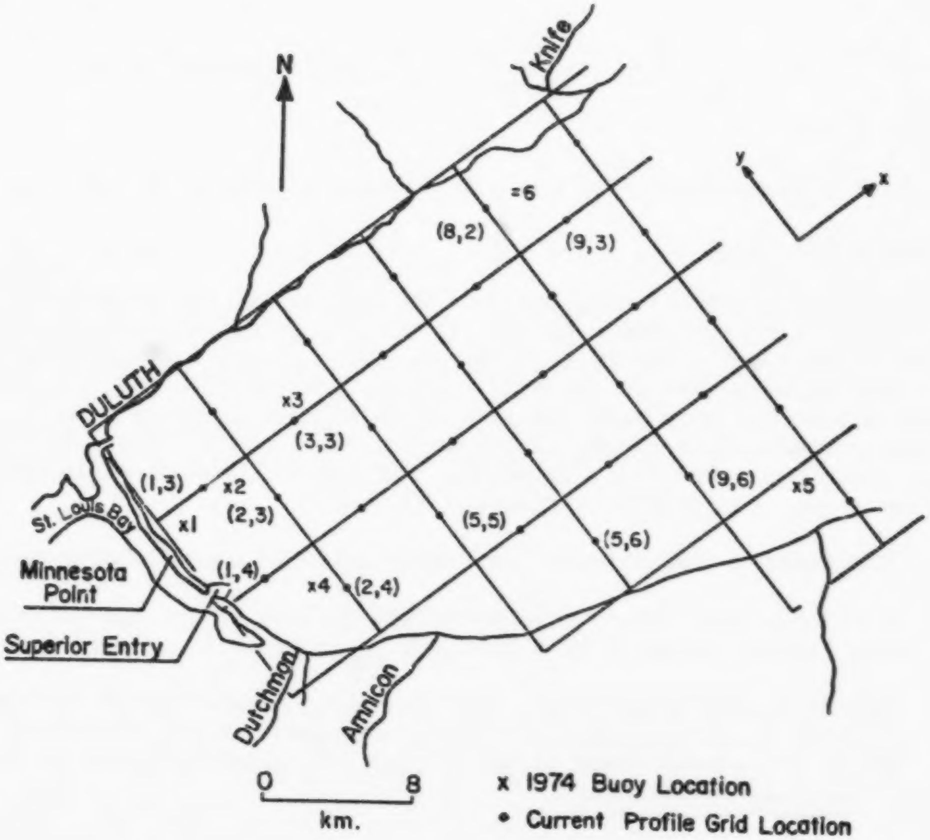
N
Knife
y
x
=6
(8,2)
(9,3)
DULUTH
x3
(3,3)
(1,3)
x2
St. Louis Bay
x1
(2,3)
(5,5)
(9,6)
x5
(5,6)
Minnesota Point
(1,4)
x4
(2,4)
Superior Entry
Dutchman
Amnicon
0
8
km.
x 1974 Buoy Location
• Current Profile Grid Location

Figure 45. Current meter station locations.

where

$$C_o = 0$$

$$\theta_n = if + \nu\beta_n^2$$

Assuming that F(t) changes slowly over the small interval from T_{k-1} to T_k made it possible to further reduce the effort in obtaining the integral by approximating it in closed form using the average value of F(t) over that interval:

$$\int_{T_{k-1}}^{T_k} F(t)e^{-\theta_n(T_k-t)} \simeq \bar{F} \int_{T_{k-1}}^{T_k} e^{-\theta_n(T_k-t)}dt$$

$$= \frac{\bar{F}}{\beta_n^4\nu^2+f^2} [e^{-\beta_n^2\nu\Delta t}(-\beta_n^2\nu\cos f\Delta T+f\sin f\Delta T) + \beta_n^2\nu]$$

$$- \frac{i\bar{F}}{\beta_n^4\nu^2+f^2} [e^{-\beta_n^2\nu\Delta T}(-\beta_n^2\nu\sin f\Delta T-f\cos f\Delta T) + f]$$

The time integral involving the water slopes is treated in the same manner.

Modeling Procedure

Six current-monitoring stations were set up in the western tip of Lake Superior during the summer months of 1974, to provide data for the calibration of the model. Figure 45 shows the locations of the current-meter stations superimposed on the grid used for the current profile model. Surface currents were measured at a depth of approximately 2 meters and bottom currents at a height of 1.8 meters above the lakebed. Stations 1, 2, and 4 were monitored for both surface and bottom currents while only surface currents were recorded at stations 3, 5, and 6.

The current profile model was implemented in the following manner:

1) First, the Rand Corporation model was applied to the entire Lake Superior basin using a grid of 81 x 56 depth locations with a spacing of 6 km.

2) Time-dependent water levels and transports were computed for the northeast and westerly winds, previously described in the section on transports, and stored every 12 minutes for the points located in the western arm of the lake.

3) The resulting water-level histories were spatially interpolated and extrapolated to obtain the x and y components of the water slope at each of the transport locations, and these values were stored for use by the current model.

4) Finally, the current profile model was run, using the previously obtained water slopes and the original wind-forcing functions to predict currents in the western arm. Special attention was given to points at or near locations where current meter data were available.

Before the model could be used, it was necessary to better understand the effects of the vertical-eddy viscosity ν. Figure 46 shows the computed current profiles using two different values of ν. The surface currents are displaced to the right of the wind due to coriolis effects, and the subsurface currents rotate clockwise with depth in a modified Ekman spiral, causing a reversal of the currents near the bottom. Raising the viscosity has the effect of decreasing the currents and somewhat altering the shape of the profile. Lower viscosities decrease the momentum transfer between layers of water, tending to uncouple the surface and bottom currents and also to decrease the bottom drag. Thus, in the case of Figure 46, both the surface current and bottom-return current increase while the transport changes only slightly.

Because little is known about the actual value of the vertical-eddy viscosity, the current model was "calibrated" by varying ν and matching predicted surface current speeds with measured values in the lake. A comparison of peak surface currents versus corrresponding wind speeds is shown in Figure 47. Stations 2 and 3 were selected because they are most likely to be free from shore effects for northeast winds. Some of the scatter in the points is probably caused by the fact that the wind measurements, obtained from the Duluth Coast Guard, were generally taken only at 6-hour intervals, so little is known about their speeds and directions in the interim period. Also the surface-current measurements, although averaged hourly, are expected to be influenced by the violent wave turbulence caused by higher winds. The relationship between the wind speeds and the surface-current speeds is a complicated one which depends on the wind stress, wind duration, total depth of the water, wave height, and vertical-eddy viscosity. In reality, the value of the vertical-eddy viscosity must also vary as a function of depth because of turbulence. When a wind stress appears over the water, a turbulent surface layer associated with wave action is developed, which implies a large surface-eddy viscosity. Deeper, the flow becomes more laminar implying a lower eddy viscosity. At the bottom the eddy viscosity may increase somewhat due to a thin layer of turbulence where the current speeds suddenly approach zero. In the current profile model, the vertical-eddy viscosity parameter had to be taken as a constant in order to find a solution to the differential equation. To calibrate the model, a value of .007 m^2/sec was used for ν, which yielded peak currents at the depth of the surface meters of about 36 cm/sec near stations 2 and 3 for the modeled 13 m/sec (30 mph) northeast wind.

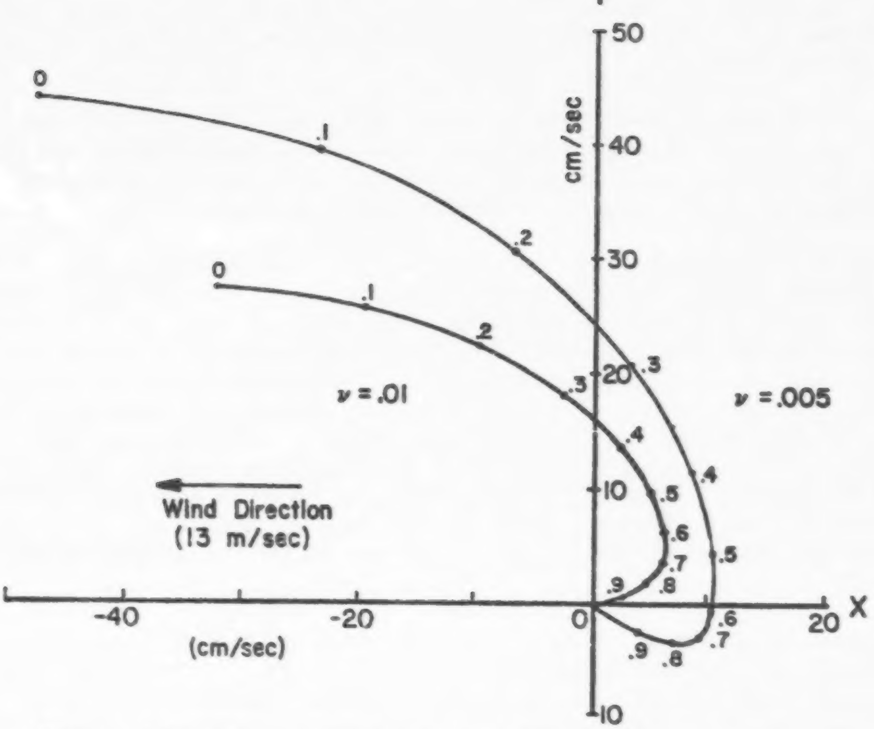

Figure 46. Current profiles for two values of ν. Vectors plotted every one-tenth of the relative depth.

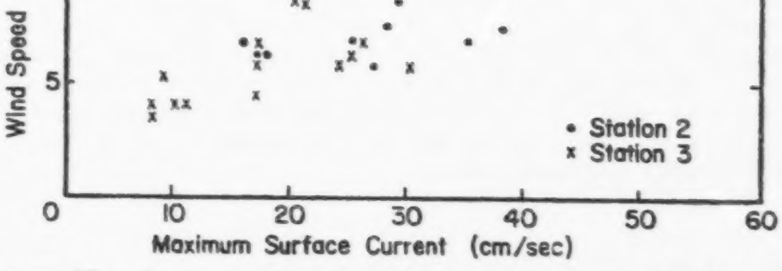

Figure 47. Peak measured surface currents vs. wind speed for several northeast winds.

Results

A detailed analysis of the model on currents is treated elsewhere (Maanum, 1977). The primary need for modeling currents came from the interest in movement of the sediment after its resuspension from major sediment deposition areas in the vicinity of the harbor entries and from dredging disposal areas. It is seen from Figure 48 that for the times of high turbulence, the bottom currents for westerly winds would transport the bottom layer of water towards the northeast shore, indicating an upswelling along that shore. For a small area east of the Superior entry, however, the bottom currents point towards Dutchman Creek, making this location a more suitable dredging disposal site from the standpoint of currents.

For the northeasterly winds, the bottom layer of water generally moves out in an easterly direction similar to the transport patterns near the axis of the arm. The results for the wind directions modeled here generally confirm the measured current patterns. The bottom currents treated here pertain to thermally unstratified conditions which are important in questions of the occurrence of high turbidity and dredging disposal.

TURBIDITY TRANSPORT MODEL

A combination of 1) transports from the numerical model, 2) information on the erosion along the south shore, and 3) turbidity settling measured in the lab, Figure 49, produced the preliminary information needed for the numerical modeling of turbidity transport and location of the settling areas which become potential resuspension sources. A nearly maximum severity condition was modeled. This entailed northeasterly winds at 13 m/sec (30 mph) for 40 hours, followed by a lull in the wind and a subsequent westerly wind patterned after actual weather observations. The boundary conditions for the model were as follows: Erosion took place at a uniform rate throughout the northeasterly wind, with the distribution along the south shore provided from data on the relative shore erosion rates. Because of the high turbulence no settling was allowed during the easterly, but at the end of the storm a settling rate was applied everywhere except at the source locations. The turbidity-source locations consisted of 1.5 x 3 kilometer blocks, i.e. half a grid square, staggered adjacent to the south shore. (More experimental work on the boundary conditions is essential for further detailed turbidity modeling.) In a sense, the horizontal eddy diffusivity process was automatically taken into account by the unavoidable mixing after each time step of the influx of higher turbidity from adjacent cells, with the suspended load already present in a particular grid space. The flux of turbidity into each grid space was determined by the transports and concentration in neighboring cells. The results for the turbidity plumes are shown in Figure 50 at various stages of the storm. The total suspended load for red clay is 1.3×10^6 metric tons, resulting from an input of 500 mg/ℓ constant suspended load at a source point at Amnicon which is comparable to real values for such storms. This value of total suspended load is roughly equal to ∿ 25% of the yearly lakeshore

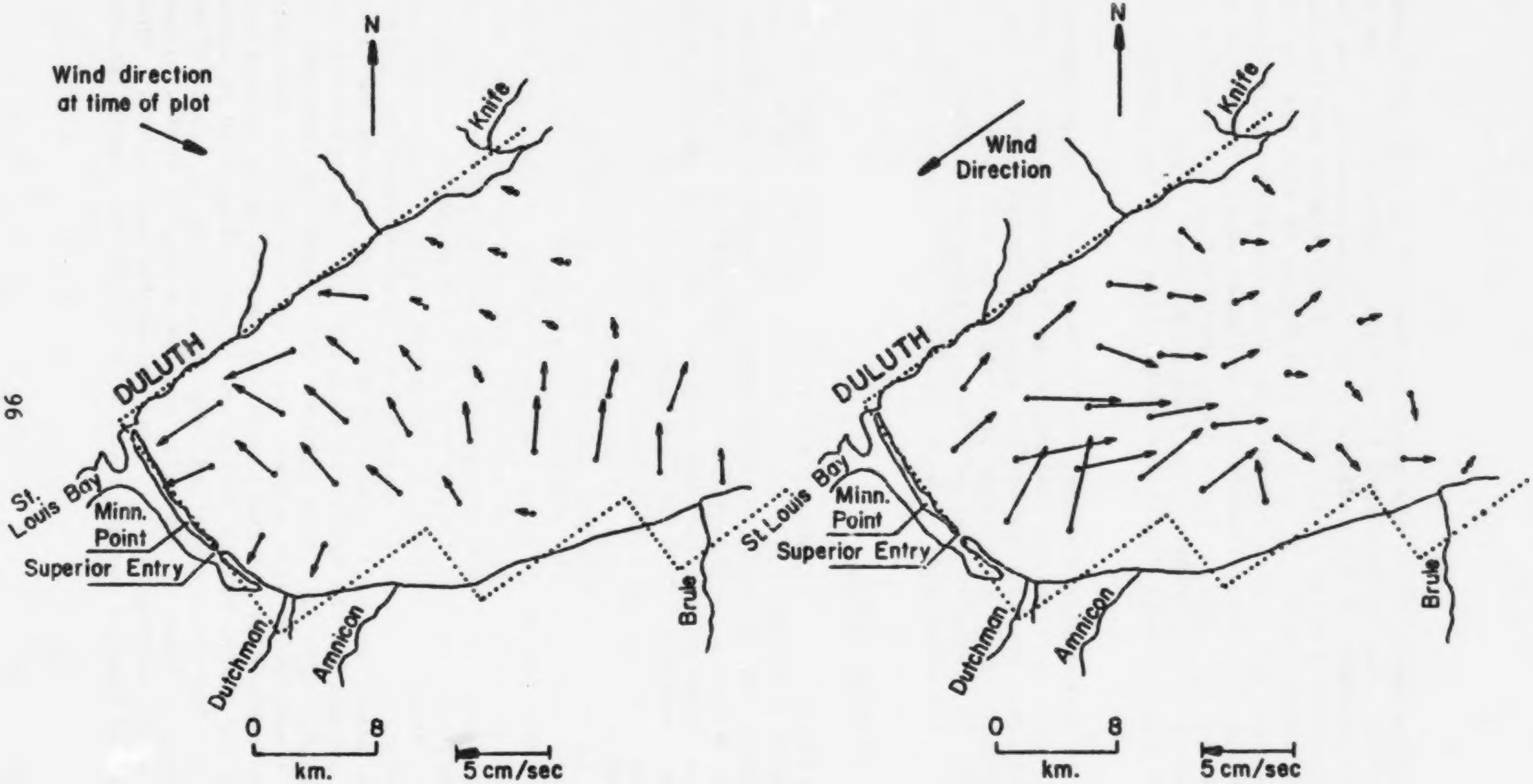
Wind direction at time of plot
N
Knife
DULUTH
St. Louis Bay
Minn. Point
Superior Entry
Dutchman
Amnicon
Brule
0
8
km.
5 cm/sec
Wind Direction
St. Louis Bay

Figure 48. Computed bottom currents near Duluth measured 1.8 m above the lake bed after 24 hours of west wind and 30 hours of east wind.

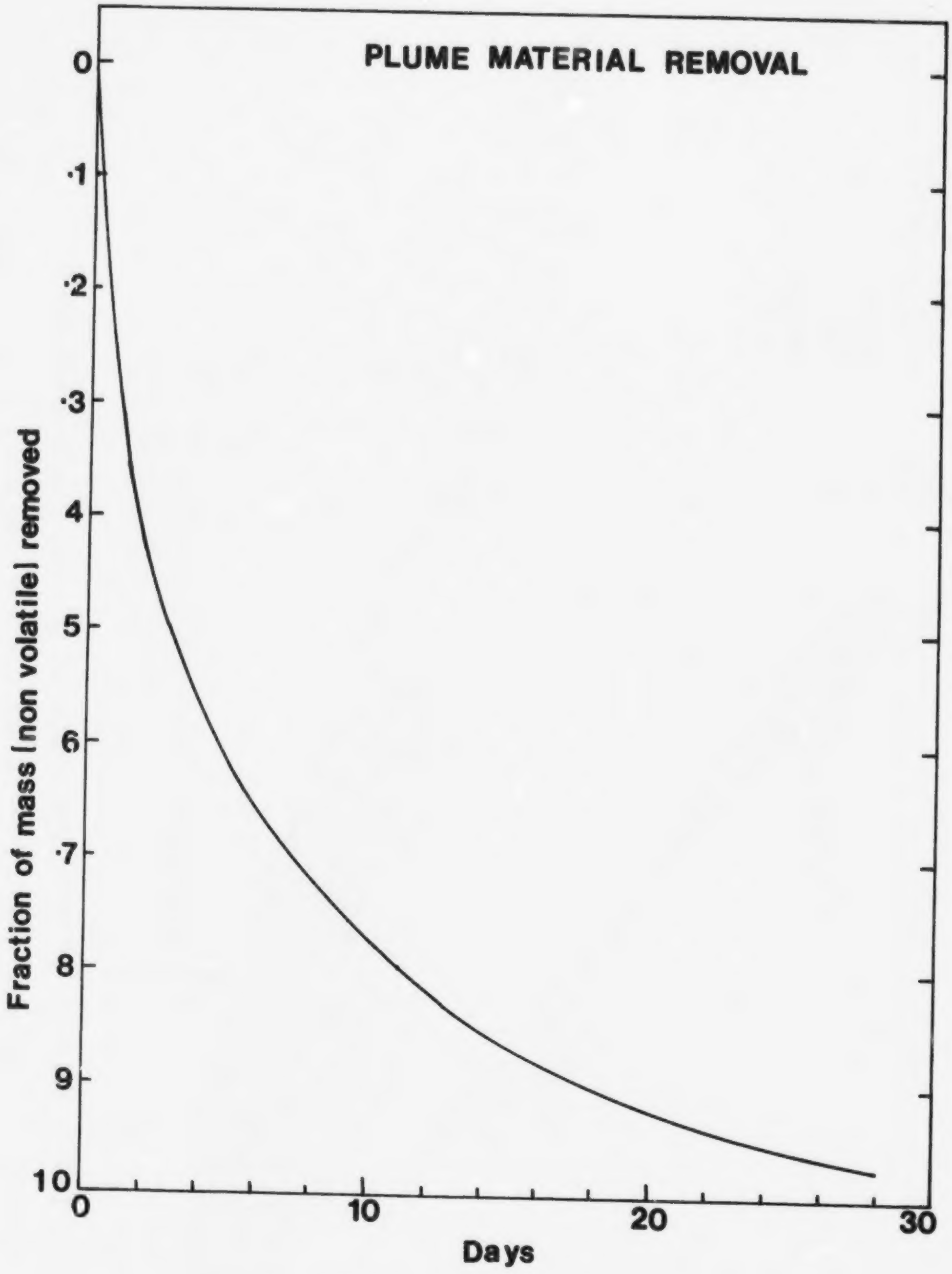

Figure 49. Lake sample settling in lab.

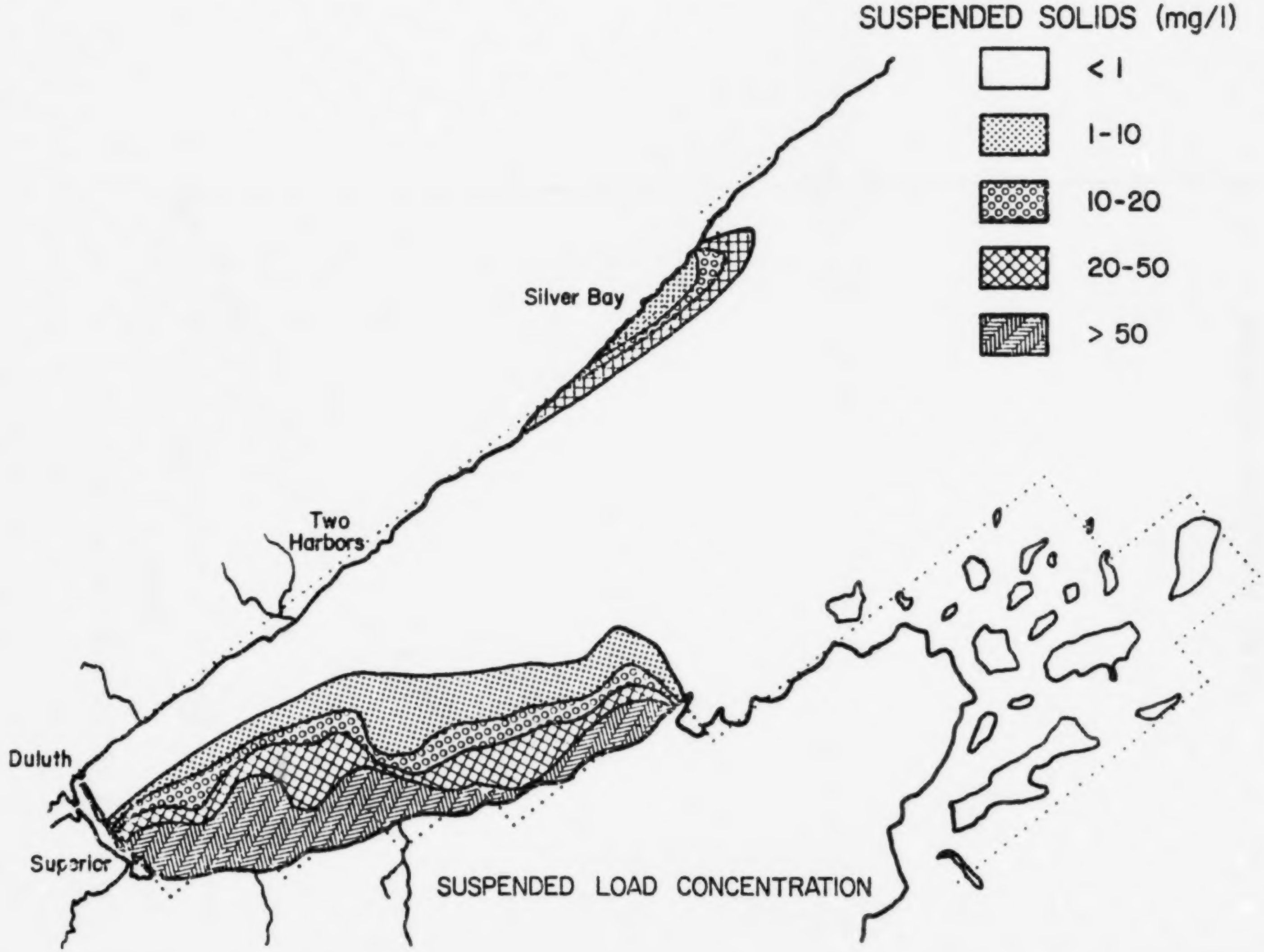
SUSPENDED SOLIDS (mg/l)
< 1
1-10
10-20
20-50
> 50
Silver Bay
Two Harbors
Duluth
Superior
SUSPENDED LOAD CONCENTRATION

MODEL TIME = 42 hours (2 hours into decay of 13 m/sec Northeasterly Wind)

Figure 50. Modeled suspended solids distribution at several stages of the storm.

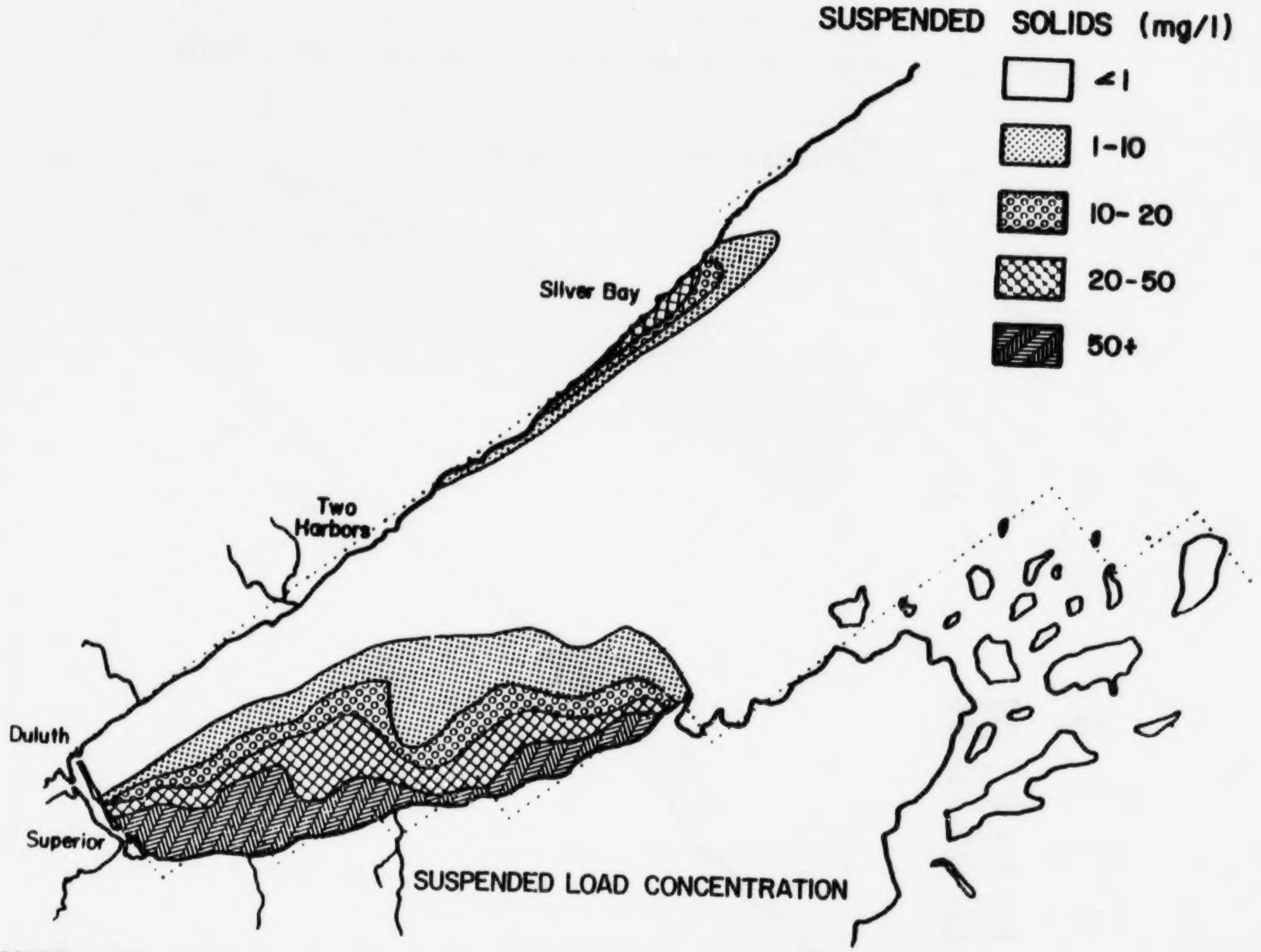
SUSPENDED SOLIDS (mg/l)
<1
1-10
10- 20
20-50
50+
Silver Bay
Two Harbors
Duluth
Superior
SUSPENDED LOAD CONCENTRATION

MODEL TIME = 60 hours (12 hours after end of 13 m/sec Northeasterly Wind)

Figure 50. (continued)

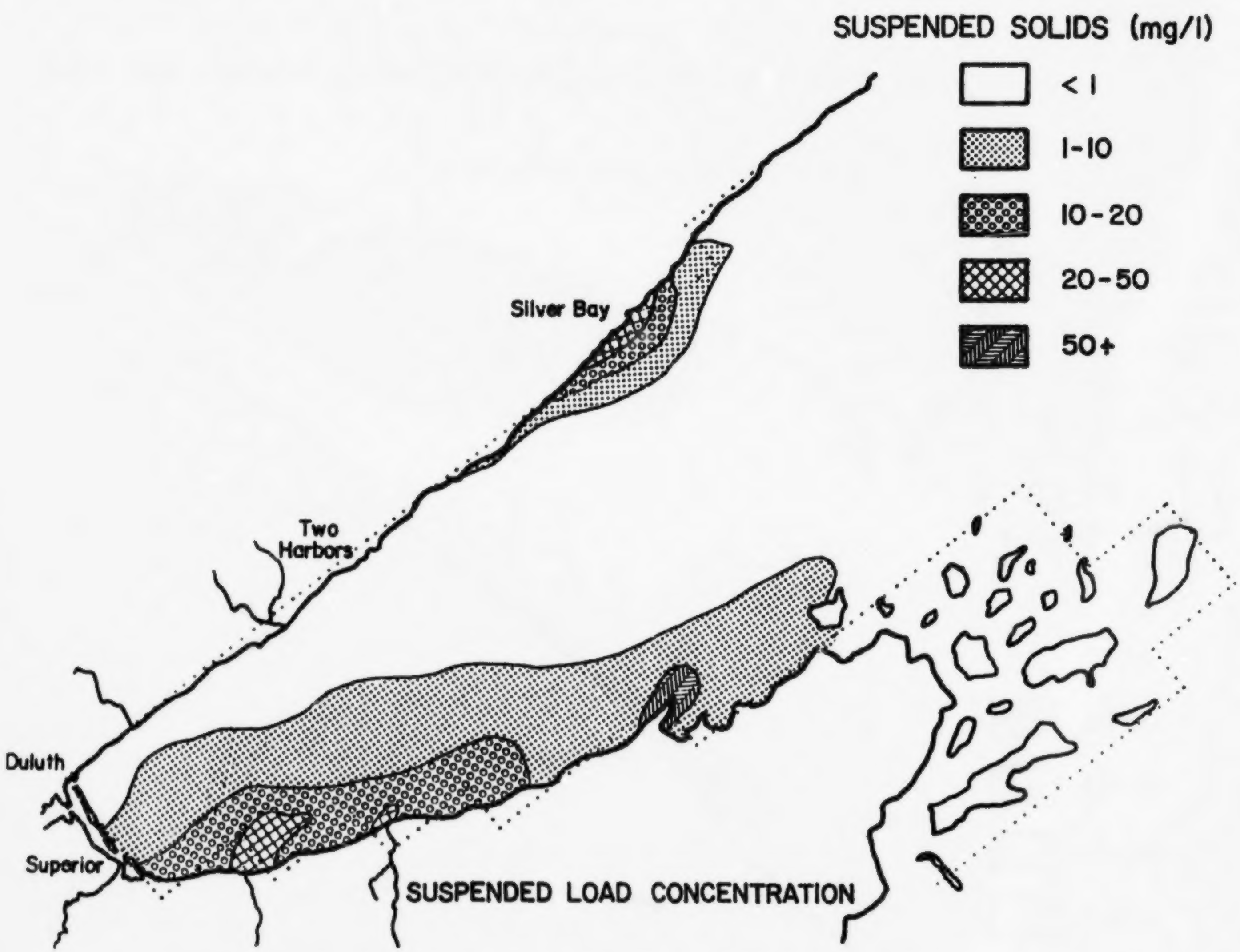
SUSPENDED SOLIDS (mg/l)
< 1
1-10
10-20
20-50
50+
Silver Bay
Two Harbors
Duluth
Superior
SUSPENDED LOAD CONCENTRATION

MODEL TIME = 120 hours (18 hours after end of 11 m/sec Westerly Wind)

Figure 50. (continued)

erosion input from the entire red clay bank erosion in Douglas and Bayfield Counties. Experimental data indicate that the major portion of the erosion takes place during three to five severe northeasterly storms occurring per season. It is interesting to compare the shape of calculated plumes to the plume observed in the Landsat image for April 3, 1975, Figure 51. This plume was due largely to resuspension in the near-shore areas of Douglas and Bayfield Counties and areas off Minnesota and Wisconsin Points. It looks much like the model plume. The deposition areas produced in this model are shown in Figure 52. Notice the high deposition rate east of the Superior entry to the Duluth-Superior Harbor, Figure 52A. The Nemadji River output is also near here ,though its load is normally transported in a southeasterly direction. On navigation charts and USGS maps, this area is shown as actually about 4 meters shallower than the adjacent areas of the lake. This roughly corresponds to about half of the amount of material which would be deposited there at the rates shown in Figure 52B, taking the age of the lake at 10,000 years. Of course, this is a rough result, probably fitting the data better than the roughness of the model deserves; yet it generally reflects the actual conditions quite well. Some available data on cores and sediment traps is yet to be analyzed and will possibly be done in the future. There is a general need for measurements necessary to describe the boundary conditions which would closely approximate the actual erosion source.

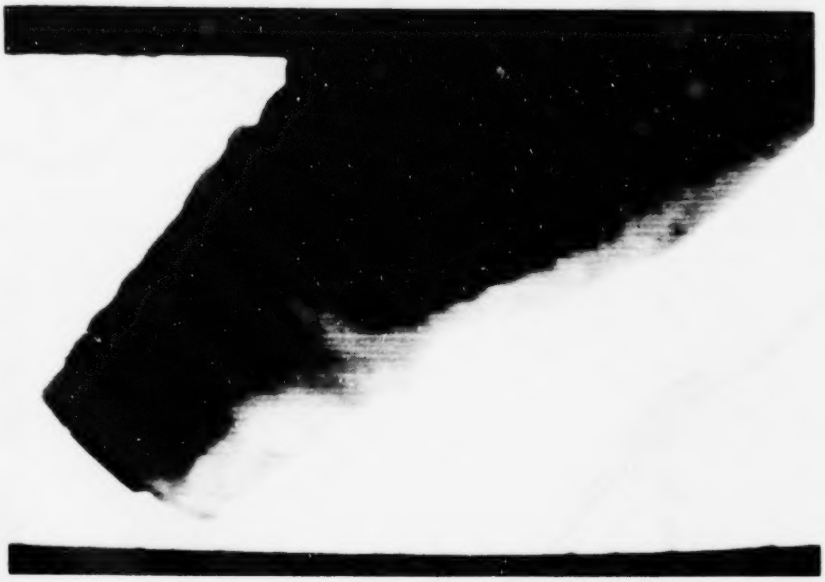

Figure 51. Landsat image for 03APR75.

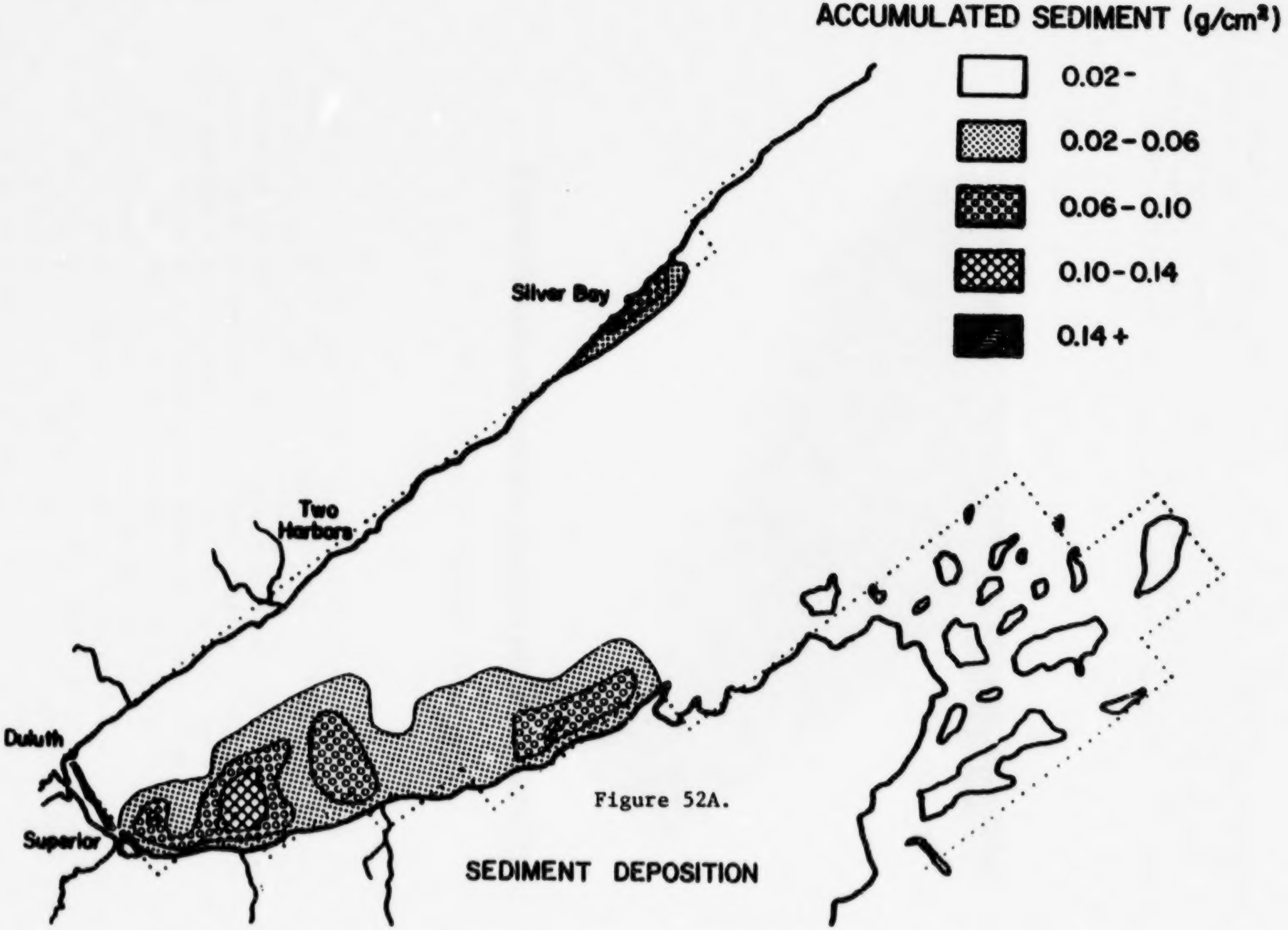
ACCUMULATED SEDIMENT (g/cm²)
0.02-
0.02-0.06
0.06-0.10
0.10-0.14
0.14+
Silver Bay
Two Harbors
Duluth
Superior
Figure 52A.
SEDIMENT DEPOSITION

MODEL TIME = 60 hours (12 hours after end of 13 m/sec Northeasterly Wind)

Figure 52. Modeled sediment accumulation at different stages of the storm.

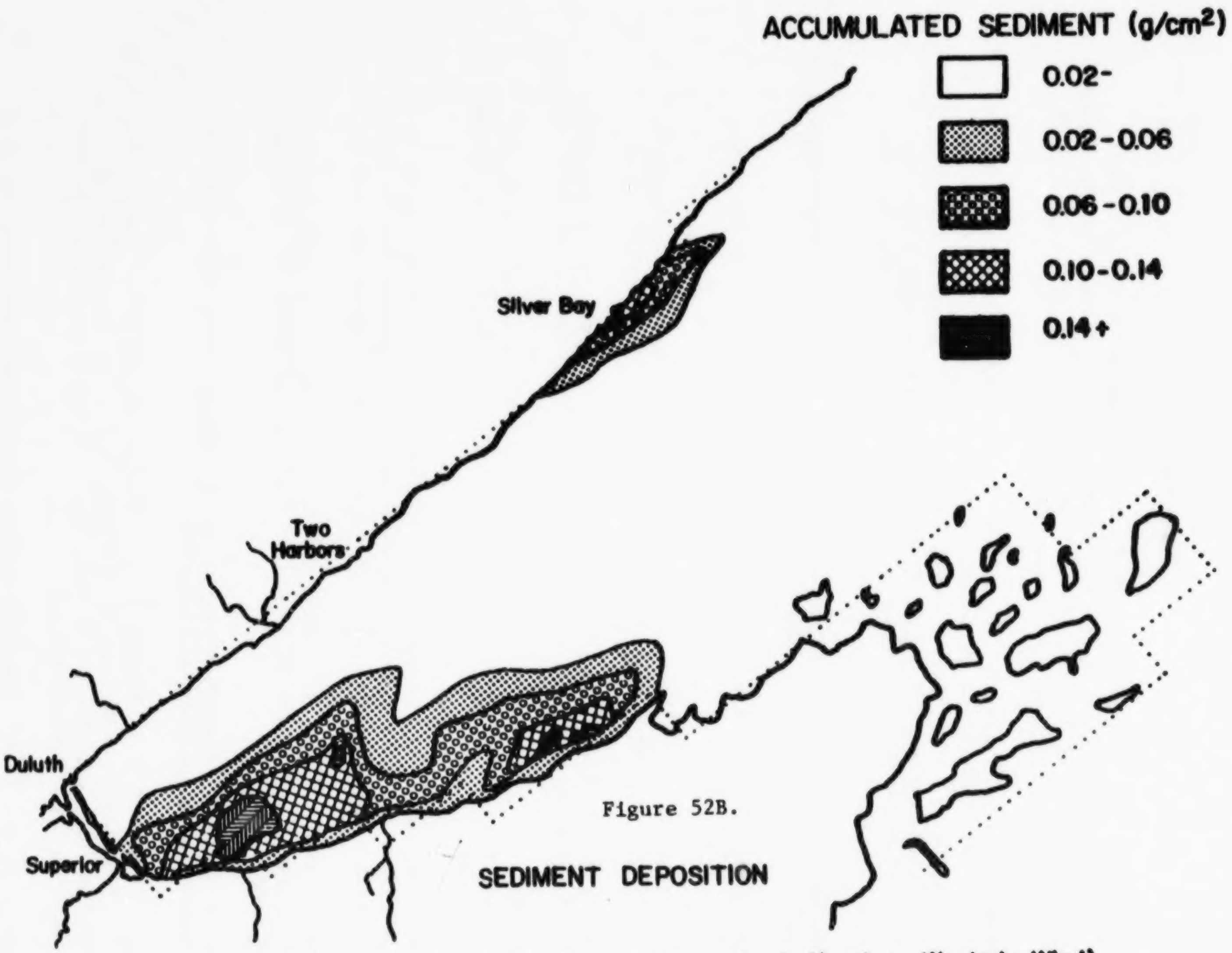
ACCUMULATED SEDIMENT (g/cm²)
0.02-
0.02-0.06
0.06-0.10
0.10-0.14
0.14+
Silver Bay
Two Harbors
Duluth
Superior

Figure 52B.

SEDIMENT DEPOSITION

MODEL TIME = 120 hours (18 hours after end of 11 m/sec Westerly Wind)

Figure 52. (continued)

REFERENCES

Bahnick, D. A., J. W. Horton, R. K. Roubal, and A. B. Dickas, 1972. "Effects of South Shore Drainage Basin and Clay Erosion on the Physical and Chemical Limnology of Western Lake Superior." Proc. 15th Conf. Great Lakes Research, Int. Assoc. Great Lakes Res.

Baumgartner, D. J., W. F. Rittall, G. R. Dittsworth, and A. M. Teeter, 1973. "Investigation of Pollution in Western Lake Superior due to Discharge of Mine Tailings, Data Report 1971." Studies Regarding the Effect of the Reserve Mining Company Discharge in Lake Superior, Pacific Northwest Environmental Research Laboratory Paper No. 10, U.S. E P A , Washington, D.C., p. 423.

Forristall, G. Z., 1974. "Three-Dimensional Structure of Storm-Generated Currents." J. Geophys. Res., 79(18), 2721-2729.

Hutchinson, G. E., 1957. A Treatise on Limnology. Wiley: New York, Vol. 1, p. 263.

Leenderste, J. J., 1967. Aspects of a Computational Model for Long-Period Water-Wave Propagation. RM5294-PR, The Rand Corporation.

Maanum, W. E., 1977. Numerical Prediction of Currents and Transports in Western Lake Superior. M.S. Thesis, University of Minnesota, Duluth.

Mortimer, C. H. and E. J. Fee, 1976. "Free Surface Oscillations and Tides of Lakes Michigan and Superior." Phil. Trans. Roy. Soc. London, 281, 1-61.

Rao, D. B. and D. J. Schwab, 1976. "Two-Dimensional Normal Modes in Arbitrary Enclosed Basins on a Rotating Earth: Application to Lakes Ontario and Superior." Phil. Trans. Roy. Soc. London, 281, 63-96.

Ruschmeyer, O. R., T. A. Olson, and H. M. Bosch, 1961. Lake Superior Studies 1956-61. Public School of Health, University of Minnesota, Minneapolis.

Sydor, M. 1973. Current Patterns and Turbidity. U.S. Army Corps of Engineers Report DACW-37-74-C-0014.

Tsai, Y. J. and Y. C. Chang, 1974. "Prediction and Verification of Storm Surges in Lake Ontario and Lake Erie." Stone and Webster Engineering Corporation, Boston, Mass. Paper presented at the 17th Conf. on Great Lakes Research.

Wilson, B. W., 1960. "Note on Surface Wind Stress Over Water at High and Low Wind Speeds." J. Geophys. Res., 65(10) 3377-3382.

APPENDIX A

SOUTH SHORE DATA FOR THE 1975 RUNOFF

Note: Data enclosed in parenthesis ( )are interpolated from measured data.

TABLE A-1. SUSPENDED LOAD TRANSPORTED FOR SNOW RUNOFF (APRIL 10 - 27, 1975) IN METRIC TONS

River	Load South of Hwy 13	Load Between Hwy 13 and Lower Station	Load From Lower Station to Lake	Total Load Discharged
Nemadji				84,848
Dutchman	224	88	5	317
Morrison	149	146		295
Amnicon	2,093	350		2,443
Ten	260	102	6	368
Wagner	134	124	6	264
Hanson	47	81		128
Middle	1,583	138	15	1,736
Poplar	351	920	12	1,283
Bardon	225	192	9	426
Pearson	220	446	23	699

Unnamed Stream #	Total Load Discharged	Unnamed Stream #	Total Load Discharged	Unnamed Stream #	Total Load Discharged
1	6	6	20	11	24
2	66	7	29	12	17
3	39	8	41	13	14
4	20	9	90	14	54
5	12	10	74	15	13

Total load from all unnamed streams 519 metric tons.

TABLE A-2. LOAD TRANSPORTED DURING RAIN EVENT (APRIL 28 - MAY 5, 1975) IN METRIC TONS

River	Load South of Hwy 13	Load Between Hwy 13 and Lower Station	Load From Lower Station to Lake	Total Load Discharged
Nemadji				22,044
Dutchman	108	30.8	1.8	140.6
Morrison	17	29.2		46.2
Amnicon	616	98		714
Ten	26	35.7	1.6	63.3
Wagner	11.4	18.6	1.6	31.6
Hanson	4	16.2		20.2
Middle	218	48.3	6	272.3
Poplar	71	278	4.8	358.8
Bardon	48	67.2	2.4	117.6
Pearson	29	103	11	143

Unnamed Stream #	Total Load Discharged	Unnamed Stream #	Total Load Discharged	Unnamed Stream #	Total Load Discharged
1	0.4	6	1.3	11	1.6
2	4.4	7	1.9	12	1.1
3	2.6	8	2.7	13	0.9
4	1.3	9	6.0	14	3.6
5	0.8	10	4.9	15	0.9

Total from all unnamed streams 34.4 metric tons.

TABLE A-3. SOUTH SHORE STREAM CHARACTERISTICS

River	Total Basin Area (km^2)	Total Lengths Main Streams / Intermittents (km)	South of Hwy 13			Between Hwy 13 and Downstream Station			Between Downstream Station and Mouth		
			Basin Area (km^2)	Main Streams (km)	Inter-mittents (km)	Basin Area (km^2)	Main Streams (km)	Inter-mittents (km)	Basin Area (km^2)	Main Streams (km)	Inter-mittents (km)
Nemadji	1191	105									
Dutchman	19	30.1 2.7	14	24.0	1.3	5	5.6	1.4	0.5	0.5	0
Morrison	13	20.4 7.2	8	11.6	4.3	5	8.8	2.9	0	0	0
Amnicon	111 * 349 +	~ 182 * 6.4 *	98 *	~160 *	5.0 *	13	21.1	1.4	0	0	0
Ten	17	20.8 24.0	13	15.3	20.6	4	4.8	3.4	0.3	0.6	0
Wagner	13	7.9 17.1	7	2.7	11.6	5	4.5	5.5	0.3	0.6	0
Hanson	11	1.4 12.2	4	1.4	3.5	6	0	8.7	0	0	0
Middle	59 * 124 +	57.0 * 25.7 *	52 *	48.8 *	20.8 *	6	6.6	4.5	0.8	1.6	0
Poplar	55 * 104 +	65.8 * 38.3 *	23 *	38.9 +	11.1 *	31	25.6	27.2	1.0	1.3	0
Bardon	32	26.7 38.1	24	16	32.3	8	9.7	5.8	0.8	1.0	0
Pearson	27	26.7 53.4	13	16	6.8	12	3.1	46.7	2.6	3.5	0

+ University of Wisconsin measurement   * includes only portion within red clay belt

TABLE A-4. SOUTH SHORE UNNAMED STREAM CHARACTERISTICS

Unnamed Stream #	Total Basin Area (km^2)	Total Length (km)	
		Main Streams	Inter-mittents
1	0.5	0.5	0.2
2	3.6	6.6	0.5
3	2.3	3.7	0.5
4	1.6	1.8	0.3
5	0.8	1.3	0
6	1.0	1.4	0.6
7	1.3	0	3.1
8	2.1	0	4.3
9	3.9	0	9.7
10	4.1	0	7.9
11	1.0	0	2.6
12	1.0	0	1.8
13	0.8	0	1.4
14	3.1	0	5.8
15	0.8	0	1.4

TABLE A-5. SOUTH SHORE EROSION DATA (1975) FOR NEMADJI GOLF COURSE AND HWY 53

Date	Water Sample Description	Turbidity (NTU)	Suspended Solids (mg/ℓ)	Stage (cm)	Discharge (m^3/sec)	Total Load (Metric Tons Per Day)
April 12	N-12-1	50.0	61.7 (58.2)	298	21.0	105
	N-12-2		54.7			
April 13			(158)	(348)	(53.1)	725
April 14			(261)	(399)	(85.2)	1922
April 15			(364)	(450)	(118)	3692
April 16	N-16-1	143	472 (476)	497	150	6150
	N-16-2		(479)			
April 17	N-17-1 (D) Hwy 53	220	580 (540)	504	152	7080
	N-17-2 (I) Hwy 53	215				
April 18	N-18-1	148	417	542	163	6472
	N-18-2	143	(460)			
	N-18-3 (D) Hwy 53	152				
	N-18-4 (I) Hwy 53	158				
April 19	N-19-1	162	523 (524)	509	154	6975
	N-19-2	162	530			
	N-19-3		521			
April 20			(494)	(495)	(148)	6324
April 21	N-21-1	148	465	481	142	5508
	N-21-2	152	463			
	N-21-3		439 (448)			
	N-21-4		432 (UWS)			
	N-21-5		457			
	N-21-6		416 (UWS)			
April 22	N-22-1	205	852	455	127	9360
April 23	N-23-1 Hwy 53	242	1055	351		
	N-23-2 Golf Course	260	927 (1059)	476	140	12801
	N-23-3	258	1113			
	N-23-4		1065			
	N-23-5		1004			

(continued)

TABLE A-5. (continued)

Date	Water Sample Description	Turbidity (NTU)	Suspended Solids (mg/ℓ)		Stage (cm)	Discharge (m^3/sec)	Total Load (Metric Tons Per Day)
April 24	N-24-1	192	423		512	155	5665
	N-24-2	190	425	(424)			
	N-24-3	187	405				
	N-24-4		425				
April 25	N-25-1	148	392		489	147	5031
	N-25-2	148	401	(397)			
	N-25-3	148	409				
	N-25-4		387				
April 26				(347)	(466)	(132)	3946
April 27				(307)	(443)	(116)	3090
April 28	N-28-1	142		(290)	420	101	2540
April 29	N-29-1	200	557		456	127	6120
April 30				(420)	(462)	(131)	4753
May 1	N-1-1	108	284	(285)	469	135	3319
	N-1-2		286				
May 2	N-2-1	100	257		390	80.4	1785
May 3				(232)	(366)	(65.3)	1310
May 4				(207)	(343)	(50.2)	898
May 5	N-5-1	85	182		319	35.1	552
May 6				(173)	(310)	(29.2)	436
May 7			165		(301)	(23.2)	331
May 23	N-23-1	26.0	29.5			6.0	15.2

TABLE A-6. SOUTH SHORE EROSION DATA (1975) FOR DUTCHMAN, HWY 13

Date	Water Sample Description	Turbidity (NTU)	Suspended Solids (mg/ℓ)	Stage (cm)	Discharge (m^3/sec)	Total Load (Metric Tons Per Day)
April 7	D-7-1 D-7-2	65.5 65.0	(50)		0.11	0.49
April 8			(55)		0.14	0.67
April 9			(60)		0.17	0.88
April 10	D-10-1 D-10-2	66.0	71 61.5 (66)		0.23 0.37	1.29 2.13
April 11			(67)			
April 12			(75)		0.54	3.49
April 13			(84)		0.71	5.14
April 14	D-14-1 (I)	70.5	93.3 (92.6)		0.85	6.80
	D-14-2 (D)	70.5	92.0			
April 15	D-15-2 D-15-3	60.5	58.0 73.7 (66)	51	2.17	12.4
April 16	D-16-1 D-16-2	85.0	119	ICE JAM	3.86	39.7
April 17	D-17-2	66.0	53	ICE JAM	3.48	16.0
April 18	D-18-1	75.5	107	ICE JAM	3.09	28.5
April 19	D-19-1	74.5	83		2.72	19.5
April 20			(86)		2.36	17.5
April 21	D-21-2	68.5	86	51	2.08	15.5
April 22	D-22-1	79.5	(107)	53	2.36	21.8
April 23	D-23-2	97.5	128	51	2.08	23.0
April 24	D-24-1	70.0	49	43	1.20	5.1
April 25	D-25-2	71.0	48	38	0.69	2.9

(continued)

TABLE A-6. (continued)

Date	Water Sample Description	Turbidity (NTU)	Suspended Solids (mg/ℓ)	Stage (cm)	Discharge (m^3/sec)	Total Load (Metric Tons Per Day)
April 26			(76)		1.19	7.8
April 27			(104)		1.70	15.3
April 28	D-28-1	113	132	52	2.21	25.2
April 29			(105)		4.11	37.3
April 30	D-30-1	80.0	78		1.47	9.9
May 1	D-1-1 (D)	70.0	(70.5)	41	0.57	3.5
May 2			(78)	(34)	0.45	3.0
May 3			(86)	(33)	0.38	2.8
May 4			(93)	(30)	0.28	2.3
May 5	D-5-1 (D)	76.0	(100)	25	0.14	1.2
May 6			(80)	(25)	0.14	0.94
May 7			(60)	24	0.11	0.59

TABLE A-7. SOUTH SHORE EROSION DATA (1975) FOR DUTCHMAN MOUTH, MORRISON HWY 13, AND MORRISON MOUTH

Date	Water Sample Description	Turbidity (NTU)	Suspended Solids (mg/ℓ)	Stage (cm)	Discharge (m^3/sec)	Total Load (Metric Tons Per Day)
Dutchman, Mouth						
April 9	D-9-1	65.0	43.0			
April 15	D-15-1	69.0	82.0		2.19	
April 16	D-16-1		216			
	D-16-2	112				
April 17	D-17-1	88.0	110			
April 18	D-18-1		162			
	D-18-2 (D)	100				
	D-18-3 (I)	102				
April 21	D-21-1	85.0	134			
April 23	D-23-1	140	241			
April 25	D-25-1	80.5	77		0.75	
April 30					1.37	
Morrison, Hwy 13						
April 16	Mo-16-1		67			
April 25	Mo-25-1	52.0	45		0.34	
April 28	Mo-28-1	91.5	103			
April 30	Mo-30-1 (D)	64.5			0.93	
May 5	Mo-5-1	62.0			0.34	
Morrison, Mouth						
April 16	Mo-16-1	118				
	Mo-16-2		259			
April 25	Mo-25-2	83.0	93			

TABLE A-8. SOUTH SHORE EROSION DATA (1975) FOR AMNICON, HWY 13

Date	Water Sample Description	Turbidity (NTU)	Suspended Solids (mg/ℓ)		Stage (cm)	Discharge (m^3/sec)	Total Load (Metric Tons Per Day)
April 10	A-10-1 A-10-2	16.5	12.5 14.3	(13.4)	61	0	0
April 11				(40.3)	(74)	0	0
April 12				(68.2)	(89)	(3.09)	18.2
April 13				(96.0)	(104)	(7.65)	63.4
April 14	A-14-1 A-14-2	60.6	125 119	(122)	(117)	(10.5)	110
April 15				(100)	(137)	(17.0)	147
April 16	A-16-1 A-16-2 (5 br after A-16-1)	59.5	55 107	(81)	157	24.8	173
April 17	A-17-1 (D) A-17-2 (I)	38.0 36.5	50		178	32.1	138
April 18	A-18-1 (D)	37.0	59		178	32.1	164
April 19	A-19-1	29.5	58		169	28.3	142
April 20				(45)	(175)	(31.4)	122
April 21	A-21-1	25.0	31		183	34.7	93
April 22				(51)	(183)	34.7	153
April 23	A-23-1	32.5	71		193	39.1	240
April 24				(66)	183	34.7	198
April 25				(62)	(178)	(32.1)	172
April 26				(58)	(173)	(30.2)	152

(continued)

TABLE A-8. (continued)

Date	Water Sample Description	Turbidity (NTU)	Suspended Solids (mg/ℓ)	Stage (cm)	Discharge (m^3/sec)	Total Load (Metric Tons Per Day)
April 27			(54)	(165)	(27.7)	129
April 28	A-28-1	54.5	71	170	29.0	178
April 29	A-29-1	30.5	(50)	183	34.7	150
April 30	A-30-1	25.0	30	183	34.7	90
May 1	A-1-1 (D)	21.0	24	165	27.7	57
May 2			(22)	155	23.2	44
May 3			(19)	(147)	(20.1)	33
May 4			(17)	(140)	(17.6)	26
May 5	A-5-1 (D)	16.5	(14)	132	15.9	19
May 6			(11)	(124)	(12.9)	12
May 7			(8)	117	9.63	7
May 23	A-23-1	9.5	3.8 (7)			

TABLE A-9. SOUTH SHORE EROSION DATA (1975) FOR TEN HWY 13, WAGNER HWY 13, WAGNER MOUTH, AND HANSON MOUTH

Date	Water Sample Description	Turbidity (NTU)	Suspended Solids (mg/ℓ)		Stage (cm)	Discharge (m^3/sec)	Total Load (Metric Tons Per Day)
Ten, Hwy 13							
April 10	T-10-1	75.0	63.3	(59)			
	T-10-2		56.0				
April 14				(200)	(112)*	(3.40)	58.7
April 15	T-15-1	113	235	(227)	46*	3.96	77.7
	T-15-2		219				
April 16	T-16-1 (D)	103	160		107*	2.69	37.2
	T-16-2 (I)	102					
April 17	T-17-1	70.5	69		58	2.53	15.1
April 18	T-18-1	91.0	123		53	2.17	23.0
April 19	T-19-1	73.0	104		39	1.13	10.2
April 20				(98)	(36)	(0.91)	7.6
April 21				(92)	(33)	(0.79)	6.3
April 22	T-22-2	69.0	86		29	0.66	4.9
April 23	T-23-1	69.5	41	(90)	32	0.75	5.8
April 24				(86)	(25)	(0.54)	4.0
April 25				(82)	(28)	(0.62)	4.4
April 26				(78)	(20)	(0.39)	2.6
April 27				(74)	(18)	(0.31)	2.0
April 28	T-28-1	102	71		23	0.46	2.8
April 29	T-29-1	85.5	120		37	0.97	10.0
April 30	T-30-1	76.0	64		36	0.91(1.04)	5.0

* Ice Obstruction

(continued)

TABLE A-9. (continued)

Date	Water Sample Description	Turbidity (NTU)	Suspended Solids (mg/ℓ)	Stage (cm)	Discharge (m^3/sec)	Total Load (Metric Tons Per Day)
May 1	T-1-1 (D)	65.0	(55)	17	0.28	1.3
May 2			(50)	(15)	(0.25)	1.1
May 3			(45)	(15)	(0.25)	0.97
May 4			(40)	(15)	(0.25)	0.86
May 5	T-5-1 (D)	70.0	(90)	14	0.20	1.6
May 6		(60)		(14)	(0.21)	1.1
May 7		(55)		(13)	(0.18)	0.87
Wagner, Hwy 13						
April 15	W-15-1 W-15-2	63.0	70.7 56.7			
April 22	W-22-2	53.5				
April 28	W-28-1	135	143			
May 1	W-1-1 (D)	61.0				
May 5	W-5-1 (D)	60.0				
Wagner, Mouth						
April 22	W-22-1	61.5	75			
Hanson, Mouth						
April 10	H-10-1	70.0	53.7			

TABLE A-10. SOUTH SHORE EROSION DATA (1975) FOR MIDDLE HWY 13, AND MIDDLE MOUTH

Date	Water Sample Description	Turbidity (NTU)	Suspended Solids (mg/ℓ)	Stage (cm)	Discharge (m^3/sec)	Total Load (Metric Tons Per Day)
Middle, Hwy 13						
April 14			(80)	99	11.9	82.2
April 15	M-15-1 M-15-2	55.0	179 (178) 177	107	14.4	221
April 16	M-16-1	28.0	(80)	107	14.4	99.4
April 17	M-17-2	37.5	96	114	18.0	149
April 18			(90)	130	24.6	192
April 19	M-19-1	26.5	83	127	24.0	172
April 20			(65)		23.5	132
April 21	M-21-1	20.5	47	119	22.9	93.2
April 22	M-22-1	16.5	55	122	22.3	106
April 23	M-23-1	21.5	55	135	25.8	122
April 24			(44)	(127)	(24.0)	91.3
April 25			(34)	(122)	(22.3)	65.6
April 26			(26)	(112)	(16.7)	37.5
April 27			(16)	(107)	(14.4)	19.9
April 28	M-28-1 M-28-2 (ditch near river)	16.0 245	7 (16) 486	102	12.6	17.4
April 29	M-29-1	20.5	5 (65)	109	15.4	86.7
April 30	M-30-1	20.5	29	113	17.3	43.4

(continued)

TABLE A-10. (continued)

Date	Water Sample Description	Turbidity (NTU)	Suspended Solids (mg/ℓ)	Stage (cm)	Discharge (m^3/sec)	Total Load (Metric Tons Per Day)
May 1			(22)	102	12.6	23.9
May 2	M-2-1	10.0	15	93	10.3	13.4
May 3			(13)		(9.74)	10.9
May 4			(11)		(8.01)	7.62
May 5	M-5-1	7.5	(9)	76	6.85	5.32
May 6			(9)		(6.17)	4.80
May 7			(9)	69	5.52	4.29
Middle, Mouth						
April 8	M-8-1	20.5	20.0	*		
	M-8-2		19.7			
April 11	M-11-1	40.5		*		
April 16	M-16-10	40.0		*		
April 18	M-18-1 (D)	85.0	279	*		
	M-18-2 (I)	89.5				

* Because of the depth and current at this station, a bottom profile could not be taken.

TABLE A-11. SOUTH SHORE EROSION DATA (1975) FOR POPLAR HWY 13 AND POPLAR MOUTH

Date	Water Sample Description	Turbidity (NTU)	Suspended Solids (mg/ℓ)		Stage (cm)	Discharge (m^3/sec)	Total Load (Metric Tons Per Day)
Poplar, Hwy 13							
April 10	P-10-1 P-10-2	12.0	6.9 2.5	(4.7)	(25)	(0.51)	0.21
April 14	P-14-2 P-14-3 P-14-4	40.0	71.3 76.0	(73)	(51) Ice Blockage	(3.26)	20.5
April 15	P-15-1 P-15-2	76.5	159 167	(163)	(64)	(4.56)	64.2
April 16				(108)	69	5.17	48.2
April 17	P-17-2	30.5	52		71	5.47	24.6
April 18				(61)	75	5.86	30.9
April 19	P-19-1	20.5	70		80	6.40	38.7
April 20				(61)		6.54	34.4
April 21	P-21-1	16.0	51		83	6.68	29.4
April 22	P-22-2	13.5	34		75	5.86	17.2
April 23	P-23-2	15.0	34			(8.55)	25.1
April 24	P-24-2	9.4	12		77	6.12	6.34
April 25				(10)		(5.75)	4.97
April 26				(8)		(5.35)	3.69
April 27				(6)		(4.98)	2.58
April 28	P-28-1	16.0	3	(5)	64	4.62	1.99
April 29	P-29-1	16.0	10	(45)	70	5.30	20.6
April 30				(40)		(4.90)	16.9
May 1				(35)		(4.53)	13.7

(continued)

TABLE A-11. (continued)
-2-

Date	Water Sample Description	Turbidity (NTU)	Suspended Solids (mg/ℓ)	Stage (cm)	Discharge (m^3/sec)	Total Load (Metric Tons Per Day
May 2	P-2-1	8.9	(15)		(4.13)	5.35
May 3			(13)		(3.74	4.20
May 4			(11)		(3.37)	3.20
May 5	P-5-1	7.0	(9)	48	2.97	2.31
May 6			(9)		(2.15	1.67
May 7			(9)	33	1.35	1.05
Poplar, Mouth						
April 14	P-14-1 P-14-2	60.0	92.7 (88) 83.7		(5.49)	41.7
April 15			(119)		(7.73)	79.5
April 16	P-16-1	50.0	151		(8.75)	114
April 17	P-17-1	56.0	85 (158)		(9.26)	126
April 18	P-18-1	65.5	165		(9.94)	142
April 19			(184)		(10.8)	172
April 20			(160)		(11.1)	153
April 21			(134)		(11.3)	131
April 22	P-22-1	32.0	87	142	12.0	90.3
April 23	P-23-1	35.0	91	165	17.6	138
April 24	P-24-1	30.5	32	142	12.0	33.2
April 25			(26)		(9.74)	12.9
April 26			(21)		(9.06)	16.4
April 27			(16)		(8.44)	11.6

(continued)

TABLE A-11. (continued)
-3-

Date	Water Sample Description	Turbidity (NTU)	Suspended Solids (mg/ℓ)	Stage (cm)	Discharge (m^3/sec)	Total Load (Metric Tons Per Day)
April 28			(13)		(7.82)	8.78
April 29			(118)		(8.95)	91.2
April 30			(105)		(8.30)	75.3
May 1	P-1-1	25.0	(40)	122	6.61	24
May 2			(39)		(7.05)	23.8
May 3			(34)		(6.31)	18.6
May 4			(29)		(5.72)	14.3
May 5	P-5-1	16.5	(23)	116	4.93	9.79
May 6			(23)		(3.65)	7.26
May 7			(23)		(2.29)	4.56

TABLE A-12. SOUTH SHORE EROSION DATA (1975) FOR BARDON HWY 13 AND BARDON MOUTH

Date	Water Sample Description	Turbidity (NTU)	Suspended Solids (mg/ℓ)	Stage (cm)	Discharge (m^3/sec)	Total Load (Metric Tons Per Day)
Bardon, Hwy 13						
April 14	B-14-1 B-14-2	50.5	92.3 (92.6) 92.0		(0.71)	5.66
April 15	B-15-1 B-15-2	93.5	272 (275) 279		(1.50)	35.7
April 16	B-16-1	80.0	159		(2.29)	31.5
April 17			(131)	64	3.12	35.3
April 18			(103)	71	5.77	51.3
April 19	B-19-1	51.5	75	60	3.96	25.7
April 20			(55.5)		(2.52)	12.1
April 21	B-21-1	36.5	36	36	1.08	3.3
April 22			(38.5)		(1.64)	5.46
April 23	B-23-1	44.5	41	48	2.21	7.82
April 24	B-24-1	36.0	41	33	0.63 (0.96)	3.41
April 25			(40)		(0.85)	2.94
April 26			(40)		(0.74)	2.54
April 27			(40)		(0.62)	2.15
April 28	B-28-1	44.5	16 (60)	58	3.77	19.5
April 29	B-29-1	64.5	10 (100)	41	1.35	11.7
April 30			(80)		(0.99)	6.9
May 1	B-1-1 (D)	45.0	(60)	24	0.62	3.2
May 2	B-2-1 (D)	39.5	(54)	19	0.45	1.8

(continued)

TABLE A-12. (continued)

Date	Water Sample Description	Turbidity (NTU)	Suspended Solids (mg/ℓ)	Stage (cm)	Discharge (m^3/sec)	Total Load (Metric Tons Per Day)
May 3			(48)		(0.41)	1.5
May 4			(42)		(0.37)	1.3
May 5	B-5-1	36.0	(36)	15	0.35 (0.33)	1.0
May 6			(30)		(0.23)	0.68
May 7			(25)	9	0.14	0.3
Bardon, Mouth						
April 9	B-9-1 (D)	39.5	35.7 (31)	Ice Blockage	0.21	
	B-9-2 (I)	36.0	27.0			
April 14	B-14-3	102	186 (185)			
	B-14-4	105	184			
April 16	B-16-2	108	327			
April 17	B-17-1 (D)	115	201			
	B-17-2 (I)	105				
April 18	B-18-1	130	311			
April 21	B-21-2	60.0	73			
April 23	B-23-2	70.0	91			
April 24	B-24-2	51.0	35	36	1.20	
May 1	B-1-2 (D)	60.5		29	0.74	

TABLE A-13. SOUTH SHORE EROSION DATA (1975) FOR PEARSON HWY 13 AND PEARSON MOUTH

Date	Water Sample Description	Turbidity (NTU)	Suspended Solids (mg/ℓ)	Stage (cm)	Discharge (m^3/sec)	Total Load (Metric Tons Per Day)
Pearson, Hwy 13						
April 14	Pe-14-1 Pe-14-2	41.0	49.3 (51) 52.7	20	0.15	0.67
April 15			(105)	(30)	(0.40)	3.61
April 16			(158)	(41)	(0.76)	10.45
April 17			(210)	(53)	(1.33)	24.1
April 18	Pe-18-3 Pe-18-4	89.5 89.5	(200)	53	1.33	22.9
April 19	Pe-19-1	85.0	220	51	1.19	22.7
April 20			(140)	(42)	(0.82)	9.85
April 21	Pe-21-2	44.0	39 (50)	33	0.48	2.07
April 22			(50)	(28)	(0.33)	1.40
April 23	Pe-23-1	45.5	68	38	0.67	3.95
April 24			(65)	(36)	(0.58)	3.26
April 25	Pe-25-1		61	(33)	(0.48)	2.53
April 26			(58)	(28)	(0.33)	1.63
April 27			(54)	(23)	(0.19)	0.90
April 28	Pe-28-1	95.0	119	28	0.33	3.34
April 29	Pe-29-1	71.5	81	38	0.67	4.68
April 30			(75)	(30)	(0.40)	2.58
May 1	Pe-1-1 (D)	55.0	70	22	0.17	1.05
May 2	Pe-2-1 (D)	44.5	(64)	17	0.12	0.64

(continued)

TABLE A-13. (continued)

-2-

Date	Water Sample Description	Turbidity (NTU)	Suspended Solids (mg/ℓ)	Stage (cm)	Discharge (m^3/sec)	Total Load (Metric Tons Per Day)
May 3			(60)	(17)	(0.11)	0.57
May 4			(55)	(16)	(0.10)	0.48
May 5	Pe-5-1	42.0	(50)	15	0.094	0.40
May 6			(50)	(13)	0.072	0.31
May 7			(50)	10	0.054	0.23
Pearson, Mouth						
April 9	Pe-9-1 (I)	39.5	37.3		0	0
April 14	Pe-14-2 (D)	74.0			(0.49)	5.21
	Pe-14-3 (I)	74.0	126 (123)			
	Pe-14-4		120			
April 15			(183)		(1.26)	19.9
April 16	Pe-16-1 (D)	96.5	238 (243)		(24.1)	50.5
	Pe-16-2		249			
April 17			(400)	86	4.19	145
April 18	Pe-18-1	115	397	85	4.19	144
	Pe-18-2	115				
	Pe-18-3	152				
April 19			(430)		(3.79)	141
April 20			(280)		(2.58)	62
April 21	Pe-21-1	74.5	81	48	1.53	10.7
April 22			(81)		(1.03)	7.19
April 23			(113)		(2.13)	20.8

(continued)

TABLE A-13. (continued)
-3-

Date	Water Sample Description	Turbidity (NTU)	Suspended Solids (mg/ℓ)	Stage (cm)	Discharge (m^3/sec)	Total Load (Metric Tons Per Day)
April 24			(147)		(1.84)	2.34
April 25			(138)		(1.52)	18.2
April 26			(131)		(1.03)	11.7
April 27			(122)		(0.61)	6.47
April 28			(270)		(1.03)	24.0
April 29			(184)		(2.12)	33.7
April 30			(170)		(1.26)	18.5
May 1			(159)		(0.55)	7.55
May 2	Pe-2-2	59.0	(145)	38	0.38	4.73
May 3			(136)		(0.35)	4.09
May 4			(125)		(0.32)	3.49
May 5			(114)		(0.30)	2.93
May 6			(114)		(0.23)	2.26
May 7			(114)		(0.17)	1.65

☆ U.S. GOVERNMENT PRINTING OFFICE: 1979—652-550/64